

INFORMATION TO USERS

This manuscript has been reproduced from the microfilm master. UMI films the text directly from the original or copy submitted. Thus, some thesis and dissertation copies are in typewriter face, while others may be from any type of computer printer.

The quality of this reproduction is dependent upon the quality of the copy submitted. Broken or indistinct print, colored or poor quality illustrations and photographs, print bleedthrough, substandard margins, and improper alignment can adversely affect reproduction.

In the unlikely event that the author did not send UMI a complete manuscript and there are missing pages, these will be noted. Also, if unauthorized copyright material had to be removed, a note will indicate the deletion.

Oversize materials (e.g., maps, drawings, charts) are reproduced by sectioning the original, beginning at the upper left-hand corner and continuing from left to right in equal sections with small overlaps. Each original is also photographed in one exposure and is included in reduced form at the back of the book.

Photographs included in the original manuscript have been reproduced xerographically in this copy. Higher quality 6" x 9" black and white photographic prints are available for any photographs or illustrations appearing in this copy for an additional charge. Contact UMI directly to order.

UMI

**A Bell & Howell Information Company
300 North Zeeb Road, Ann Arbor MI 48106-1346 USA
313/761-4700 800/521-0600**

CONTRIBUTIONS TOWARDS THE COMPUTATION OF A
PRECISE REGIONAL GEOID

by

Mehdi Najafi Alamdari

BSc. in Physics, University of Tehran, Iran, 1970

MSc. in Engineering, University of New Brunswick, Canada, 1981

A THESIS SUBMITTED IN PARTIAL FULFILLMENT OF
THE REQUIREMENTS FOR THE DEGREE OF
Doctor of Philosophy
in the
Geodesy and Geomatics Engineering

This thesis is accepted.



Dean of Graduate Studies

THE UNIVERSITY OF NEW BRUNSWICK

November, 1996

© Mehdi Najafi Alamdari, 1996



**National Library
of Canada**

**Acquisitions and
Bibliographic Services**

**395 Wellington Street
Ottawa ON K1A 0N4
Canada**

**Bibliothèque nationale
du Canada**

**Acquisitions et
services bibliographiques**

**395, rue Wellington
Ottawa ON K1A 0N4
Canada**

Your file *Votre référence*

Our file *Notre référence*

The author has granted a non-exclusive licence allowing the National Library of Canada to reproduce, loan, distribute or sell copies of this thesis in microform, paper or electronic formats.

The author retains ownership of the copyright in this thesis. Neither the thesis nor substantial extracts from it may be printed or otherwise reproduced without the author's permission.

L'auteur a accordé une licence non exclusive permettant à la Bibliothèque nationale du Canada de reproduire, prêter, distribuer ou vendre des copies de cette thèse sous la forme de microfiche/film, de reproduction sur papier ou sur format électronique.

L'auteur conserve la propriété du droit d'auteur qui protège cette thèse. Ni la thèse ni des extraits substantiels de celle-ci ne doivent être imprimés ou autrement reproduits sans son autorisation.

0-612-23868-7

Abstract

The Stokes-Helmert scheme of the geoid determination was further developed here. In this scheme the topographical masses above the geoid are condensed as a surface material layer on the geoid. The gravity field associated with this condensation is called the Helmert gravity field.

The mixed Boundary Value Problem (BVP) is first solved in the Helmert space (field). As a result, the "geoid of the Helmert earth" or the "Helmert co-geoid" is determined. Then, the co-geoid is transformed to the geoid by applying the correction for the indirect effect. For its determination the co-geoid is decomposed into two parts: the long wavelength part, called the reference spheroid is determined using satellite only analysis; the short wavelength part called the residual (high-frequency) geoid is determined using terrestrial gravity data. The reference spheroid plays the role of a reference surface to which the residual geoid is referred. Both parts are precisely corrected for the Helmert condensation effect.

The long wavelength reference gravity field is constructed, from the satellite data, to compute the Helmert reference spheroid. In the meantime, some quantities in the reference field are computed. These quantities are: the direct topographical effect on gravity, Helmert's reference gravity anomaly, secondary indirect topographical effect on gravity, and the reference spherical correction to the boundary condition. They are all evaluated to a 2nd degree approximation.

In the residual geoid, the generalized Stokes integral, taken over a spherical cap of radius $\psi_0 = 6^\circ$ and employing a modified spheroidal kernel designed to counteract the truncation, is used. The contribution of the gravity data outside the cap is called the truncation error, minimized by the modified kernel. It is estimated using a geopotential model. The gravity data used in the Stokes integration, are the residual (high-frequency) $5' \times 5'$ mean Helmert gravity anomalies, referred to the co-geoid.

These residual values are obtained from the "observed" gravity anomalies (the whole values) on the topography. For this, the observed values are first Helmertized by applying the direct topographical effect on gravity. They are reduced to residual component by subtracting the Helmert reference gravity anomalies on the topography (discussed above). Then, they are downward continued to the geoid. The values on the geoid are transferred to the co-geoid by applying the secondary indirect topographical effect and the spherical correction to the boundary condition, both reduced by their reference values.

The error in the Helmert co-geoid is a combination of two errors: that of the spheroid and that of the residual geoid. The error in the spheroid is the result of the errors in the satellite potential coefficients. The spheroidal heights are correlated, and the correlation is a function of the geopotential model used. The correlation distance is about 900 *km*. The error in the residual geoidal heights are due to the errors in the terrestrial gravity data. They are also correlated through the gravity data being shared by the Stokes integrals at the two points in question.

Contents

Abstract	ii
List of Tables	vii
List of Figures	viii
Acknowledgments	x
1 Introduction	1
1.1 Gravimetric Determination of the Geoid	2
1.1.1 Helmert's method	3
1.2 The Stokes-Helmert Scheme	4
1.2.1 Generalized Stokes-Helmert Scheme	10
1.2.2 Flowchart of the Operations	12
1.3 Topics of the Investigation	13
2 Higher-degree Reference Field in the Helmert Space	18
2.1 Introduction	18
2.1.1 Actual Gravity Field of the Earth	18
2.1.2 Anomalous Gravity Field of the Earth	19
2.2 Satellite-derived Gravity Field of the Earth	24
2.3 Higher-degree Reference Field	26

2.4	Helmertization of the Higher-degree Reference Field	28
2.4.1	Residual Topographical Potential V	29
2.4.2	Helmert's Higher-degree Reference Field	35
2.5	Evaluation of the Anomalous Quantities on the Helmert co-geoid . . .	38
3	Numerical Evaluation of the Residual Helmert Co-geoid	41
3.1	Modified Spheroidal Stokes's Integrator	41
3.2	Numerical Evaluation of the Modified Spheroidal Stokes Integral . . .	43
3.2.1	The Residual Helmert Gravity Anomaly	49
3.3	Truncation Error of the Modified Spheroidal Stokes Integral	50
3.4	Downward Continuation of Mean Helmert's Gravity Anomalies	56
4	Numerical Results	62
4.1	Reference Quantities	62
4.1.1	Reference Spheroid of Degree 20 in Canada	62
4.1.2	Reference Gravity Anomaly of Degree 20 in Canada	64
4.2	Helmert's Reference Quantities in Canada	67
5	Accuracy of the Helmert Co-geoid	76
5.1	Introduction	76
5.2	Variance of the spheroid of degree L	77
5.3	Variance of δN and $\Delta(\delta N)$	81
5.3.1	Covariance of δN	82
5.3.2	Numerical evaluation of the $\rho_{\delta N}$	85
5.3.3	Relative Accuracy of the Geoid	88
6	Conclusions and recommendations	90
6.1	The Stokes-Helmert Scheme	90
6.2	The Helmert Reference Spheroid	91
6.3	Accuracy of the Geoid	92

6.4 Recommendations	93
Vita	100

List of Tables

4.1	Spheroid N_{20} in Canada and its mean "commission error"	64
4.2	Δg_{20} in Canada and their mean "commission error"	67
4.3	N_{20}^h in Canada	72
4.4	Δg_{20}^h in Canada	72

List of Figures

1.1	Flowchart of the Operations in the Stokes-Helmert Scheme	14
3.1	The three zones in the Stokes integrator	44
3.2	Errors in the residual geoid, obtained by the GIN95.f integrator (size of inner zone used is $2^\circ \times 2^\circ$). Contour interval is 0.02 <i>m</i>	47
3.3	Smoothed errors in the residual geoid, obtained by the GIN95.f integrator (size of inner zone is $4^\circ \times 4^\circ$). Contour interval is 0.02 <i>m</i>	48
3.4	The truncation error (for $\psi_0 = 6^\circ$) in Canada (from the GFZ93A model). Contour interval is 0.04 <i>m</i>	53
3.5	Difference in truncation error, obtained from OSU91A and GFZ93A models. Contour interval is 0.02 <i>m</i>	54
3.6	Contribution of downward continuation of Helmert's gravity anomaly to the Helmert co-geoid. Contour interval is 0.1 <i>m</i>	61
4.1	N_{20} derived from GRIM4-S4 model. Contour interval is 5 <i>m</i>	63
4.2	Ellipsoidal correction to N_{20} . Contour interval is 0.1 <i>m</i>	65
4.3	Higher-degree approximation of N_{20} , compared to the ellipsoidal approximation. Contour interval is 0.5 <i>mm</i>	66
4.4	Δg_{20} derived from GRIM4-S4 model. Contour interval is 5 <i>mGal</i>	68
4.5	Ellipsoidal correction to Δg_{20} . Contour interval is 0.2 <i>mGal</i>	69
4.6	Direct topographical effect on spheroid, based on the centre of mass conservation model. Contour interval is 0.02 <i>m</i>	70

4.7	DTE_{20} , based on the centre of mass conservation model. Contour interval is 0.05 <i>mGal</i>	71
4.8	$SITE_{20}$, based on the centre of mass conservation model. Contour interval is 0.01 <i>mGal</i>	73
4.9	D_{20}^S (spherical correction to the Δg_{20}) in Canada. Contour interval is 0.01 <i>mGal</i>	74
5.1	Accuracy (error variance) performance of GRIM4-S4 model in different latitudes	78
5.2	Error power spectrum of the GRIM4-S4 model	80
5.3	Error covariance function of the spheroid of degree 20 along a meridian	81
5.4	Intersection of the integration domains	82
5.5	Integration over the area ϑ , for $\psi < \psi_0$	87
5.6	Correlation function of the residual geoid	87

Acknowledgments

I would like to express my sincere appreciation to Prof. Dr. Petr Vaníček for his useful ideas on the theory of precise geoid determination and his guidance in the "geoid meetings" and every time during this undertaking. I would like to appreciate Prof. Alfred Kleusberg for his ideas in testing the gravity data for the geoid computation. I would appreciate Prof. Zdeněk Martinec for his useful discussions in the theory of precise geoid determination.

A heartfelt word of thanks goes to my wife, Nasrin, and my children Sam and Sanas for their understandings.

Chapter 1

Introduction

The work presented in this dissertation is an outcome of a research contract done on the precise determination of the geoid by a working group to which the author was a member. During the past five years, the working group refined a theory for the precise determination of the geoid. This theory has been crystallized in a method called the "Stokes-Helmert Scheme" [Vaníček and Martinec, 1994]. The group employed the scheme to compile a precise geoid for Canada [Vaníček et al., 1995a]. The author's responsibility in the group was partly to look after the long wavelength part of the geoid: examining different global geopotential models and assessing their accuracies. A more detailed description of the author's contribution towards the geoid computation is given in Sec. (1.3).

In this introductory chapter, the whole picture of the geoid determination will be briefly explained in the section called the Stokes-Helmert scheme. Before this, the gravimetric determination of the geoid based on the Stokes theory and the Helmert method is explained.

1.1 Gravimetric Determination of the Geoid

In the gravimetric method, the geoidal height is obtained as a by-product of the third or mixed Boundary Value Problem (*BVP*) [Heiskanen and Moritz, 1981, p. 36] solved for the disturbing potential T ,

$$\nabla^2 T = 0. \quad (1.1)$$

This is the Laplace differential equation. Geoid is the boundary and

$$\Delta g = -\frac{\partial T}{\partial H} - \frac{2}{R}T \quad (1.2)$$

is the boundary condition—the spherical approximation of the "fundamental equation of physical geodesy" [Heiskanen and Moritz, 1981, eqn. (2-151f)], where Δg is the boundary value (the gravity anomaly referred to the geoid), R is the mean radius of the earth, and H is the orthometric height. The condition for T to satisfy the Laplace equation is to be a harmonic function. T is harmonic outside ($r > R$) the earth and

$$T = \frac{c}{r} + O\left(\frac{1}{r^3}\right) \quad \text{for } r \rightarrow \infty, \quad (1.3)$$

[Martinec, 1996]. The condition on the existence of the solution for T , is that Δg should not contain the first-degree harmonics [ibid]. This condition is satisfied in the geocentric coordinates system and the solution is given by the Stokes formula

$$T(\Omega) \doteq \frac{R}{4\pi} \int \int_{\epsilon} \Delta g(\Omega') S(\psi(\Omega, \Omega')) d\Omega', \quad (1.4)$$

where ϵ denotes the earth, Ω is the geocentric direction (with components of the geocentric latitude φ and longitude λ) defining position on the geoid of the computation point, and Ω' is the direction defining position of the integration point. $S(\psi)$ is the Stokes kernel, a function of ψ —the spherical distance between the two positions. The geoidal height N , referred to a geocentric reference ellipsoid, is then derived from T using the Bruns formula

$$N = \frac{T}{\gamma_0}, \quad (1.5)$$

where γ_0 is the normal gravity on the reference ellipsoid.

1.1.1 Helmert's method

There arise complications in the application of Stokes's formula to the real earth, because T is not a harmonic function everywhere on the geoid, as it is required by the Laplace equation and the gravity anomaly is not very well known on the geoid. These complications arise because of the existence of topographical masses above the geoid.

Condensation of the topographical masses along the plumb lines into a surface material layer on the geoid, based on Helmert's second condensation reduction method [Heiskanen and Moritz, 1981, Sec. (3-7)], creates a different gravity field called Helmert's gravity field with the following characteristics:

1. the isostatic equilibrium of the crust is mostly preserved, i.e., the replacement of the topography by the condensed layer does not significantly alter the equilibrium, and as such preserves the main features of the gravity field,
2. the Stokes formula is applicable in this field anywhere on and above the "geoid in Helmert's space" (Helmert co-geoid) without any complication, and
3. the transformation back to the real space (indirect effect) can be numerically evaluated.

Denoting the gravity potential of the earth by W and the Helmert gravity potential by W^h , one can write

$$W^h = W - V, \quad (1.6)$$

where V is the change in the gravity potential due to the condensation. In analogy to the earth gravity field, the Helmert gravity field is characterized by the Helmert disturbing potential T^h . Unlike T , T^h is a harmonic function outside the Helmert co-geoid, since there remain no attracting masses outside the co-geoid in the Helmert field, thus it satisfies the Laplace differential equation

$$\nabla^2 T^h = 0. \quad (1.7)$$

This implies that the Stokes formula, as a solution to the Laplace equation will determine the T^h outside the co-geoid. The Boundary here is the equipotential surface of the Helmert field counterpart to the geoid in the real field. It is the Helmert co-geoid, and the boundary condition is similar to eqn. (1.2), as

$$\Delta g^h = -\frac{\partial T^h}{\partial H} - \frac{2}{R}T^h, \quad (1.8)$$

where Δg^h is the boundary value (Helmert's gravity anomaly referred to the co-geoid).

The Helmert co-geoid departs from the geoid by at most a few metres [Heiskanen and Moritz, 1981, Sec. (3-7)]. It is the Helmert condensation indirect effect—called the Primary Indirect Topographical Effect (*PITE*). It can be numerically evaluated since the difference of the Helmert model earth from the real earth is mathematically described.

1.2 The Stokes-Helmert Scheme

There are researchers who have given thoughts to the precise determination of the geoid. Wichiencharoen [1982] by computing indirect effect on the geoid, Wang and Rapp [1990] by computing the terrain effect on the geoid, and Heck [1992] by considering the Helmert second condensation method. In the Stokes-Helmert scheme, presented herein, a thorough investigation of the Helmert condensation idea for a precise determination of the geoid was conducted by Vaníček and Martinec [1994]. In this scheme the BVP is first solved in the Helmert space. The solution (Helmert co-geoid) is then transformed back into the real space (the geoid) by precise evaluation of the *PITE*.

The main goal of the Stokes-Helmert scheme is to provide a theory accurate enough for computing the geoid, as the final product, to the accuracy of 1 *cm* in a distance of 100 *km* or 10 *cm* in a regional extent. This goal will be achieved if all the corrections and transformations of the observed gravity anomaly to the Helmert space are carried

out to the accuracy of $10 \mu Gal$ [Vaníček and Martinec, 1994]. This in turn implies that any effect on gravity, during the transformations, larger than $10 \mu Gal$ has to be investigated and taken into account.

The scheme can be visualized from different perspectives. In one view it can be described in the following four steps:

1. Transforming the "observed gravity anomaly" (Δg_t) on the earth surface into Helmert's gravity anomaly (Δg_t^h), referred to the same surface.
2. Downward continuing of Δg_t^h to the Helmert co-geoid.
3. Solving the BVP in the Helmert space, i.e., solving for the Helmert co-geoid using the generalized Stokes formula.
4. Transforming the co-geoid to the geoid by evaluating the *PITE*.

To carry out the transformations, the mathematical descriptions of the differences, both in gravity and potential, between the actual gravity field and the Helmert field are required. The difference in the potential (V ; eqn. (1.6)), called "residual topographical potential" is given by

$$V = V^t - V^c, \quad (1.9)$$

where V^t is the gravitational potential of the topography and V^c is the gravitational potential of the condensation layer. Assuming ρ as the density of the topography and σ as the surface density of the condensed topography, the two potentials are given by the Newton integral, as

$$V^t = G \int \int \int_{\tau} \frac{\rho}{\ell} d\tau, \quad (1.10)$$

$$V^c = G \int \int_{\zeta} \frac{\sigma}{\ell} d\zeta, \quad (1.11)$$

where τ and ς characterize the volume of the topography and the surface of the geoid respectively. G is the gravitational constant and ℓ is the spatial distance between the computation point and the integration point. These potentials will be elaborated in Sec. (2.4.1).

The potential V is the tool for the transformations from the actual space to the Helmert space and back to the actual space. As it is understood from the three equations above, it is the mass density difference between the topography and its condensation that is required for the evaluation of the potential V . As the first approximation, the topographical density is modelled as the lateral density distribution within the topography. Martinec and Vaníček [1994b] show that an approximate knowledge of the distribution (good to about 5%) would ensure the required accuracy in the evaluation of V (and the gravity transformations).

Based on the potential V , the four steps above can be further explained as follows

- Step 1: Δg_t is computed from the observed gravity g_t by subtracting from it the normal gravity γ_t on the telluroid,

$$\Delta g_t = g_t - \gamma_t, \quad (1.12)$$

where γ_t is obtained from normal gravity on the reference ellipsoid (γ_0) using Taylor series expansion of the normal gravity along the normal direction (n),

$$\begin{aligned} \gamma_t &= \gamma_0 + \left. \frac{\partial \gamma}{\partial n} \right|_0 H^N + \frac{1}{2} \left. \frac{\partial^2 \gamma}{\partial n^2} \right|_0 (H^N)^2 + \dots \\ &\doteq \gamma_0 + \mathit{grad} \gamma|_0 H^N, \end{aligned} \quad (1.13)$$

where H^N is the normal height [Vaníček and Krakiwsky, 1986, Sec. (16.4)]. The effect of the neglected terms in the Taylor series expansion is smaller than $1 \mu Gal$ at a maximum elevation of 4000 m [Vaníček and Martinec, 1994]. Denoting the term $(\mathit{grad} \gamma|_0 H^N)$ as the sum of the three terms:

$$\mathit{grad} \gamma|_0 H^N = -0.3086 (mGal/m) H^N - LE - AE; \quad (1.14)$$

and comparing with the previous equation, yields

$$\begin{aligned} LE &= \left(-\frac{\partial\gamma}{\partial n}\Big|_0 - 0.3086 \right) H^N \\ AE &= -\frac{1}{2} \frac{\partial^2\gamma}{\partial n^2}\Big|_0 (H^N)^2, \end{aligned} \quad (1.15)$$

where -0.3086 is the global mean gradient of normal gravity, LE is the "Latitude Effect" and AE is the "Altitude Effect" on the normal gravity. The normal height H^N is compared to the Helmert orthometric height H by the equation

$$H = H^N \left(\frac{\gamma_0 - 0.1543 H}{g_t + 0.0424 H} \right). \quad (1.16)$$

This equation is worked out from the definitions of the normal and orthometric height systems [ibid]. The difference between orthometric and normal heights defines the separation between quasigeoid and the geoid. The separation is negligible at sea but may reach to a maximum of 2 m in mountains. Assuming the maximum value, the two heights can be used interchangeably in the corrective terms LE and AE , as was approximated by Vaníček and Martinec [1994, eqns. (22) and (37)],

$$\begin{aligned} LE &\doteq \left(\frac{2}{a} \gamma_0(\phi) + 2 \omega^2 - 0.3086 \right) H \\ AE &\doteq -4.81 \times 10^{-8} (mGal/m^2) H^2, \end{aligned} \quad (1.17)$$

where ω is the angular velocity of the earth spin, and ϕ is the latitude.

The Δg_t is then transformed to Helmert's space by applying the residual topographical effect on gravity, i.e., by constructing Helmert's gravity anomaly Δg_t^h . This effect is the vertical gradient of potential V evaluated on the topography. It is called the Direct Topographical Effect on gravity— DTE . Its value on the topography is derived as

$$DTE_t = - \frac{\partial V}{\partial H}\Big|_t. \quad (1.18)$$

A similar effect on gravity arises from the condensation of the atmosphere on the geoid. It is called the Direct Atmospheric Effect on gravity— DAE , and the value on topography is given as

$$DAE_t = - \left. \frac{\partial V^a}{\partial H} \right|_t, \quad (1.19)$$

where V^a is the residual atmospheric potential, defined in much the same way as the residual topographical potential. A combined topographical and atmospheric residual potential may be denoted as

$$V^* = V + V^a. \quad (1.20)$$

Hence,

$$\Delta g_t^h = \Delta g_t - DTE_t - DAE_t = \Delta g_t + \left. \frac{\partial V^*}{\partial H} \right|_t. \quad (1.21)$$

In practice, DTE_t and DAE_t , being vertical gradients, are approximated by the geocentric radial (r) derivatives of V and V^a . The error committed by the approximation is much less than $10 \mu Gal$.

- Step 2: Δg_t^h is reduced downward to the geoid along the plumb line. This requires the vertical gradient of Helmert gravity to be known, which it is not. In practice, thus, an alternative approach is used [Vaníček et al., 1996]. In this approach the Helmert gravity anomaly on the geoid is determined from the anomalies on the topography, using inverse Poisson's integral transformation [Heiskanen and Moritz, 1981, eqn. (1-89)]. The downward reduction can be written as

$$\Delta g_g^h = \Delta g_t^h + D\Delta g^h, \quad (1.22)$$

where $D\Delta g^h$ is called the downward continuation of Δg^h .

For the precise evaluation of the geoid, Δg_g^h is further reduced to the co-geoid (the boundary) to which the sought Helmert's disturbing potential T^h is also

referred. For this, a reduction called the Secondary Indirect Topographical and atmospheric Effect on gravity—*SITE*, evaluated on the geoid,

$$SITE \doteq \frac{2}{R} V_g^*, \quad (1.23)$$

is applied [Vaníček and Martinec, 1994, eqn. (40)]. V_g^* here is the potential V^* evaluated on the geoid. The *SITE* may account for up to 300 μGal . It is evaluated using spherical approximation, without deteriorating the required accuracy. The Helmert anomaly reduced by the corrections discussed so far is denoted by Δg_h^h .

The Stokes formula, to be used in the next step, is based on the approximate (spherical approximation) boundary condition eqn. (1.8). To correct for this approximation, another correction, denoted by D^S ,

$$D^S \doteq \frac{2}{R} \left[\frac{a \omega^2}{\gamma_0(\phi)} + f \left(-\frac{1}{3} + \cos(2\phi) \right) \right] T_g^h, \quad (1.24)$$

is needed [Vaníček and Martinec, 1994, eqn. (29)]. The D^S correction may reach up to 160 μGal . It may be evaluated using a high resolution (e.g., 360/360) geopotential model, taking T for the Helmert disturbing potential T^h .

Assembling all the corrections into one equation yields

$$\begin{aligned} \Delta g_h^{h*} &= \Delta g_g^h + SITE + D^S \\ &= g_t - (\gamma_0 - 0.3086 H - LE - AE) + \left. \frac{\partial V^*}{\partial H} \right|_t \\ &\quad + D \Delta g^h + \frac{2}{R} V_g^* + D^S, \end{aligned} \quad (1.25)$$

where Δg_h^{h*} is the anomaly to be used in the Stokes integral.

- Step 3: The Stokes formula is now employed to compute the Helmert co-geoid from Δg_h^{h*} . There are, however, some practical considerations involved here. They will be further discussed in Sec. (3.1).

- Step 4: The computed co-geoid is then corrected for the indirect effect due to the transformations from real space to the Helmert space. It is a combination of the Primary Indirect Topographical (*PITE*) and Atmospheric (*PIAE*) Effects on the geoid, [Vaníček and Martinec, 1994],

$$PITE + PIAE = \frac{V_g^*}{\gamma_0}, \quad (1.26)$$

The *PITE* amounts to at most some 1-2 *m*. It should be evaluated using the spherical approximation of the geoid, versus the planar approximation used in common practice. This better approximation improves the geoid by as much as 0.5 *m* [Martinec and Vaníček, 1994a]. Assuming a laterally varying density distribution for the topography, compared to the constant density $\rho_0 = 2.67 \text{ g cm}^{-3}$, further improves the *PITE*, i.e., to the accuracy of 1 *cm* [Martinec, 1993].

Helmert's condensation reductions *DTE* and *DAE* do have some impact on the physical parameters of the earth. They may either change, even though slightly, the mass or the location of the centre of mass of the earth, depending on the formulation of the surface layer density [Martinec, 1993]. As a result, the Helmert co-geoid represents a "model earth" which is slightly different in mass or in the centre of mass. But the changes are compensated when transforming the co-geoid to the geoid by applying the corresponding *PITE* and *PIAE* corrections.

1.2.1 Generalized Stokes-Helmert Scheme

Because of the sparse gravity data on the earth surface, the gravimetric method alone cannot be used in determination of the whole spectrum of the geoid. A combined method, using two types of data: extraterrestrial (satellite); and terrestrial (surface) data, is employed. The first data, Sec. (2.2), are homogeneous and available in low-frequency band, since satellites barely sense the earth gravity field in high-frequency

band which is strongly attenuated at the satellite altitude. The second data, surface gravity anomalies, are reliable only in the high-frequency band, since the gravity observations on the earth surface are only distributed in a local or regional extent. Both kinds of data carry information about the same gravity field of the earth. For a proper use of the data, in the geoid determination, one should assign proper statistical weights to each data type. This is not a trivial task. One way to take advantage of both data is to define a clear cut frequency delimitation between the data types to avoid correlation [Vaníček et al., 1987]. The degree/order 20/20 potential term is shown to be a reasonable break [Vaníček and Krakiwsky, 1986, Ch. 23], since the terms up to degree 20 are determined to a good accuracy from the analysis of satellite orbits. Hence, the geoid is determined in two parts.

The long wavelength part (the main features up to 20/20) is determined from a satellite-derived geopotential field, Sec. (2.3). For the reasons discussed in the next paragraph, this part of the geoid is called the higher-degree reference spheroid, and the field originating the spheroid is called the higher-degree reference field.

The remaining part (the short wavelength features), called the residual (high-frequency) geoid, is determined from terrestrial gravity, using spheroidal Stokes's integral [Vaníček and Krakiwsky, 1986, eqn. (24.28)], employing spheroidal kernel of degree $L = 20$. The integral, as a high-pass filter, automatically cuts off the low-frequency contribution of the surface data and refers the residual geoid exactly to the higher-degree spheroid. Thus, the spheroid plays the role of a reference surface—the reference spheroid.

The spheroidal Stokes's integral, as with the original Stokes's integral, has to be extended over the entire earth, even though the contribution of the "distant" gravities to this integral is minimal. For the lack of gravity observations in remote areas, the spheroidal kernel is modified in a way that minimizes the contribution of the distant gravities [Vaníček and Sjöberg, 1991]. Then, the integral is called the "generalized Stokes integral". More on the modification theory is found in Sec. (3.1).

The (minimum) contribution of the "distant" gravities, called the "truncation error" is estimated separately, using a high resolution geopotential model, Sec. (3.3).

Let us complete this section by briefly explaining another generalized technique for the precise determination of the geoid. Sideris and She [1995] applied a technique to compute a high-resolution geoid for Canada. In their approach, a higher-degree (360) spheroid is first derived from a global geopotential model, e.g., OSU91A [Rapp et al., 1991]. The spheroid is then used as a reference surface for the residual geoid computed from the Stokes integral (eqns. (1.4) and (1.5)) employing the original Stokes's kernel, and the terrestrial gravity anomalies reduced by the geopotential field. The original kernel is used in order to correct for the deficiency in the geopotential model by the terrestrial data. For the numerical evaluation, the (convolution) Stokes integral and other terms such as the indirect effects and the accuracy estimate of the geoid, were treated using the Fast Fourier Transform [Schwarz et al., 1990; Forsberg and Sideris, 1993; Sideris and Li, 1993].

1.2.2 Flowchart of the Operations

In practice, surface gravity data are available in the form of mean anomalies, representing $5' \times 5'$, $1^\circ \times 1^\circ$ or even larger geographical cells, while satellite data are given in the form of potential coefficients. Hence, the numerical evaluation of the geoid involves mean anomalies.

In the absence of a homogeneous and properly densified network of point gravity anomalies (with known orthometric heights), a grid of mean anomalies, derived from point values, may represent the gravity field better. Averaging the "observed" point anomalies in a geographic cell suppresses the observational errors in data collection, in the meantime, however, smoothes the gravity field. The degree of smoothness depends on the area of the cell. Any quantity of the gravity field, e.g., the geoid, derived from mean anomalies is a smoothed model of the reality. Practically, in geoid determination, the mean anomalies associated with smaller cells eliminate only the

local surface irregularities of the gravity field without affecting the geoid solution.

A flowchart of the operations required at each step of the geoid evaluation, an improved version compared to Vaníček et al. [1995a], is shown in Fig. 1.1. In this diagram, the circles stand for input data and rectangles denote computational blocks.

The list of input (I) data sets required is:

- I1 - the first 20/20 potential coefficients of a satellite-derived field;
- I2 - $5' \times 5'$ mean incomplete Bouguer anomalies;
- I3 - global topographical height model (given by harmonic coefficients);
- I4 - local detailed topography, such as $1 \text{ km} \times 1 \text{ km}$, and $5' \times 5'$ topography;
- I5 - global atmospheric density model;
- I6 - normal gravity field and the corresponding reference ellipsoid;
- I7 - combined (satellite and terrestrial) global geopotential field of high resolution (e.g., 360/360);
- I8 - topographical density model.

Operations required to evaluate the Helmert higher-degree reference spheroid (N_{20}^h) are shown in the sequence of boxes on the left hand side of the Fig. 1.1 and the operations associated with the residual Helmert co-geoid are shown on the right hand side. The operations in the dash-line blocks are so far only proposed, and have not been implemented yet.

1.3 Topics of the Investigation

Contributions of this research towards the geoid determination theory are mostly in the area of the reference field in the Helmert space, i.e., all the operational blocks in

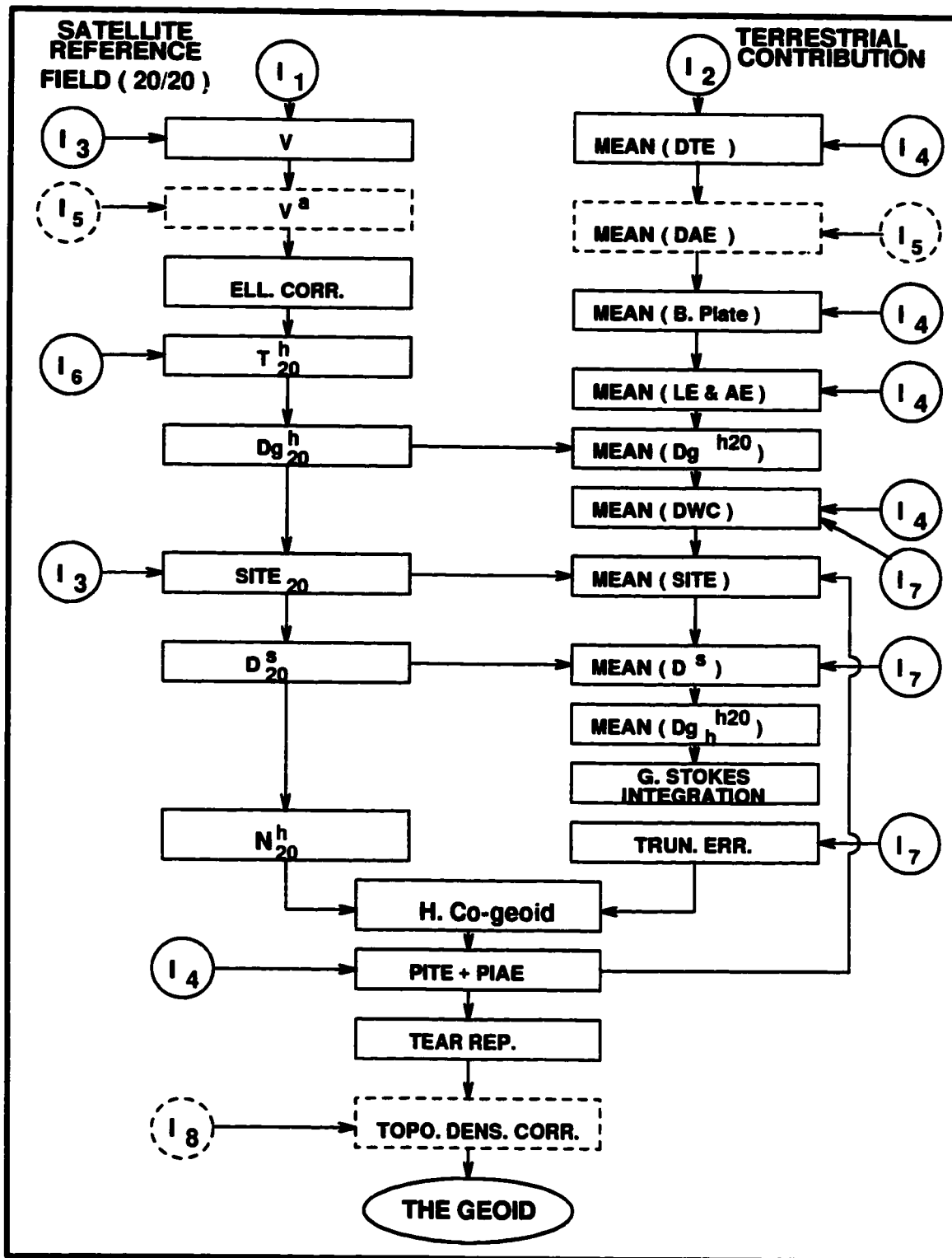


Figure 1.1: Flowchart of the Operations in the Stokes-Helmert Scheme

the left column of the diagramme (Fig. 1.1) except for the atmospheric condensation corrections.

The most appropriate satellite gravity field was selected as the reference gravity potential field (20/20), after investigating and examining the accuracy performance of different global geopotential models of the GEM-T and GRIM4 families, Sec. (4.1.1). For the reduction of the selected reference field on the geoid, the satellite-derived potential coefficients were corrected for the ellipticity of the geoid ("ellipsoidal approximation"), Sec. (2.5). The desirability of an even better approximation (compared to the ellipsoidal approximation) was studied; it was concluded that the ellipsoidal approximation is good enough for the 1 *cm* accuracy.

The reference residual topographical potential V_{20} was formulated in a harmonic series expansion, Sec. (2.4.2), in terms of a series of squared-topography harmonics, derived from the topography model TUG87 [Wieser, 1987]. The reference field was then Helmertized by applying the potential V_{20} , Sec. (2.4.2). The Helmert reference potential was then reduced to the Helmert disturbing potential (T_{20}^h) by subtracting the normal potential induced by the GRS-80 reference ellipsoid, Sec. (2.4.2). The reference gravity anomaly Δg_{20}^h , shown by Dg_{20}^h in the Fig. 1.1, was formulated, Sec. (2.4.2). The reference spherical correction D_{20}^S , Sec. (2.5), derived from the Helmert disturbing potential, and the $SITE_{20}$, Sec. (2.4.2), all derived from V_{20} , were then generated. These fields are to be subtracted, in the sequences shown in Fig. 1.1, from the mean "observed" values to eliminate the long wavelength components. Finally, the high-frequency Δg_h^{h20} , shown by Dg_h^{h20} in the Fig. 1.1, is obtained. The Helmert reference spheroid N_{20}^h was derived from T_{20}^h . It constitutes the long wavelength component of the Helmert co-geoid.

Improvements of the high-frequency Stokes's integrator were implemented and the truncation error of the integrator has been formulated and estimated. The original software (integrator) had been designed to accept either point or mean gravity anomalies of different resolutions as the input data and to predict point anomalies

wherever necessary. These features caused an unnecessary complexity of the software and slowed down the computation. With the availability of the mean anomalies of the $5' \times 5'$ resolution throughout Canada, the software was streamlined. As a result, the CPU time required for running the software was considerably reduced. With this faster software, an optimum size of the inner zone was studied. The truncation error of the integrator was estimated using different high resolution geopotential models to investigate an optimum model.

The software developed to carry out the research herein described is as follows:

sfroid.f - to evaluate a higher-degree spheroid, employing "spherical", "ellipsoidal", and "higher-degree" approximations, using a given geopotential model. The ellipsoidal correction (approximation) to the spheroid, using eqn. (2.99), and the higher-degree correction, compared to the ellipsoidal correction, considering eqn. (4.3), are numerically evaluated.

sfrod3.f - to evaluate a higher-degree spheroid, eqn. (2.101), and the accuracy estimate of the spheroid due to the errors of the geopotential model.

sfrod4.f - to evaluate the error variance, Fig. 5.1, error power spectrum of a geopotential model, Fig. 5.2, and error covariance of a satellite-derived spheroid, Fig. 5.3.

hgrvan.f - to evaluate the reference quantities: V_{20} (eqn. (2.69)), Δg_{20} (eqn. (2.38)), DTE (eqn. (2.86)), Δg_{20}^h (eqn. (2.87)), $SITE_{20}$ (eqn. (2.90)), and the ellipsoidal correction to the gravity anomaly (eqn. (2.100)), using a geopotential model and a topographical model.

sphelm.f - to evaluate the V_{20} and the Helmert spheroid N_{20}^h , eqn. (2.102).

dsterm.f - to evaluate the D^S term, eqn. (2.103), and its accuracy, using a combined geopotential model.

trnerr.f - to evaluate the truncation error, eqn. (3.11), of the generalized Stokes integral and the accuracy of the truncation error. This program was originally written as `zbysto.f` by Martinec [1993]. The program is modified by different input option. Some features such as profile option and error estimation, were added to the program.

hdelgtr.f - to compute high-frequency mean Δg_t^h from mean Bouguer anomaly [Heiskanen and Moritz, 1981, eqn. (3-19)], reduced by the reference gravity anomaly on topography, and corrected for some mean anomalies discussed in Sec. (3.2.1).

avrage.f - to average a high resolution mean anomalies, e.g., $5' \times 5'$, to a smother mean anomalies, e.g., $1^\circ \times 1^\circ$.

GIN95.f - to evaluate the generalized Stokes integral, Sec. (3.1), using the integration cap of radius $\psi_0 = 6^\circ$. This is a new version of the original GIN program described in [Gang Chang et al., 1986; Vaníček et al., 1987].

crltion.f - to evaluate the error correlation, as a function of spherical distance, between residual geoidal heights, eqn. (5.32).

chnseq.f - to change the sequence (order) of data in a sequential file to the sequence required by the GIN95.f routine. As a requirement with GIN95.f, an input file of gravity anomalies, assigned with latitudes and longitudes, has to be ordered for latitudes from south to north, and for longitudes from west to east.

Chapter 2

Higher-degree Reference Field in the Helmert Space

2.1 Introduction

2.1.1 Actual Gravity Field of the Earth

Potential

The actual gravity potential of the earth W is the sum of the gravitational potential (W_g) and the centrifugal potential (W_c),

$$W = W_g + W_c, \quad (2.1)$$

In satellite dynamics applications the gravitational potential, a harmonic function outside the earth, is expressed as an infinite series of harmonic functions, formulated in a geocentric coordinates system as

$$W_g(r, \Omega) = \frac{GM}{r} - \frac{GM}{r} \sum_{n=2}^{\infty} \left(\frac{a}{r}\right)^n W_n(\Omega), \quad (2.2)$$

where r is the geocentric radius, Ω is the geocentric direction, G is the gravitational constant, M is the mass of the earth, a is the radius of the Brillouin sphere (a

geocentric sphere with minimal radius enclosing the whole earth), W_n are the surface spherical harmonics,

$$\forall n \geq 2 \quad W_n(\Omega) = \sum_{m=0}^n [\overline{W}_{nm}^C \overline{Y}_{nm}^C(\Omega) + \overline{W}_{nm}^S \overline{Y}_{nm}^S(\Omega)], \quad (2.3)$$

where \overline{W}_{nm}^C and \overline{W}_{nm}^S are the unitless and normalized potential coefficients, \overline{Y}_{nm}^C and \overline{Y}_{nm}^S are the normalized spherical harmonics of degree n and order m , [Heiskanen and Moritz, 1981, eqns. (1-73)],

$$\begin{aligned} \overline{Y}_n^C &= \sqrt{2n+1} P_n(\sin \varphi) & m=0, \\ \begin{pmatrix} \overline{Y}_{nm}^C \\ \overline{Y}_{nm}^S \end{pmatrix} &= \sqrt{2(2n+1) \frac{(n-m)!}{(n+m)!}} \begin{pmatrix} \cos m\lambda \\ \sin m\lambda \end{pmatrix} P_{nm}(\sin \varphi) & m \neq 0, \end{aligned} \quad (2.4)$$

where P_n are the Legendre polynomials and P_{nm} are the associated Legendre functions.

Gravity

The actual gravity g , the magnitude of the gravity vector, of the earth is the absolute value of the gradient of the actual potential. The gravity vector defines the vertical (H) direction, hence, g equals the vertical gradient of the potential with negative sign [Vaníček and Krakiwsky, 1986],

$$g = |\nabla W| = -\frac{\partial W}{\partial H}. \quad (2.5)$$

2.1.2 Anomalous Gravity Field of the Earth

Disturbing Potential

Since the variation of the actual gravity potential (W) of the earth is very small compared to its magnitude, the bulk of the potential is expressed mathematically in such a way that the remaining part, called the disturbing or anomalous potential

T , is small and thus easily handled using even linear approximations. The closest model potential to the actual potential, yet easy to handle mathematically, is the normal potential U generated by the "normal body" (the reference ellipsoid) of the earth with the mass equal (ideally) to the mass of the earth, co-axial with the earth, and spinning with the same velocity as the earth. The actual potential can, then, be written as

$$W = U + T. \quad (2.6)$$

The normal potential is expressed as

$$U = U_g + W_c. \quad (2.7)$$

where U_g is the gravitational part of the normal potential and W_c is the centrifugal potential of the earth. U_g is a harmonic function and can be expanded, in the geocentric coordinates system, in an infinite series of harmonic functions [Heiskanen and Moritz, 1981, eqn. (2-88)], as

$$U_g(r, \varphi) = \frac{GM^*}{r} - \frac{GM^*}{r} \sum_{n=2,4,\dots}^{\infty} \left(\frac{a^*}{r}\right)^n J_n^N P_n(\sin \varphi), \quad (2.8)$$

based on the four "Stokes's constants" a^* , b^* , M^* , and ω . J_n^N are the normal potential coefficients [ibid, eqn. (2-92)],

$$J_n^N = (-1)^{\frac{n}{2}+1} \frac{3e^n}{(n+1)(n+3)} \left(1 - 0.5n + 2.5n \frac{J_2^N}{e^2}\right), \quad (2.9)$$

defined only for the even degrees n . All of the coefficients corresponding to the odd degrees are zero. In this formula e is the first eccentricity, J_2^N is the second degree coefficient, representing the flattening of the normal ellipsoid. It is determined from the four given constants [Bomford, 1971, P. (479)]. It is useful to mention here that the coefficients J_n^N decrease to zero for $n > 8$ [Vaníček and Kleusberg, 1987].

The normal gravity γ , the magnitude of the normal gravity vector, in analogy to the actual gravity, is given as the derivative of the normal potential along the normal

direction (n). It can be also approximated to a good accuracy by the derivative along the H ,

$$\gamma = |\nabla U| \doteq -\frac{\partial U}{\partial H}. \quad (2.10)$$

The most recent international formula for the normal gravity, as part of GRS-80, is given by Moritz [1980].

Considering eqns. (2.7), (2.1), and (2.6), we obtain T as

$$T(r, \Omega) = W_g(r, \Omega) - U_g(r, \Omega). \quad (2.11)$$

T is about 5 orders of magnitude smaller than W_g [Vaníček and Martinec, 1994], and it is a harmonic function outside the earth, since both W_g and U_g are harmonic functions. Considering eqns. (2.2) and (2.8), the spectral form of T is obtained as

$$T(r, \Omega) = \frac{GM}{r} T_0 - \frac{GM}{r} \sum_{n=2}^{\infty} \left(\frac{a}{r}\right)^n T_n(\Omega), \quad (2.12)$$

where T_0 , the 0-th degree harmonic, goes to zero for $M^* = M$, T_n are the disturbing potential surface harmonics,

$$\forall n \geq 2 \quad T_n(\Omega) = \sum_{m=0}^n [\bar{T}_{nm}^C \bar{Y}_{nm}^C(\Omega) + \bar{T}_{nm}^S \bar{Y}_{nm}^S(\Omega)]. \quad (2.13)$$

\bar{T}_{nm}^C and \bar{T}_{nm}^S are the disturbing potential coefficients. In the derivation of T , it was assumed that both eqns. (2.2) and (2.8) are referred to the same coordinates system, i.e., the reference ellipsoid is geocentric (the mean earth ellipsoid). For a non-geocentric ellipsoid, first-degree harmonics appear in the spectral form of T [Heiskanen and Moritz, 1981, eqn. (2-176a)].

Gravity Anomaly

The gravity anomaly Δg , as a function of T , is defined by the "fundamental equation of physical geodesy" [Heiskanen and Moritz, 1981, eqn. (2-148)]:

$$\Delta g = -\frac{\partial T}{\partial H} + \frac{1}{\gamma} \frac{\partial \gamma}{\partial H} T, \quad (2.14)$$

or in terms of potential U (see eqn. (2.10))

$$\Delta g = -\frac{\partial T}{\partial H} - \frac{1}{\gamma} \frac{\partial^2 U}{\partial H^2} T. \quad (2.15)$$

The spherical approximation of the equation [Heiskanen and Moritz, 1981, eqn. (2-154)], reads

$$\Delta g = -\frac{\partial T}{\partial r} - \frac{2}{r} T. \quad (2.16)$$

Substituting for T (from eqn. (2.12)) and its partial derivative with respect to the geocentric radius r ,

$$\frac{\partial T}{\partial r} = -\frac{GM}{r^2} T_0 + \frac{GM}{r^2} \sum_{n=2}^{\infty} (n+1) \left(\frac{a}{r}\right)^n T_n(\Omega), \quad (2.17)$$

into eqn. (2.16) yields

$$\Delta g(r, \Omega) = \frac{GM}{r^2} T_0 + \frac{GM}{r^2} \sum_{n=2}^{\infty} (n-1) \left(\frac{a}{r}\right)^n T_n(\Omega). \quad (2.18)$$

The sources of error in the spherical approximation of Δg are the following approximations,

$$\frac{\partial T}{\partial H} \approx \frac{\partial T}{\partial r}, \quad \frac{1}{\gamma} \frac{\partial^2 U}{\partial H^2} \approx \frac{2}{r}. \quad (2.19)$$

The error caused by the approximation of the vertical derivative of T with the radial derivative is due to the difference between geodetic and geocentric latitudes. It is of a relative order of $5.5 \times 10^{-6} \sin^2 2\phi$ [Vaníček and Martinec, 1994]. Assuming 300 *mGal* as maximum value for the vertical derivative of T , the maximum error is about 2 μGal which is negligible. A large error comes from the second approximation.

For a rigorous evaluation of Δg on the geoid, the second error must be eliminated. This is done by considering the D^S term (see eqn. (1.24)) in the eqn. (2.15). This term is defined for T^h by Vaníček and Martinec [1994, eqn. 27]; in the real space it reads

$$D^S = \left(\frac{1}{\gamma_0} \frac{\partial^2 U}{\partial H^2} \Big|_0 - \frac{2}{R} \right) T_g, \quad (2.20)$$

where T_g is the disturbing potential on the geoid and R is the mean radius of the earth

$$R = (a^{*2} b^*)^{\frac{1}{3}}, \quad (2.21)$$

and

$$\frac{1}{\gamma_0} \left. \frac{\partial^2 U}{\partial H^2} \right|_0 \doteq \frac{2}{a^*} \left[1 + \frac{\omega^2 a^*}{\gamma_0} + f^* \cos 2\phi + \frac{f^{*2}}{16} (11 + 12 \cos 2\phi + \cos 4\phi) \right]. \quad (2.22)$$

This equation, as a power series in the flattening f^* of the reference ellipsoid, was derived by Vaníček and Martinec [1994, eqn. 22]. Denoting

$$D^S = D(\phi) T_g, \quad (2.23)$$

from eqn. (2.15) we get

$$\Delta g = - \left. \frac{\partial T}{\partial r} \right|_g - \frac{2}{R} T_g - D(\phi) T_g. \quad (2.24)$$

Substituting for T_g , and for its radial derivative from their harmonic series, one obtains the rigorous harmonic expansion of the gravity anomaly on the geoid, as

$$\Delta g(\Omega) = \frac{GM}{r_g^2} \Delta g_0(\Omega) + \frac{GM}{r_g^2} \sum_{n=2}^{\infty} \left(\frac{a}{r_g} \right)^n \Delta g_n(\Omega), \quad (2.25)$$

where

$$\begin{aligned} \Delta g_0(\Omega) &= (1 - r_g D(\phi)) T_0 \\ \forall n \geq 2 \quad \Delta g_n(\Omega) &= (n - 1 - r_g D(\phi)) T_n(\Omega), \end{aligned} \quad (2.26)$$

and

$$r_g = r_g(\Omega) \quad (2.27)$$

is the geocentric radius of the geoid.

Geoidal Height

The geoidal height N is derived from the disturbing potential T (evaluated on the geoid, T_g) using Bruns second formula

$$N(\Omega) = \frac{T_g(\Omega)}{\gamma_0}. \quad (2.28)$$

This formula is obtained from the Taylor series expansion (the linear part) of the normal potential U on the reference ellipsoid, assuming $U_0 = W_0$:

$$U_g = U_0 + \left. \frac{\partial U}{\partial H} \right|_0 N + \frac{1}{2} \left. \frac{\partial^2 U}{\partial H^2} \right|_0 N^2 + \dots, \quad (2.29)$$

where W_0 is potential on the geoid. For the condition $U_0 \neq W_0$, a correction to the Taylor series must be applied [Heiskanen and Moritz, 1981, eqn. (2-178)]. Considering eqn. (2.10), and after some manipulations of the series, we get

$$N(\Omega) = \frac{T_g(\Omega)}{\gamma_0} + \frac{1}{2\gamma_0} \left. \frac{\partial \gamma}{\partial H} \right|_0 N^2 + \dots \quad (2.30)$$

Approximating $\gamma_0 = 10^6 \text{ mGal}$, $\frac{\partial \gamma}{\partial H} = 0.3 \text{ mGal/m}$, the second degree (in N) term, a correction to the Bruns formula, is in the order of $1.5 \times 10^{-7} N^2$, which for $|N| = 100 \text{ m}$ it is less than 1.5 mm . For a centimetre geoid, this correction is negligible [Vaníček and Martinec, 1994].

2.2 Satellite-derived Gravity Field of the Earth

The long wavelength features of the earth gravity field can be determined from orbit perturbations analysis of low orbiting satellites. In the satellite altitude, the high frequency features of the earth gravity field are attenuated, i.e., the amplitudes of the features of degree 20 and higher reduces by more than 40% [Vaníček and Krakiwsky, 1986, Sec. (23-4)]. The gravity field derived this way is called satellite-derived geopotential model. The model is usually given by a series of spherical harmonic functions with derived coefficients.

A recently derived family of geopotential models by "Deutsches Geodätisches Forschungsinstitut, Abt.I" (DGFI) is called the GRIM4 models [Schwintzer et al., 1991]. These models had been originally designed for the orbit restitution of the ERS-1 altimeter satellite to the accuracy of one decimetre (in the radial direction). GRIM4-S4 is a purely satellite-derived model complete to 60/60. Observations to 31 satellites with different inclination angles, distributed between 0° and 90°, were used to derive the model. The observations (satellite tracking data) comprise of optical observations to satellites (1962-1971), satellite laser ranging since 1971, and Doppler range rates since 1978. These data reveal gravitational orbit perturbations of satellites to be composed of wide band spectrum of variations.

A single satellite in an inclined orbit is subject only to some wavelengths of the earth gravitation, so that the relative amplitudes of individual periodic components contained in the satellite data are mainly dependent on the satellite inclination. This means that the relative power spectrum of the data changes with the inclination. As a result, only a combination of the tracking data obtained from an assembly of satellites with different inclinations, distributed between 0 to 90 degrees, provides a complete picture of the gravity field. This has been the case with the satellites used in the derivation of the GRIM4 models.

An analysis of sensitivity of the geopotential coefficients of GRIM4-S1 model to orbital information was conducted by Schwintzer et al. [1991]. It has shown that the contribution of the orbital perturbation information to the potential coefficients decreases, from 100% to 0%, by increasing the degree and order of the coefficients. The situation is quite opposite for the a priori stochastic information, based on the Kaula rule, imposed on the coefficients. That is, as the degree and order of the coefficients increase, they become more dependent on the a priori information than on the real orbital information. However, the coefficients of degree 0 up to 25/25 are shown to be well determined—being more than 50% dependent on the orbit perturbation data.

In the adjustment of the satellite tracking observations, the external gravity potential of the earth is formulated as a series of spherical harmonics in the coordinates system defined by the tracking station network. In order to prevent aliasing effects, the upper bound of the series is selected as high (in frequency) as to exhaust all periodicities that may exist in the observations. By constraining the coordinates system to coincide with a geocentric system, the adjustment yields a field lacking the first degree harmonics. The low frequency part (of degree less or equal to L) of the satellite field is then formulated as

$$\hat{W}_L(r, \Omega) = \frac{G\hat{M}}{r}\hat{W}_0 - \frac{G\hat{M}}{r} \sum_{n=2}^L \left(\frac{\hat{a}}{r}\right)^n \hat{W}_n(\Omega), \quad (2.31)$$

where \hat{M} is mass of the earth plus the mass of the atmosphere obtained from the satellite observations, \hat{W}_0 , the zero-th degree coefficient, equals to unity if the mass is fixed to the initial value (\hat{M}) prior to the adjustment. \hat{a} is a pre-selected scale (the semi-axis of the earth; an approximation of the Brillouin radius), and \hat{W}_n are surface harmonics of the satellite potential, see eqn. (2.3).

2.3 Higher-degree Reference Field

As it was discussed in Sec. (1.2.1) and (2.2), a satellite-derived gravity field is more appropriate to be employed in derivation of the long wavelength part of the geoid because

- it is the most unambiguous and unbiased, available so far, in its constituents because a group of well distributed satellites in inclination is used to provide the full coverage of the earth;
- the terrestrial gravity data collected so far, around the globe, are yet sparse. The data are inadequate to yield homogeneous global features of the gravity field of the earth.

To facilitate this, the gravity potential W is modelled differently than in the eqn. (2.6).

Following the same ideology as in Sec. (2.1.2), W may be decomposed into its (low-frequency) long wavelength part (W_L) and the remaining high-frequency part (W^L) as

$$W = W_L + W^L. \quad (2.32)$$

Now, W_L is selected from the satellite field (eqn. (2.31)) and denoted as the higher-degree reference potential. Referring this potential to the potential U , yields

$$\hat{W}_L = U + \delta U, \quad (2.33)$$

where δU is the higher-degree reference potential referred to the second-degree potential U . Comparing the equation (above) with the equation

$$W_L = U + T_L, \quad (2.34)$$

derived from eqn. (2.6) for $L > 8$ (see Sec. (2.1.2)), reveals that

$$\delta U = T_L, \quad (2.35)$$

where T_L is the long wavelength part of the disturbing potential T , expressed as eqn. (2.12). Considering the eqns. (2.8) and (2.31) in the eqn. (2.11), using the satellite field, for $n \leq L$, we get

$$\delta U = T_L(r, \Omega) = \frac{G\hat{M}}{r} T_0 - \frac{G\hat{M}}{r} \sum_{n=2}^L \left(\frac{\hat{a}}{r}\right)^n T_n(\Omega), \quad (2.36)$$

where

$$\begin{aligned} T_0 &= \hat{W}_0 - \frac{M^*}{\hat{M}} \\ \forall n \geq 2 \quad T_n(\Omega) &= \hat{W}_n(\Omega) - \left(\frac{M^*}{\hat{M}}\right) \left(\frac{a^*}{\hat{a}}\right)^n J_n^N P_n(\sin \varphi). \end{aligned} \quad (2.37)$$

The higher-degree reference gravity anomaly Δg_L on the geoid is directly obtained from eqn. (2.25), using the satellite field, and by taking only the first L harmonics,

$$\Delta g_L(\Omega) = \frac{G\hat{M}}{r_g^2} \Delta g_0(\Omega) + \frac{G\hat{M}}{r_g^2} \sum_{n=2}^L \left(\frac{\hat{a}}{r_g}\right)^n \Delta g_n(\Omega). \quad (2.38)$$

Based on $\delta U(T_L)$, evaluated on the geoid, the reference spheroid N_L referred to the reference ellipsoid, is derived from the Bruns formula

$$N_L(\Omega) = \frac{T_L(\Omega)}{\gamma_0(\Omega)}, \quad (2.39)$$

or in the spectral form as

$$N_L(\Omega) = \frac{GM}{r_g \gamma_0} T_0 - \frac{GM}{r_g \gamma_0} \sum_{n=2}^L \left(\frac{\hat{a}}{r_g} \right)^n T_n(\Omega). \quad (2.40)$$

The spheroid is an equipotential surface of the reference field, as the geoid is of the actual field.

2.4 Helmertization of the Higher-degree Reference Field

By Helmertization, it is meant the transformation from the real earth field to the Helmert space. This includes all the quantities defined in the field. The transformation originates from eqn. (1.6),

$$W^h = W - V,$$

where the potential V , eqn. (1.9), is a small residual quantity. Further to the discussion in Sec. (1.2), the topographical potential V^t generates a strong gravitational field capable of displacing equipotential surfaces, such as the geoid, by as much as 10^3 m [Martinec and Vaníček, 1994], while the effect of V on the geoid is at most 2 m . This implies that V is 2.5 orders of magnitude smaller than either V^t or V^c . This is why the transformation from the real earth field to the Helmert space (Helmertization of the field) can be precisely carried out, even if a precise information about the density distribution within the topography is not available.

The Helmert disturbing potential T^h , in analogy to T in the real field, is given by

$$W^h = U + T^h. \quad (2.41)$$

Substituting for W^h from eqn. (1.6), yields

$$T^h = W - U - V = T - V. \quad (2.42)$$

Considering eqns. (2.1), (2.7), and (1.9) we get

$$T^h = W_g - V^t + V^c - U_g \quad (2.43)$$

It can be seen that the gravitational potentials ($W_g - V^t$), V^c , and U_g are harmonic outside the geoid. Hence, T^h is harmonic and satisfies the Laplace eqn. (1.7). This implies that T^h can be expressed as a series of harmonic functions outside the geoid with the harmonic coefficients determined from the proper boundary condition. This problem has been already solved for T , assuming that T is a harmonic function, in the real space. The solution is expressed by eqn. (2.12). The solution, even though it does not completely fit a non-harmonic function T , fits the harmonic function T^h rigorously. Substituting for T from eqn. (2.12) in eqn. (2.42), provides rigorous harmonic expansion for T^h .

2.4.1 Residual Topographical Potential V

The residual potential V , eqn. (1.9), is defined as the difference between the two potentials V^t and V^c . Denoting by ϱ the density within the topography and σ as the surface density of the condensed topography, the two potentials can be evaluated, using Newton's integral [Martinec and Vaníček, 1994b], as

$$V^t(r, \Omega) = G \int_{\infty}^{\int_{r'=r_g(\Omega')}^{r_g(\Omega')+H(\Omega')}} \frac{\varrho(r', \Omega')}{\ell(r, \Omega, r', \Omega')} r'^2 dr' d\Omega', \quad (2.44)$$

$$V^c(r, \Omega) = G \int_{\infty} \frac{\sigma(\Omega')}{\ell(r, \Omega, r_g, \Omega')} r_g^2 d\Omega', \quad (2.45)$$

where ℓ is the spatial distance between the computation point (r, Ω) and the integration point (r', Ω') , r_g is the geocentric radius of the geoid. To evaluate the integrals,

one has to know $r_g(\Omega)$, and the densities ρ and σ . To evaluate the potential V , which is a very small quantity compared to V^t , an approximate knowledge of r_g and the densities should be good enough. The potential V has an effect of at most 2 m on the geoidal height, thus the spherical approximation of the geoid ($r_g \doteq R$) will have an effect of the order of flattening (0.003), i.e., at most 6 mm on the geoidal height [Martinec and Vaníček, 1994b]. The situation is somewhat similar with the densities.

Assuming now constant density ρ_0 within the topography and the $r_g = R$, the gravitational potential of the topography is given by the Newton integral [ibid],

$$V^t(r, \Omega) \doteq G\rho_0 \int_{\infty} \int_{z=0}^{H'} \frac{(R+z)^2}{\ell(r, \Omega, R+z, \Omega')} dz d\Omega', \quad (2.46)$$

where H' , the topographical height, is a function of Ω' reckoned along the radius vector, and equals to a sufficient accuracy to the orthometric height. We can now express the inverse distance as an infinite series of the Legendre polynomials $P_n(\cos \psi)$,

$$\frac{1}{\ell} = \frac{1}{r} \sum_{n=0}^{\infty} \left(\frac{R+z}{r} \right)^n P_n(\cos \psi), \quad (2.47)$$

convergent for $r > R+z$, where ψ is the spherical distance between the computation point and the integration point.

Substituting the inverse distance into the integral formula yields

$$V^t(r, \Omega) \doteq G\rho_0 \int_{\infty} \int_{z=0}^{H'} \frac{(R+z)^2}{r} \sum_{n=0}^{\infty} \left(\frac{R+z}{r} \right)^n P_n(\cos \psi) dz d\Omega'. \quad (2.48)$$

This equation has been further developed to

$$V^t(r, \Omega) \doteq G\rho_0 R^2 \sum_{n=0}^{\infty} \left(\frac{R}{r} \right)^{n+1} \frac{1}{n+3} \sum_{k=1}^{n+3} \binom{n+3}{k} \int_{\infty} \left(\frac{H'}{R} \right)^k P_n(\cos \psi) d\Omega', \quad (2.49)$$

by Vaníček et al. [1995b].

The evaluation of eqn. (2.45) requires a condensation model that associates the condensation density σ with the real topographical density ρ . We shall show how this works for two such models that seem to make the best physical sense.

First Condensation Model

For the evaluation of the potential of the condensation layer, we first select a model among many possible models, the condensation scheme that preserves the position of the centre of mass of the earth. The consequence of this selection is that when the residual topographical potential is expressed in a spectral form, the terms of degree 1 are identically equal to zero. As a result, the spectral form of the reference field in Helmert's space does not contain terms of degree 1 either, i.e., the field is referred to the geocentric coordinates as required in the Stokes theory. It is shown by Martinec [1993] that the condensation density

$$\sigma(\Omega') = \bar{\rho}(\Omega') H(\Omega') \left[1 + \frac{3H(\Omega')}{2R} + \frac{H^2(\Omega')}{R^2} + \frac{H^3(\Omega')}{4R^3} \right], \quad (2.50)$$

preserves the centre of mass. Here σ is the surface layer density, and $\bar{\rho}$ is the mean density of topography along the geocentric radial direction.

Substituting for the surface density from eqn. (2.50) into the eqn. (2.45), and considering constant topographical density ρ_0 , which results in $\bar{\rho} = \rho_0$, yields

$$V^c(r, \Omega) \doteq GR^2 \rho_0 \int_{\epsilon} \left(H' + \frac{3H'^2}{2R} + \frac{H'^3}{R^2} + \frac{H'^4}{4R^3} \right) \frac{1}{\ell} d\Omega'. \quad (2.51)$$

Developing the reciprocal distance into spherical harmonics,

$$\frac{1}{\ell} = \frac{1}{r} \sum_{n=0}^{\infty} \left(\frac{R}{r} \right)^n P_n(\cos \psi), \quad (2.52)$$

and substituting into these into the integral, we finally get the harmonic expression for the condensation layer potential, convergent for $r > R$,

$$V^c(r, \Omega) \doteq GR^2 \rho_0 \sum_{n=0}^{\infty} \left(\frac{R}{r} \right)^{n+1} \int_{\epsilon} f(H') P_n(\cos \psi) d\Omega', \quad (2.53)$$

where

$$f(H') = \frac{H'}{R} + \frac{3}{2} \left(\frac{H'}{R} \right)^2 + \left(\frac{H'}{R} \right)^3 + \frac{1}{4} \left(\frac{H'}{R} \right)^4. \quad (2.54)$$

Subtracting the condensation layer potential from the topographical potential, we get the harmonic expansion for the residual topographical potential V ,

$$V(r, \Omega) \doteq G\rho_0 R^2 \sum_{n=0}^{\infty} \left(\frac{R}{r}\right)^{n+1} \left[\frac{1}{n+3} \sum_{k=1}^{n+3} \binom{n+3}{k} \int_{\epsilon} \left(\frac{H'}{R}\right)^k P_n(\cos \psi) d\Omega' - \int_{\epsilon} f(H') P_n(\cos \psi) d\Omega' \right]. \quad (2.55)$$

The summation over k converges very quickly, since $H' \ll R$, and we can safely truncate it at degree 3. Then the equation for potential V is rewritten in a more transparent form

$$V(r, \Omega) \doteq G\rho_0 R^2 \sum_{n=0}^{\infty} \left(\frac{R}{r}\right)^{n+1} \frac{n-1}{2} \left[\int_{\epsilon} \left(\frac{H'}{R}\right)^2 P_n(\cos \psi) d\Omega' + \frac{n+4}{3} \int_{\epsilon} \left(\frac{H'}{R}\right)^3 P_n(\cos \psi) d\Omega' \right]. \quad (2.56)$$

It is evident that the harmonic constituent of degree 1 goes to zero, as expected.

Isolating the zero-degree term yields

$$V(r, \Omega) \doteq -\frac{G\rho_0 R}{2r} \int_{\epsilon} H'^2 d\Omega' + \frac{G\rho_0}{2} \sum_{n=2}^{\infty} \left(\frac{R}{r}\right)^{n+1} (n-1) \int_{\epsilon} H'^2 P_n(\cos \psi) d\Omega', \quad (2.57)$$

where now the higher than second degree terms in H were left out. This is possible for the reference field limited to a maximum degree L . The error caused by neglecting the H'^3 -term is smaller than $(L+1) \times 0.5 \times 10^{-3}$, which for $L = 20$ amounts to about 1%. The isolated term in the right hand side, i.e., the zero-degree residual topographical potential is denoted by V_0 .

In accordance with the definition of a surface harmonic [Heiskanen and Moritz, 1981, eqn. (1-71)], we can write

$$(H^2)_n(\Omega) = \frac{2n+1}{4\pi} \int_{\epsilon} H'^2 P_n(\cos \psi) d\Omega', \quad (2.58)$$

where $(H^2)_n$ is the surface harmonics of the squared-topography H^2 . Using this symbolism in eqn. (2.57), we get

$$V(r, \Omega) \doteq 2\pi G \rho_0 \sum_{n=0}^{\infty} \left(\frac{R}{r}\right)^{n+1} \frac{n-1}{2n+1} (H^2)_n(\Omega), \quad (2.59)$$

where

$$(H^2)_n(\Omega) = \sum_{m=0}^n \left[(H^2)_{nm}^C Y_{nm}^C(\Omega) + (H^2)_{nm}^S Y_{nm}^S(\Omega) \right]. \quad (2.60)$$

The symbols $(H^2)_{nm}^C$ and $(H^2)_{nm}^S$ denote the harmonic coefficients of the H^2 .

The presence of the zero-degree harmonic V_0 reflects the fact that this condensation model is not designed to preserve the mass of the earth. As a result, the equipotential surfaces are slightly uplifted in the Helmert space, compared to their positions in the real earth field. The amount of uplift at the earth surface ($r \doteq R$) can be evaluated from a global topographical model. Using the TUG87 model, the uplift is determined from the Bruns formula,

$$N_0 = \frac{V_0}{\gamma_0} \doteq -4 \text{ cm}, \quad (2.61)$$

where

$$V_0 = -2\pi G \rho_0 (H^2)_{00}. \quad (2.62)$$

Second Condensation Model

The second model of condensation reduction is the one that preserves the mass of the earth. This condensation requires a surface layer of density

$$\sigma(\Omega) = \bar{\rho}(\Omega) H(\Omega) \left[1 + \frac{H(\Omega)}{R} + \frac{H^2(\Omega)}{3R^2} \right], \quad (2.63)$$

[Martinec, 1993]. Following the same procedure as for the first model, starting from eqn. (2.50) onward, we end up with the spectral expression for the residual topographical potential associated with this condensation, (cf. eqn. (2.59)),

$$V(r, \Omega) \doteq 2\pi G \rho_0 \sum_{n=1}^{\infty} \left(\frac{R}{r}\right)^{n+1} \frac{n}{2n+1} (H^2)_n(\Omega), \quad (2.64)$$

where the zero-degree harmonic is zero, as prescribed, and the first-degree harmonics are

$$\begin{aligned}
 V_{10} &= \frac{2\pi}{3} G \rho_0 (H^2)_{10}, \\
 V_{11}^C &= \frac{2\pi}{3} G \rho_0 (H^2)_{11}^C, \\
 V_{11}^S &= \frac{2\pi}{3} G \rho_0 (H^2)_{11}^S.
 \end{aligned}
 \tag{2.65}$$

The first-degree harmonics describe the displacement of the origin of the coordinate system with respect to the centre of mass. Assuming ξ , η , and ζ to be the displacements in the geocentric coordinates system, it is shown by Heiskanen and Moritz [1981, p. 99] that

$$\begin{aligned}
 V_{10} &= \frac{GM}{R^2} \zeta, \\
 V_{11}^C &= \frac{GM}{R^2} \xi, \\
 V_{11}^S &= \frac{GM}{R^2} \eta.
 \end{aligned}
 \tag{2.66}$$

Using the TUG87 model, it was found that

$$\begin{aligned}
 \xi &\doteq 2.3 \text{ mm}, \\
 \eta &\doteq 7.5 \text{ mm}, \\
 \zeta &\doteq -1.5 \text{ mm}.
 \end{aligned}
 \tag{2.67}$$

In the sequel, the first condensation model will be used, since it does not violate the requirement of using a geocentric coordinates system ("forbidden harmonics"). On the other hand, the Stokes integral is blind to the presence of any zero degree harmonic. That has to be evaluated from somewhere else. This, however does not present a problem here, since the zero degree harmonic V_0 has been already determined from the earth topography, eqn. (2.62).

2.4.2 Helmert's Higher-degree Reference Field

The higher-degree reference potential in the Helmert space, denoted by W_L^h , is derived from eqn. (1.6). Taking the long wavelength part yields

$$W_L^h(r, \Omega) = \hat{W}_L(r, \Omega) - V_L(r, \Omega), \quad (2.68)$$

where \hat{W}_L replaces W_L , as we will be talking about the satellite-derived field only. Before subtracting the potential V_L (eqn. (2.59)), it is rewritten as

$$V_L(r, \Omega) \doteq \frac{GM}{r} V_0 - \frac{GM}{r} \sum_{n=2}^L \left(\frac{\hat{a}}{r}\right)^n V_n(\Omega), \quad (2.69)$$

where

$$\forall n \geq 2 \quad V_n(\Omega) = \sum_{m=0}^n [V_{nm}^C Y_{nm}^C(\Omega) + V_{nm}^S Y_{nm}^S(\Omega)], \quad (2.70)$$

and the unitless harmonic coefficients are given by

$$\begin{aligned} V_0 &= -\frac{2\pi R \rho_0}{\hat{M}} (H^2)_{00}, \\ \forall n \geq 2, m \leq n : \quad \begin{pmatrix} V_{nm}^C \\ V_{nm}^S \end{pmatrix} &= -\frac{2\pi R \rho_0}{\hat{M}} \frac{(n-1)}{(2n+1)} \left(\frac{R}{\hat{a}}\right)^n \begin{pmatrix} (H^2)_{nm}^C \\ (H^2)_{nm}^S \end{pmatrix}, \end{aligned} \quad (2.71)$$

where \hat{a} and \hat{M} were defined in Sec. (2.2). Now the Helmert reference potential can be easily derived as

$$W_L^h(r, \Omega) = \frac{GM}{r} W_0^h - \frac{GM}{r} \sum_{n=2}^L \left(\frac{\hat{a}}{r}\right)^n W_n^h(\Omega), \quad (2.72)$$

where

$$\begin{aligned} W_0^h &= \hat{W}_0 - V_0, \\ \forall n \geq 2 \quad W_n^h(\Omega) &= \hat{W}_n(\Omega) - V_n(\Omega). \end{aligned} \quad (2.73)$$

We now have to derive Helmert's higher-degree reference potential, reference gravity anomaly, and the Helmert reference spheroid, as these three quantities constitute the

"references". These quantities are obtained by "Helmertization" of their counterparts in the real earth space. This is done by transforming the quantities from the real earth field to the Helmert space by applying the corresponding corrective terms: V , DTE , and $SITE$.

The higher-degree Helmert reference potential δU^h , referred to U (see Sec. (2.3)) is

$$\delta U^h = T_L^h, \quad (2.74)$$

where the anomalous potential T_L^h is obtained directly from eqn. (2.42),

$$T_L^h(r, \Omega) = T_L(r, \Omega) - V_L(r, \Omega). \quad (2.75)$$

Considering eqns. (2.36) and (2.69) we get

$$T_L^h(r, \Omega) = \frac{GM}{r} T_0^h - \frac{GM}{r} \sum_{n=2}^L \left(\frac{\hat{a}}{r}\right)^n T_n^h(\Omega), \quad (2.76)$$

where

$$\begin{aligned} T_0^h &= T_0 - V_0 \\ \forall n \geq 2 \quad T_n^h(\Omega) &= T_n(\Omega) - V_n(\Omega). \end{aligned} \quad (2.77)$$

The Helmert gravity anomaly Δg^h , like its counterpart in the real field, Sec. (2.1.2), is defined by the equation

$$\Delta g^h = -\frac{\partial T^h}{\partial H} + \frac{1}{\gamma} \frac{\partial \gamma}{\partial H} T^h, \quad (2.78)$$

where Δg^h and T^h both refer to the Helmert co-geoid. Let us re-write the similar equation for Δg and T on the geoid, in the real space (eqn. (2.14)):

$$\Delta g = -\frac{\partial T}{\partial H} + \frac{1}{\gamma} \frac{\partial \gamma}{\partial H} T. \quad (2.79)$$

Subtracting the last two equations yields

$$\Delta g^h = \Delta g - \frac{\partial(T^h - T)}{\partial H} + \frac{1}{\gamma} \frac{\partial \gamma}{\partial H} (T^h - T). \quad (2.80)$$

Substituting for $(T^h - T)$ from eqn. (2.42) we get

$$\Delta g^h = \Delta g + \frac{\partial V}{\partial H} - \frac{1}{\gamma} \frac{\partial \gamma}{\partial H} V. \quad (2.81)$$

Because of the residual V , we can use the spherical approximation (eqn. (2.19), on the geoid),

$$\frac{1}{\gamma} \frac{\partial \gamma}{\partial H} = -\frac{1}{\gamma} \frac{\partial^2 U}{\partial H^2} \approx -\frac{2}{R}, \quad (2.82)$$

and the radial derivative of V instead of the vertical derivative [Vaníček and Martinec, 1994] in the the right hand side, as

$$\Delta g^h = \Delta g + \frac{\partial V}{\partial r} + \frac{2}{R} V. \quad (2.83)$$

The last term of the equation is the *SITE*, see eqn. (1.23). This equation defines also the relation between the long wavelength terms as

$$\Delta g_L^h = \Delta g_L + \frac{\partial V_L}{\partial r} + \frac{2}{R} V_L, \quad (2.84)$$

or

$$\Delta g_L^h = \Delta g_L + \frac{\partial V_L}{\partial r} + SITE_L, \quad (2.85)$$

The partial derivative in the right hand side is the higher-degree direct topographical effect on gravity (cf. eqn. (1.18)), referred to the geoid. Taking the radial derivative of eqn. (2.69), we get

$$-\frac{\partial V_L}{\partial r}(r, \Omega) = -\frac{GM}{r^2} V_0 + \frac{GM}{r^2} \sum_{n=2}^L \left(\frac{\hat{a}}{r}\right)^n (n+1) V_n(\Omega). \quad (2.86)$$

Considering eqns. (2.38) and (2.86) in eqn. (2.85) we find on the Helmert co-geoid, that

$$\Delta g_L^h(r_{g'}, \Omega) = \frac{GM}{r_g^2} \Delta g_0^h(r_g, \Omega) + \frac{GM}{r_g^2} \sum_{n=2}^L \left(\frac{\hat{a}}{r_g}\right)^n \Delta g_n^h(r_g, \Omega) + SITE_L, \quad (2.87)$$

where $r_{g'}$ is the radius of the Helmert co-geoid, r_g is the radius of the geoid, and

$$\begin{aligned} \Delta g_0^h(r_g, \Omega) &= \Delta g_0(\Omega) - V_0 \\ \Delta g_n^h(r_g, \Omega) &= \Delta g_n(\Omega) + (n+1) V_n(\Omega), \end{aligned} \quad (2.88)$$

or substituting for $\Delta g_0(\Omega)$ and $\Delta g_n(\Omega)$ from eqns. (2.26), we get

$$\begin{aligned} \Delta g_0^h(r_g, \Omega) &= (1 - r_g D(\phi)) T_0 - V_0 \\ \forall n \geq 2 \quad \Delta g_n^h(r_g, \Omega) &= (n - 1 - r_g D(\phi)) T_n(\Omega) + (n + 1) V_n(\Omega). \end{aligned} \quad (2.89)$$

Substituting for V from eqn. (2.69) yields the higher-degree $SIT E_L$

$$SIT E_L \doteq \frac{2G\hat{M}}{R^2} V_0 - \frac{2G\hat{M}}{R^2} \sum_{n=2}^L \left(\frac{\hat{a}}{R} \right)^n V_n(\Omega). \quad (2.90)$$

Helmert's reference spheroid or the higher-degree Helmert co-geoid is derived from δU^h or T_L^h , eqn. (2.76), on the geoid, using Bruns's formula,

$$N_L^h(\Omega) = \frac{G\hat{M}}{r_g \gamma_0} T_0^h - \frac{G\hat{M}}{r_g \gamma_0} \sum_{n=2}^L \left(\frac{\hat{a}}{r_g} \right)^n T_n^h(\Omega). \quad (2.91)$$

Considering eqns. (2.75) and (2.39) we can write

$$N_L^h(\Omega) = N_L(\Omega) - \frac{V_L(\Omega)}{\gamma_0(\Omega)}. \quad (2.92)$$

The last term in the equation is the residual topographical effect on the reference spheroid. It can be given in terms of the harmonics of potential V , eqn. (2.69), as

$$\frac{V_L}{\gamma_0} \doteq \frac{G\hat{M}}{r\gamma_0} V_0 - \frac{G\hat{M}}{r\gamma_0} \sum_{n=2}^L \left(\frac{\hat{a}}{r} \right)^n V_n(\Omega). \quad (2.93)$$

2.5 Evaluation of the Anomalous Quantities on the Helmert co-geoid

To evaluate the Helmert anomalous quantities, e.g., eqn. (2.76), on the Helmert co-geoid, one has to know the equation of the co-geoid. The separation between the Helmert co-geoid and the geoid is at most $2m$ (*PITE*, Sec. (1.2)). Using the radii $r_{g'}$ and r_g interchangeably in the evaluation of the anomalous quantities does not make sensible differences. Hence, we consider only the geoid whose equation is

$$r = r_g(\Omega). \quad (2.94)$$

The geoid can only be described by mathematical expressions of an infinite complexity such as an infinite series. In the equations relating anomalous quantities, however, the geoid can be modelled by either the mean earth sphere or more precisely it can be approximated by the mean earth ellipsoid,

$$r_g \doteq r_E(\Omega), \quad (2.95)$$

of the major semi-axis \hat{a} and the flattening f . Selection of the "ellipsoidal geoid" in the equations, brings about the so-called ellipsoidal approximation of the anomalous quantities. For a small flattening f , the equation of the ellipsoid is given by Bomford [1971, p. 565] as

$$r_E(\Omega) = \hat{a} (1 - f \cos^2 \theta + 0(f^2)), \quad (2.96)$$

where θ is the co-latitude, and $0(f^2)$ represents the terms of the order of squared-flattening. By substituting r_E for r in T_L^h , the radial term changes to

$$\forall n \leq 20 : \quad \left(\frac{\hat{a}}{r_E} \right)^{n+1} \doteq 1 + (n+1) f \cos^2 \theta + 0(f^2). \quad (2.97)$$

The effect of the squared-flattening terms in T_L^h , for $L=20$, is smaller than 3×10^{-3} , so they can be neglected. Hence, the ellipsoidal approximation of the disturbing potential reads

$$T_L^h(\Omega) = \frac{G\hat{M}}{\hat{a}} T_0^h - \frac{G\hat{M}}{\hat{a}} \sum_{n=2}^L [1 + (n+1) f \cos^2 \theta] T_n^h(\Omega), \quad (2.98)$$

and the ellipsoidal approximation of T_L^h compared to the spherical approximation, ($r_g \doteq \hat{a}$), will then be given by the correction

$$T_L^h(r, \Omega) \Big|_{r=r_E} - T_L^h(r, \Omega) \Big|_{r=\hat{a}} \doteq f \cos^2 \theta T_0^h - \frac{G\hat{M}}{\hat{a}} \sum_{n=2}^L (n+1) f \cos^2 \theta T_n^h(\Omega), \quad (2.99)$$

called the ellipsoidal correction to the disturbing potential. The correction is considerable and may have an impact of up to one metre on the geoidal height, see chapter 4.

It is useful to show the ellipsoidal correction to the reference gravity anomal Δg_L (eqn. (2.38)). As with the disturbing potential, we can write

$$\Delta g_L(\Omega)|_{r=r_B} - \Delta g_L(\Omega)|_{r=\hat{a}} \doteq f \cos^2\theta \Delta g_0(\Omega) - \frac{GM}{\hat{a}^2} \sum_{n=2}^L (n+1) f \cos^2\theta \Delta g_n(\Omega), \quad (2.100)$$

In practice, the anomalous quantities in the real earth field: eqns. (2.36), (2.38), (2.40) or the quantities in the Helmert space: eqns. (2.76), (2.87), (2.91), (2.90), are required to be evaluated on the geoid/co-geoid using the ellipsoidal approximation of the geoid. The ellipsoidal approximation of the eqns. (2.40) and (2.91), read

$$N_L(\Omega) \doteq \frac{GM}{\hat{a}\gamma_0} T_0 - \frac{GM}{\hat{a}\gamma_0} \sum_{n=2}^L [1 + (n+1) f \cos^2\theta] T_n(\Omega) \quad (2.101)$$

and

$$N_L^h(\Omega) \doteq \frac{GM}{\hat{a}\gamma_0} T_0^h - \frac{GM}{\hat{a}\gamma_0} \sum_{n=2}^L [1 + (n+1) f \cos^2\theta] T_n^h(\Omega) \quad (2.102)$$

respectively.

It is worth to give here the spectral formula of the reference D_L^s term, evaluated on the geoid. From eqns. (2.23) and (2.12) and using ellipsoidal approximation, we obtain

$$D_L^s \doteq \frac{GM}{\hat{a}} D(\phi) T_0 - \frac{GM}{\hat{a}} \sum_{n=2}^L [1 + (n+1) f \cos^2\theta] D(\phi) T_n(\Omega). \quad (2.103)$$

Chapter 3

Numerical Evaluation of the Residual Helmert Co-geoid

3.1 Modified Spheroidal Stokes's Integrator

The residual (high-frequency) Helmert co-geoid is evaluated from the residual Helmert gravity anomaly using the generalized (spheroidal) Stokes integral,

$$N^L(\Omega) \doteq \frac{R}{4\pi\gamma_0} \int \int_{\epsilon} \Delta g^L(\Omega') S^L(\psi) d\Omega', \quad (3.1)$$

where Δg^L in this chapter denotes the high-frequency Helmert gravity anomaly evaluated on the co-geoid. S^L is the high-frequency Stokes kernel or the spheroidal Stokes kernel, referred to degree- L spheroid,

$$S^L(\psi) = \sum_{n=L+1}^{\infty} \frac{2n+1}{n-1} P_n(\cos \psi). \quad (3.2)$$

The kernel, as a function of spherical distance ψ , decreases to zero faster, compared to the original (ellipsoidal) Stokes kernel [Vaníček and Krakiwsky, 1986]. This characteristic of the kernel is advantageous since the gravity from distant areas contributes little to the result of integration.

In order to further minimize the contribution of "remote" gravity to the Stokes integral, Molodenskij et al. [1961] proposed the idea of the modification of the Stokes kernel. The kernel is modified in such a way as to make it converge to zero at a shorter distance from the computation point, so that the integration can be "truncated" closer to the computation point. Theoretically, there is no modification that would give zero contribution of the remote gravity to the integral. Some contribution always persists. This is called the truncation error of the modified Stokes integral, truncated close to the computation point.

The idea could be extended to the spheroidal Stokes integral as well. In Vaníček and Kleusberg [1987], the modification of the spheroidal Stokes kernel for a spherical cap of radius $\psi_0 = 6^\circ$ was first proposed. The spheroidal Stokes kernel is modified by adding low-frequency constituents to the kernel,

$$S^{*L}(\psi) = S^L(\psi) - S_L^*(\psi) = S^L(\psi) - \sum_{l=2}^L \frac{2l+1}{2} \hat{t}_l P_l(\cos \psi), \quad (3.3)$$

where the amplitudes \hat{t}_l are determined, to minimize the truncation error.

It is, of course, the truncation error of the modified Stokes integral:

$$N^{*L}(\Omega) \doteq \frac{R}{4\pi\gamma_0} \int \int_{\epsilon} \Delta g^L(\Omega') S^{*L}(\psi) d\Omega', \quad (3.4)$$

that is minimized. The modified integral is different from the original (eqn. (3.1)) integral by

$$\begin{aligned} \delta N^m &= \frac{R}{4\pi\gamma_0} \int \int_{\epsilon} (S^L(\psi) - S^{*L}(\psi)) \Delta g^L d\Omega' \\ &= \frac{R}{4\pi\gamma_0} \int \int_{\epsilon} S_L^*(\psi) \Delta g^L d\Omega'. \end{aligned} \quad (3.5)$$

Since the modification of the Stokes kernel is carried out in the low-frequencies, the modification will not affect the Stokes integral, i.e., δN^m will be zero if the residual Helmert gravity anomalies Δg^L are not contaminated by any low frequency errors. This requires the low-frequency component (Δg_L) to be known properly, since the residual anomaly is obtained from the "observed" anomaly by subtracting the

satellite-derived (low-frequency) reference anomaly. The spectral form of the δN^m will be derived later in Sec. (3.3), when dealing with the truncation error.

3.2 Numerical Evaluation of the Modified Spheroidal Stokes Integral

The modified spheroidal (high-frequency) Stokes integral is evaluated over the spherical cap C_0 of radius $\psi_0 = 6^\circ$, (see above)

$$N^{*L}(\Omega) \doteq \frac{R}{4\pi\gamma_0} \int \int_{C_0} \Delta g^L(\Omega') S^{*L}(\psi) d\Omega'. \quad (3.6)$$

Gravity anomalies on the earth surface are given as mean values for geographical cells. To accommodate the mean anomalies, the Stokes integral is reduced, without any loss of generality, to a summation of partial integrals over the cells c_i inside the spherical cap,

$$\begin{aligned} N^{*L}(\Omega) &= \sum_i \frac{R}{4\pi\gamma_0} \int \int_{c_i} \overline{\Delta g_i}^L S^{*L}(\psi) dc \\ &= \sum_i \frac{R}{4\pi\gamma_0} \overline{\Delta g_i}^L \int \int_{c_i} S^{*L}(\psi) dc. \end{aligned} \quad (3.7)$$

Since a mean anomaly is, by definition, constant over the corresponding cell, it can be taken outside the partial integral, so that each partial integral could be expressed as a product of the integral mean (within the cell) of the kernel with the cell area.

If the kernel behaves linearly within the cell, the integral mean of the kernel can be approximated by the kernel value at the centre of the cell. This behaviour of the kernel may be true over a smaller size cell or over a cell located reasonably far from the computation point. The modified spheroidal Stokes kernel is assumed linear over $5' \times 5'$ cells, located at spherical distances of some arc minutes from the computation point [Vaníček and Kleusberg, 1987]. The kernel is assumed linear over even larger ($1^\circ \times 1^\circ$) cells, located farther than 1 arc degree from the computation

point. This property of the kernel necessitates a division of the inner zone where detailed anomalies must be used, and outer zone, where mean anomalies for larger cells could be used, Fig. 3.1.

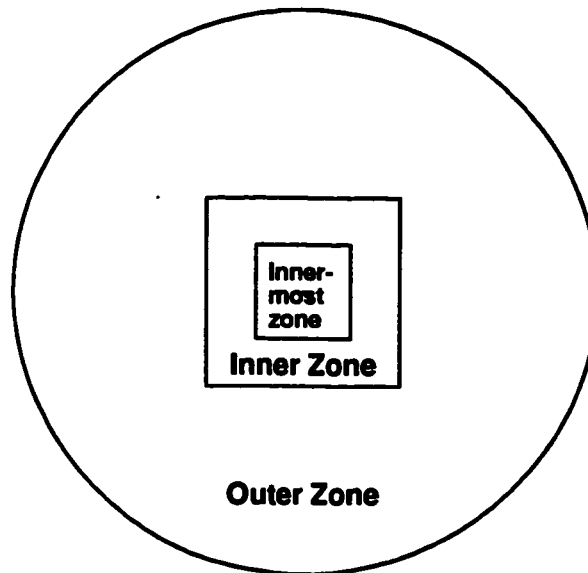


Figure 3.1: The three zones in the Stokes integrator

The linear approximation, however, is the source of some errors in the integration, which will be discussed later.

At the immediate vicinity of the computation point, the behaviour of the kernel is more involved. Because of the higher rate of change of the kernel and particularly its singularity at the computation point, an analytical solution of the Stokes integral is sought in the immediate vicinity. For this reason, the ellipsoidal surface of the integration domain is approximated by a plane tangent to the ellipsoid at the computation point. This integration domain is called the innermost zone; it is the area extending to the spherical distance of a few arc minutes from the computation point. In this zone an analytical surface, usually a plane, is fitted in the least-squares sense to the discrete equally weighting $5' \times 5'$ mean gravity anomalies. The reason for the equal weighting is simply the lack of knowledge about the proper assessment of the mean anomaly accuracies. The existing different weights implied by the observational

accuracies cannot be used, since they usually reflect only observational statistics, and not the averaging (modelling) errors of the mean anomalies which are probably more dominant. The modified spheroidal Stokes kernel, expressed as a series of trigonometric functions, is truncated (after the trigonometric functions are developed into series) to the first few terms, insuring its accuracy to 0.01% at distances $\psi < 20'$,

$$S(\psi) \doteq \frac{2}{\psi} - 3 \ln \left(\frac{\psi}{2} \right) - 4 \quad (3.8)$$

[Vaníček et al., 1987]. Because of the meridian convergence, the number of the mean anomalies inside the innermost zone increases when the computation point moves north. At the latitude of 40° the number is almost doubled compared to the equator.

Outside the innermost zone, the next area extends up to 1° and is called the inner zone. In this zone the partial integrals are computed as the kernel value at the centre of cell multiplied by the cell area, and $5' \times 5'$ mean anomalies are used. Outside the inner zone, is the outer zone which extends to the distance of $\psi_0 = 6^\circ$. In this zone the Stokes integral is treated the same way as in the inner zone but using $1^\circ \times 1^\circ$ mean anomalies. These anomalies are averaged from $5' \times 5'$ mean anomalies.

The original Stokes's integrator GIN452 used by Vaníček et al. [1987] was rewritten into a new version called GIN95.f. This new version computes residual co-geoid in three modes, single point, profile, and grid of points using $5' \times 5'$ mean anomalies in innermost and inner zones and $1^\circ \times 1^\circ$ mean anomalies in the outer zone. As a very preliminary test of the new version, the performance of the integrator was examined in the following way. It has been shown by Sjöberg [1983] that the observed land uplift in Fennoscandia caused a geoidal height change of almost 10% of the uplift, i.e., for 1 m land uplift the change in the geoid is almost 10 cm. One metre change in elevation (land uplift) is equivalent to a gravity change of 0.3 mGal. Hence, one can argue that a 0.3 mGal long wavelength change in gravity is equivalent to 10 cm change in the geoidal height. Given the observed gravity anomaly data, the integrator was assigned to compute residual geoid at a profile twice: once using the original data, the second

time using the data increased by 0.6 mGal . The difference in co-geoidal heights resulting from the two computations, ranged between 18 and 22 cm , confirming a reasonable performance of the integrator.

The integrator was further tested in an area of $5^\circ \times 10^\circ$ in south-west Canada. The integrator was assigned to compute a residual geoid, using gravity anomalies derived from the GFZ93A combined global geopotential model [Gruber and Anzenhofer, 1993] for ($n = 21\dots, 360$). The computed geoid, after being corrected for the truncation error, was compared to the geoid obtained directly from the potential coefficients of the same model using the software `sfrod3.f`, Sec. (1.3), employing spectral formula of the geoid. Discrepancies ranging between -0.12 m and $+0.28 \text{ m}$ were observed, Fig. 3.2.

The discrepancies were thought to be mostly due to the use of point values of the integration kernel rather than integral mean values. Another source of discrepancies is that, by changing computation point in steps of $5'$ in either latitude or longitude, the integration zones remain unchanged until the computation point passes through an integer degree parallel or meridian (border lines of $1^\circ \times 1^\circ$ anomalies), i.e., the exchange of gravity data sets is not smooth. As a result, sharp changes (tears) in geoidal heights occur in both directions, see Fig. 3.2.

To reduce the effect of the kernel approximation (point values for mean values) the dimensions of the inner zone were increased from $2^\circ \times 2^\circ$ to $4^\circ \times 4^\circ$. This allows a larger number of finer cells to be used by in the integration, and results in a better approximation of the Stokes integral. This resulted in a considerable improvement and the range of the discrepancies decreased to $(-0.07 \text{ m}, +0.07 \text{ m})$. Further expansion of the inner zone, e.g., to the size of $6^\circ \times 6^\circ$, caused further improvement, by a few millimeters, but the computer time spent on the integration increased by 100%.

To repair the tears, a smoothing algorithm [Vaníček et al., 1995a] was applied to the integrator's output. A comparison after smoothing showed that the tears disappear and the discrepancy range is reduced to $(-0.06 \text{ m}, +0.06 \text{ m})$, see Fig. 3.3.

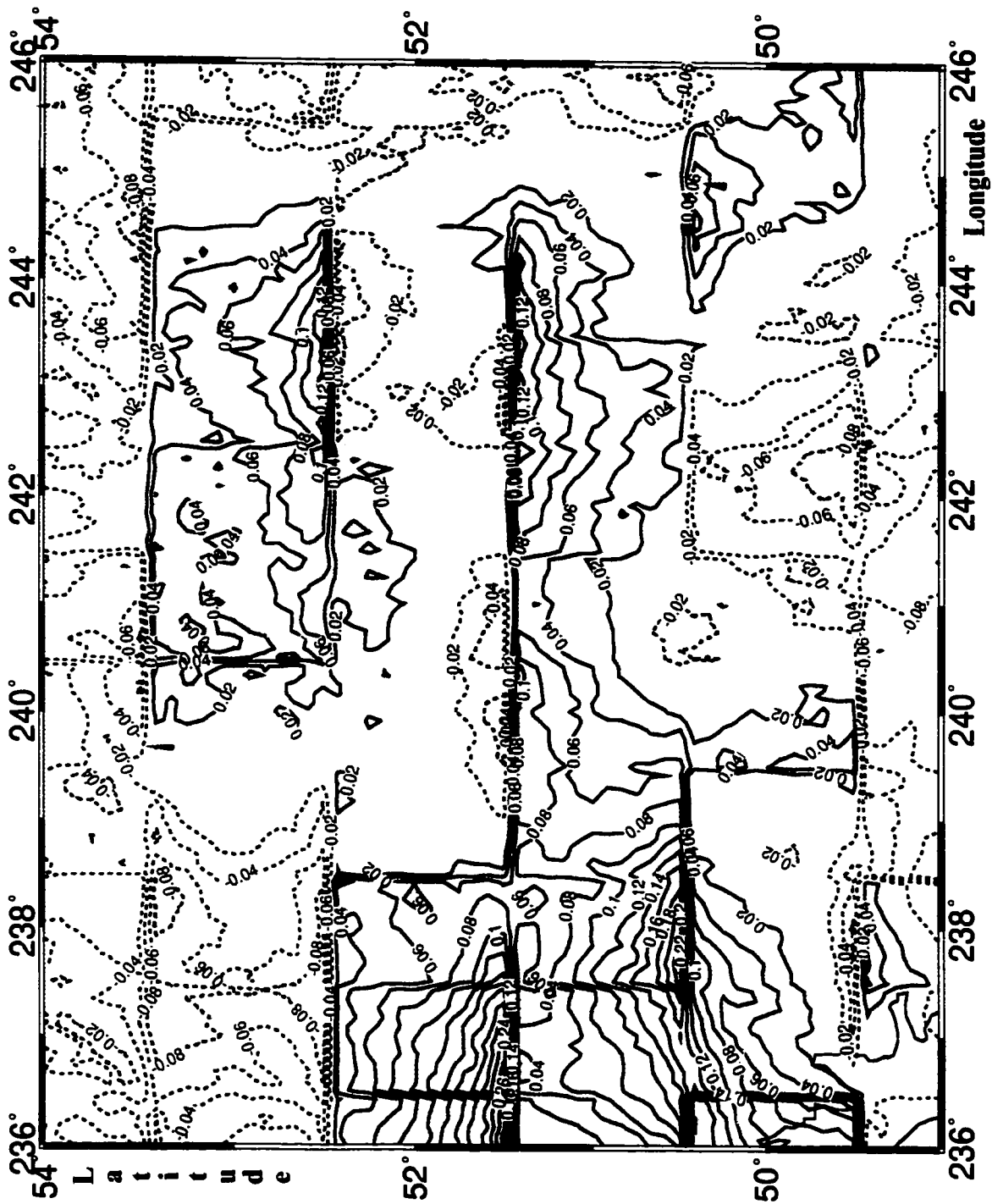


Figure 3.2: Errors in the residual geoid, obtained by the GIN95.f integrator (size of inner zone used is $2^\circ \times 2^\circ$). Contour interval is 0.02 m.

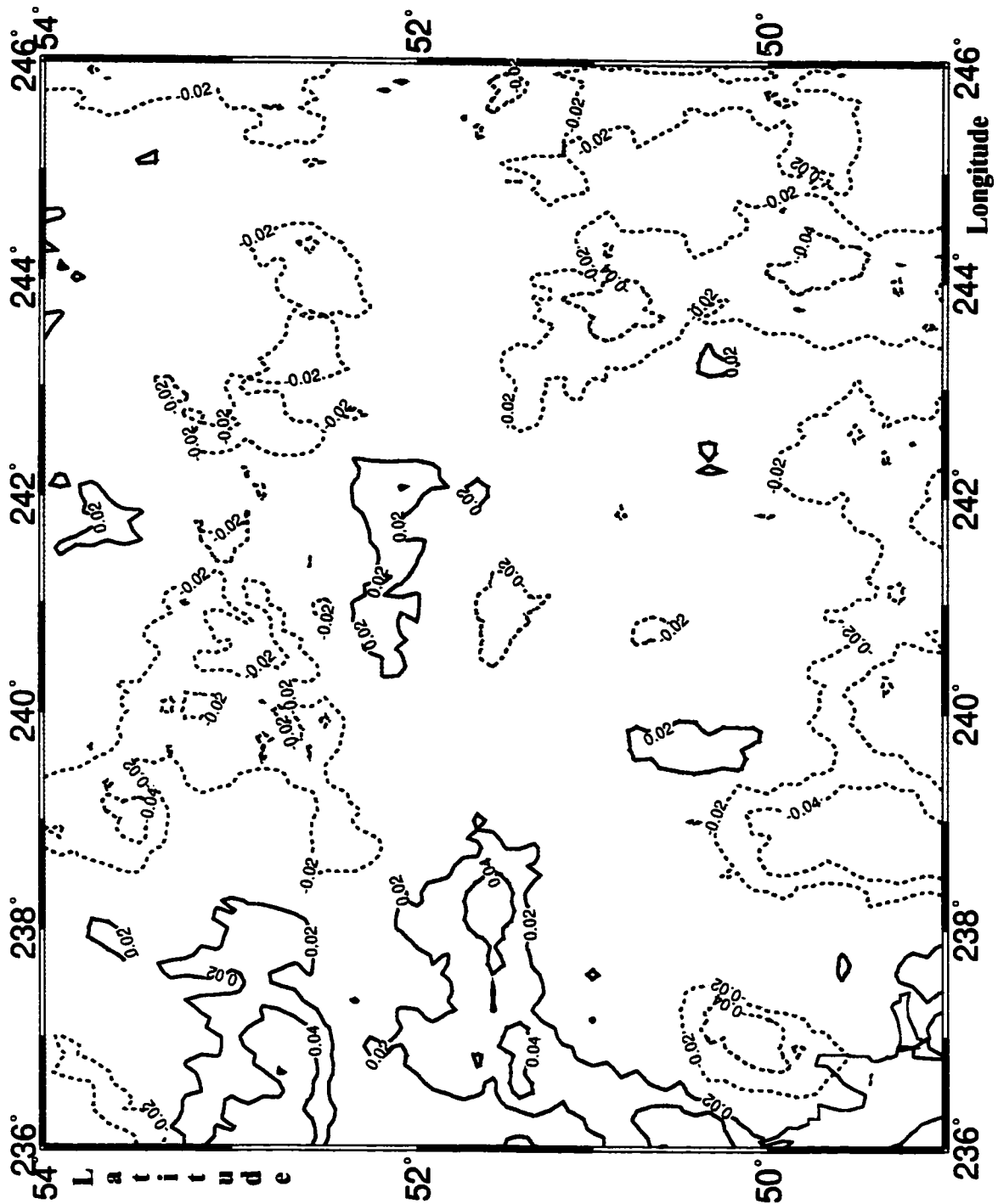


Figure 3.3: Smoothed errors in the residual geoid, obtained by the GIN95.f integrator (size of inner zone is $4^\circ \times 4^\circ$). Contour interval is 0.02 m.

Further smoothing brings another improvements by a few millimeters which is not considered significant. The 6 *cm* magnitude discrepancy is interpreted as a combination of errors of the numerical integration, and the use of point instead of mean surface gravity anomalies.

3.2.1 The Residual Helmert Gravity Anomaly

In practice, gravity data is available in the form of mean free-air or mean Bouguer gravity anomalies in regular geographic grids. The Bouguer anomalies [Heiskanen and Moritz, 1981, eqn. (3-19)], because the topographical effect is removed, are smooth and suitable for interpolation. For this reason, these anomalies are used in developing the Helmert anomalies (eqn. (1.25)). A mean Helmert anomaly (on the geoid) is expressed in terms of a mean incomplete Bouguer anomaly $\overline{\Delta g_t^B}$, on the topography, as

$$\begin{aligned} \overline{\Delta g_h^{h*}} &= \overline{\Delta g_t^B} + \overline{DTE}_t + 2\pi G \rho_0 \overline{H} + \overline{LE} + \overline{AE} \\ &\quad + D\overline{\Delta g^h} + \overline{SITE} + \overline{D^S}, \end{aligned} \quad (3.9)$$

[Vaníček et al., 1995a], where G is the gravitational constant, and ρ_0 is the topographical density. This is the formula applied in the flowchart Fig. 1.1. Overlines here denote mean values in the flowchart. As it is shown, the mean Bouguer anomaly is "Helmertized" by applying the \overline{DTE} , computed using a high resolution topography (height) model. The mean Helmert anomaly is corrected for the $(2\pi G \rho_0 \overline{H})$, denoted (B. Plate) in the flowchart, to restore the Bouguer plate reduction in the Bouguer anomalies. Then \overline{LE} and \overline{AE} are applied to correct for the spherical approximation of the global gradient ($0.3086mGal/m$) of the normal gravity. After these corrections, the resultant is considered as the Helmert gravity anomaly on the topography.

Before the downward continuation, the Helmert gravity anomaly (on the topography) is reduced to its high-frequency component, by subtracting the Helmert reference gravity anomaly $Dg_{20}^h(\Delta g_{20}^h)$, on the topography. Δg_{20}^h on the topography is computed

from its value (satellite-derived) on the geoid, from left column of the flowchart, using the Taylor's series (linear part) expansion. As a consequence of the ellipsoidal approximation applied in the reference anomaly, and the \overline{LE} and \overline{AE} effects (discussed above), the reduced Helmert gravity anomaly is considered only a high-frequency component, i.e., the low-frequency part is properly removed. The reductions discussed (so far) are handled by the routine "hdelgtr.f", see Sec. (1.3).

The (residual) high-frequency Helmert anomaly is then continued downward to the geoid by apply $D\overline{\Delta g}^h$, Sec. (3.4). After the downward continuation, the high-frequency \overline{SITE} and the high-reference \overline{D}^S are added. These high-frequency quantities are obtained from their mean values by subtracting the corresponding reference values. Finally, the Helmert anomaly, reduced to this end, is considered to be of a high-frequency character as is required by the generalized Stokes integral, Fig. 1.1.

3.3 Truncation Error of the Modified Spheroidal Stokes Integral

The (minimum) truncation error of the modified spheroidal Stokes integral, eqn. (3.4), is given by

$$\delta N^{*L} = \frac{R}{4\pi\gamma} \int \int_{\in - C_0} \Delta g^L S^{*L}(\psi) d\Omega', \quad (3.10)$$

where $\in - C_0$ is the area outside the spherical cap C_0 . A spectral form of the truncation error, in terms of gravity anomaly harmonics, was derived by Vaníček and Sjöberg [1991],

$$\delta N^{*L}(\Omega) = \frac{R}{2\gamma} \sum_{n=L+1}^{\infty} Q_n^{*L}(\psi_0) (\Delta g^L)_n, \quad (3.11)$$

where

$$\forall n > L \quad Q_n^{*L}(\psi_0) = \int_{\psi_0}^{\pi} S^{*L}(\psi) P_n(\cos \psi) \sin \psi d\psi \quad (3.12)$$

are Molodensky's like truncation coefficients [Molodenskij et al., 1960].

For the numerical evaluation of the coefficients, the integral formula above might not be a suitable one. It will be more convenient to express the coefficients in terms of the Molodensky original coefficients Q_n [Heiskanen and Moritz, 1981, eqn. (7-34)],

$$Q_n(\psi_0) = \int_{\psi_0}^{\pi} S(\psi) P_n(\cos \psi) \sin \psi d\psi, \quad (3.13)$$

where $S(\psi)$ is the original Stokes kernel

$$S(\psi) = \sum_{l=2}^{\infty} \frac{2l+1}{l-1} P_l(\cos \psi), \quad (3.14)$$

[ibid, eqn. (2-169)].

For the convenient expression of $Q_n^{*L}(\psi_0)$, let us go back to Vaníček and Sjöberg [1991]. In a search for the minimum truncation error, they found that the L_2 -norm:

$$\|.\|^2 = \int \int_{\epsilon-C_0} (.)^2 d\Omega', \quad (3.15)$$

of the sought kernel $S^{*L}(\psi)$ (eqn. (3.3)) has to be minimized. Minimizing the norm with respect to the free coefficients \hat{t}_l results in the following normal equations, [ibid, eqn. (18)],

$$\forall n = 2, \dots, L : \quad Q_n^{*L}(\psi_0) = 0. \quad (3.16)$$

Substituting for $S^{*L}(\psi)$ from eqn. (3.3), yields $L - 1$ normal equations for the $L - 1$ unknowns \hat{t}_l as

$$\forall n = 2, 3, \dots, L : \quad \sum_{l=2}^L \frac{2l+1}{2} E_{ln} \hat{t}_l = Q_n^L, \quad (3.17)$$

where Q_n^L are "high-frequency" Molodensky's coefficients,

$$Q_n^L(\psi_0) = \int_{\psi_0}^{\pi} S^L(\psi) P_n(\cos \psi) \sin \psi d\psi \quad (3.18)$$

and

$$E_{ln} = \int_{\psi_0}^{\pi} P_l(\cos \psi) P_n(\cos \psi) \sin \psi d\psi. \quad (3.19)$$

Substituting for $S^{*L}(\psi)$ from eqn. (3.3) into eqn. (3.12) and considering eqn. (3.18) yields

$$\forall n > L, \quad Q_n^{*L}(\psi_0) = Q_n^L(\psi_0) - \sum_{l=2}^L \frac{2l+1}{2} E_{ln} \hat{t}_l. \quad (3.20)$$

Now the Q_n^L are derived in terms of the Q_n . For this, the $S^L(\psi)$ (eqn. (3.2)) is written in terms of $S(\psi)$ as

$$S^L(\psi) = S(\psi) - \sum_{l=2}^L \frac{2l+1}{l-1} P_l(\cos \psi). \quad (3.21)$$

Substituting for $S^L(\psi)$ in eqn. (3.18), yields

$$Q_n^L(\psi_0) = Q_n(\psi_0) - \sum_{l=2}^L \frac{2l+1}{l-1} E_{ln}. \quad (3.22)$$

Substituting for these coefficients in eqn. (3.20), after some manipulation we finally get

$$\forall n > L, \quad Q_n^{*L}(\psi_0) = Q_n(\psi_0) - \sum_{l=2}^L \frac{2l+1}{l-1} \left(1 + \frac{l-1}{2} \hat{t}_l\right) E_{ln}. \quad (3.23)$$

These coefficients are zero for $n \leq L$, see eqns. (3.16).

In practice the truncation error, eqn. (3.11), is expressed in terms of the Helmert disturbing potential coefficients T_{nm}^h , using eqn. (2.18), in a spherical approximation $r = R$:

$$\delta N^{*L}(\Omega) = \frac{R}{2} \sum_{n=L+1}^{\infty} (n-1) Q_n^{*L}(\psi_0) T_n^h. \quad (3.24)$$

Approximating the Helmert surface harmonics T_n^h by the real harmonics T_n , we get an estimate of the truncation error. The need for this approximation arises from the fact that the numerical evaluation of the high-frequency T_n^h requires a detailed squared topography model. On the other hand, because the Q_n^{*L} coefficients converge to zero in high frequencies, the approximation does not introduce considerable error. Figure 3.4 shows an estimate of the truncation error for $\psi_0 = 6^\circ$ in Canada, using the GFZ93A combined model as a source of T_n . The error ranges between -0.24 m and $+0.36 \text{ m}$.

The truncation error estimates using different global models differ by a few centimeters. A comparison between truncation errors estimated from the GFZ93A and the OSU91A models is shown in Fig. 3.5, where differences ranging between -6 cm

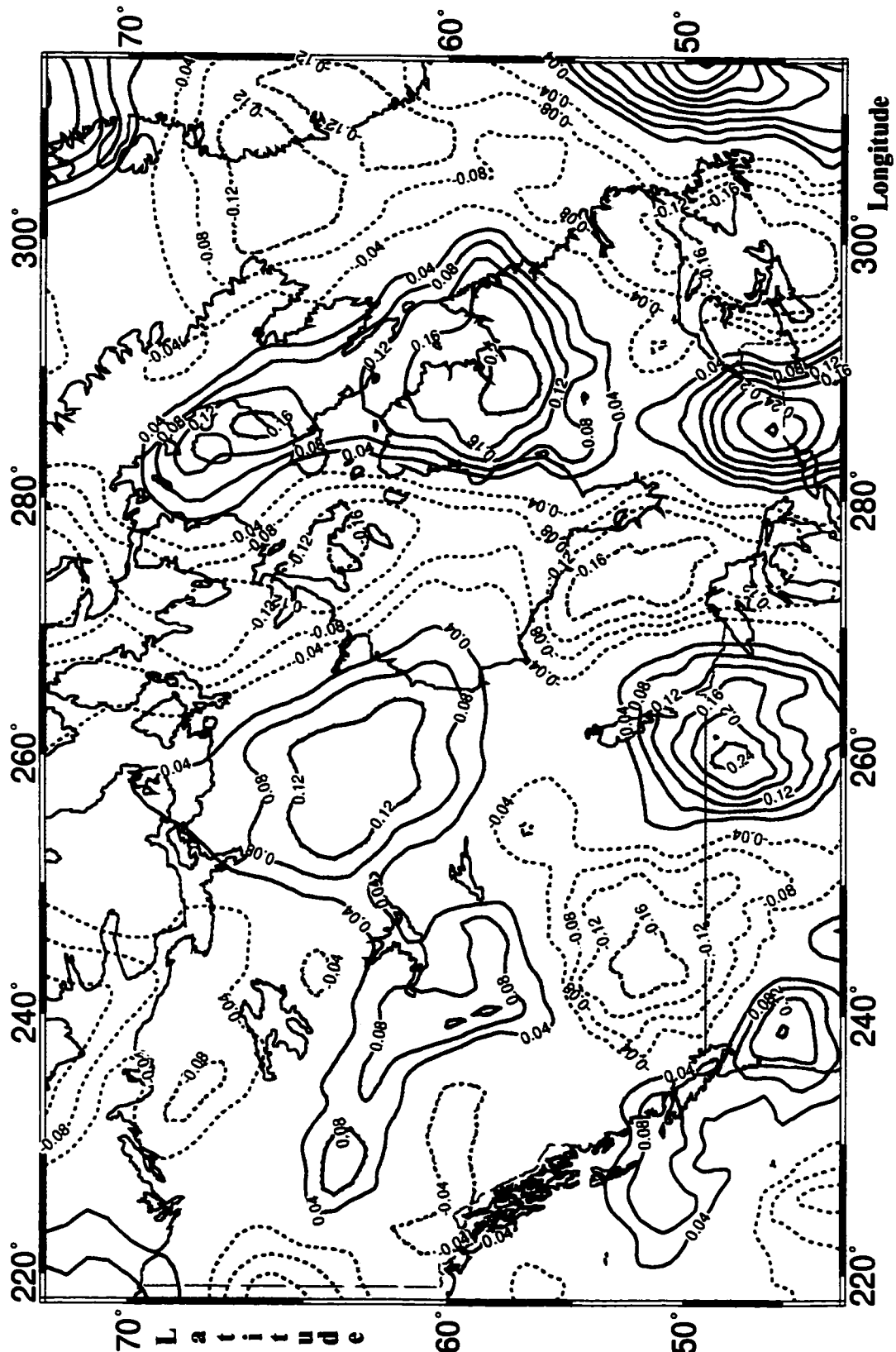


Figure 3.4: The truncation error (for $\psi_0 = 6^\circ$) in Canada (from the GFZ93A model). Contour interval is 0.04 m.

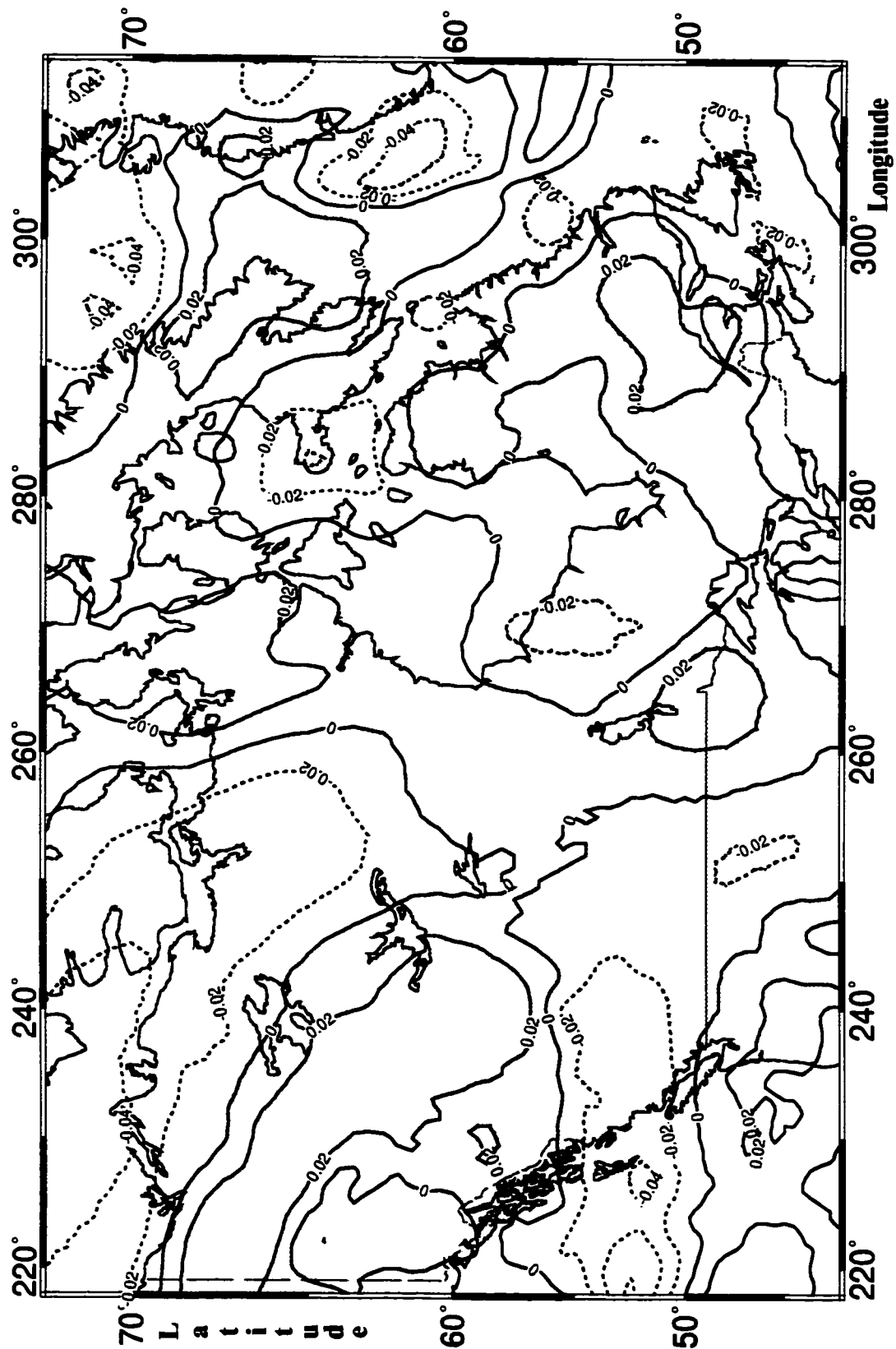


Figure 3.5: Difference in truncation error, obtained from OSU91A and GFZ93A models. Contour interval is 0.02 m.

and +5 *cm* are evident. Because of this uncertainty in global models, the truncation error should be kept to the minimum even though it is estimable from geopotential models.

In computing the truncation error, the summation over degrees n does not need to be extended all the way over all the degrees of the model used, because the truncation coefficients Q_n^{*L} converge to zero for higher degrees. This was examined by computing the truncation error selecting different upper limit for the summation. The upper limit was increased at the steps of $\Delta n = 10$ each time. It was shown that after degree $n = 120$, the change in δN^{*L} remained less than one centimetre. Hence, to the accuracy of one centimetre, the summation for Canada can be terminated at $n = 120$. The estimation uncertainty (commission error) of the truncation error, as it was computed from propagation or errors (of the potential coefficients), remained under one centimetre when the GFZ93A model was used.

Now δN^m , eqn. (3.5), the correction to the Stokes integral is evaluated. Substituting eqns. (3.3) and (3.2) into eqn. (3.5) yields

$$\delta N^m = \frac{R}{4\pi\gamma} \int \int_{\epsilon} \sum_{l=2}^L \frac{2l+1}{2} E_{ln} \hat{t}_l P_l(\cos \psi) \Delta g^L d\Omega'. \quad (3.25)$$

Changing the sequence of summation and integration yields the spectral form, in terms of the surface harmonics of the gravity anomaly,

$$\delta N^m = \frac{R}{2\gamma} \sum_{l=2}^L \hat{t}_l (\Delta g^L)_l. \quad (3.26)$$

As it was discussed in Sec. (3.1), theoretically, the correction is equal to zero. In practice, however, the reduced Helmert gravity anomaly (Sec. (3.2.1)) contains some low-frequency noise because of the noise in satellite reference field or the noise coming from "observed" anomalies. As a consequence, δN^m is not equal to zero, and has to be statistically evaluated. Finally, the high frequency co-geoid determined in (Sec. (3.2)) should be corrected by both the truncation error and by an estimate of δN^m .

3.4 Downward Continuation of Mean Helmert's Gravity Anomalies

Downward continuation of gravity anomaly in the real earth field depends on the topographical density, because of the presence of the attracting topographical masses above the geoid. In the Helmert space, however, the downward continuation of the (Helmert) anomaly is possible, since the topographical masses are condensed on the geoid. As a result, the Helmert disturbing potential T^h and the function $\frac{1}{r}\Delta g^h$, are harmonic outside the geoid. In Vaníček et al. [1996], Poisson's integral formula [Heiskanen and Moritz, 1981, eqn. (1-89)] is used for the downward continuation of the Helmert gravity anomaly. The integral reads

$$V_e(r, \Omega) = \frac{1}{4\pi} \int \int_{\epsilon} V(R, \Omega') K(r, \psi, R) d\Omega', \quad (3.27)$$

where

$$K(r, \psi, R) = \frac{R(r^2 - R^2)}{\ell^3}. \quad (3.28)$$

$V_e(r, \Omega)$ is the value of the harmonic function V at point (r, Ω) exterior to the sphere of $r = R$. The value is obtained by integrating of values $V(R, \Omega')$ on the sphere of radius R . The function K is the Poisson kernel, a function of both the computation point (r, Ω) and the integration point (R, Ω') , whose spherical and spatial distances from the computation point are ψ and ℓ respectively. The Poisson integral is immediately applicable to Helmert's gravity disturbance (δg^h) [Heiskanen and Moritz, 1981, eqn. (2-142)], as a point function. For the Helmert gravity anomaly, the integral changes to [Vaníček et al., 1996, eqn. (11)]

$$\Delta g_t^h \doteq \frac{R}{4\pi r} \int \int_{\epsilon} \Delta g_g^h K(r, \psi, R) d\Omega'. \quad (3.29)$$

The spectral form of the kernel is

$$K(H, \psi) = \sum_{n=0}^{\infty} (2n+1) \left(\frac{R}{R+H} \right)^{n+1} P_n(\cos \psi), \quad (3.30)$$

where H is the height of the computation point. The Poisson kernel, in contrast to the Stokes kernel, is non-homogeneous—a function of height of the computation point. The kernel converges to zero slowly at low altitude, and faster at high altitude.

Since in the Stokes-Helmert scheme the surface gravity data are used to evaluate only the residual ($n > 20$) co-geoid, then, only the high-frequency components of Helmert's anomalies are needed to be continued downward. This allows the high-frequency Poisson kernel

$$K^{20}(H, \psi) = \sum_{n=21}^{\infty} (2n + 1) \left(\frac{R}{R + H} \right)^{n+1} P_n(\cos \psi), \quad (3.31)$$

to be used. This kernel converges to zero at a shorter spherical distance from the computation point than the original kernel. It was shown in Vaníček et al. [1996] that for the downward continuation of anomalies to the accuracy of $10 \mu Gal$, in south-west Canada with topography ranging from 0 to 3000 m , the high-frequency Poisson integration can be evaluated out only up to spherical radius of 1 arc degree with a manageable truncation error. For the integration cap of radius $\psi_0 = 1^\circ$, a modification of the (high-frequency) kernel was sought (K^{*20}), in much the same way as the modification of the Stokes kernel, (cf. Sec. (3.3)), i.e., to minimize the contribution of "distant" ($\psi > 1^\circ$) anomalies on the Poisson's integral. The truncation error can then be estimated from global geopotential models.

The modified high-frequency Poisson integral is then adapted for the evaluation of the mean gravity anomalies on the topography from the mean anomalies on the geoid. This requires a double averaging of the kernel over geographical cells c_i on the topography and c_j on the geoid,

$$\overline{\overline{K}}_{ij}^{*20} = \frac{1}{c_i} \int \int_{c_i} \frac{R}{4\pi r} \left(\int \int_{c_j} K^{*20}(H, \psi) dc_j \right) dc_i. \quad (3.32)$$

The integration over the Helmert co-geoid is replaced by summation of partial integrals over the number of cells (J) within the spherical cap of radius $\psi_0 = 1^\circ$,

$$\overline{\Delta g}_i^{h20} \doteq \sum_{j=1}^J \overline{\overline{K}}_{ij}^{*20} \overline{\Delta g}_j^{h20}. \quad (3.33)$$

The approximation sign accounts for the fact that the truncation error of Poisson's integral is missing in the equation.

For a simultaneous evaluation of J mean anomalies on the topography from the same number J of mean anomalies on the co-geoid, the above system of linear equations is implemented for $i = 1, 2, \dots, J$. A closer look at this system of equations reveals that not all of the J mean anomalies on the topography are completely determined from the J mean anomalies on the geoid. The anomalies at the marginal points—points sitting closer than 1° spherical distance from the border of the computation area (area defined by the J anomalies on the co-geoid) are only partially determined. Actually, at these points the 1° integration cap is incomplete; there are not enough data (mean anomalies) falling inside the cap when the marginal points are considered.

For a precise evaluation of the mean anomalies on the topography, even the minimized truncation error, which may still reach to a few hundreds of μGal [Vaníček et al., 1996], has to be taken into account. The spatial form of the error reads:

$$Dg_T = \frac{R}{4\pi r} \int_{\psi_0}^{\pi} \int_0^{2\pi} \Delta g_g^{h20} K^{*20}(H, \psi) \sin \psi \, d\psi \, d\alpha. \quad (3.34)$$

Following the same reasoning as in Heiskanen and Moritz [1981, Sec. (7-4)], see also Sec. (3.3), the spectral form of the error was found to be

$$Dg_T = \frac{R}{2r} \sum_{n=0}^{\infty} Q_n^{*20}(H, \psi_0) (\Delta g_g^{h20})_n, \quad (3.35)$$

where

$$Q_n^{*20}(H, \psi_0) = \int_{\psi_0}^{\pi} K^{*20}(H, \psi) P_n(\cos \psi) \sin \psi \, d\psi, \quad (3.36)$$

and $(\Delta g_g^{h20})_n$ is the n -th ($n > 20$) surface spherical harmonic of the residual Helmert anomaly.

For an estimation of the truncation error, we may express $(\Delta g_g^{h20})_n$ in terms of T_n^h , using equation similar to eqn. (2.18) in the Helmert space on the co-geoid, and

taking the spherical approximation ($r \doteq R$),

$$\left(\Delta g_g^{h20}\right)_n \doteq \frac{GM}{R^2} (n-1) \left(\frac{a}{R}\right)^n T_n^h. \quad (3.37)$$

Now, substituting $\left(\Delta g_g^{h20}\right)_n$ from this equation into eqn. (3.35) we get

$$Dg_T \doteq \frac{GM}{2R^2} \sum_{n=0}^{\infty} (n-1) \left(\frac{a}{R}\right)^n Q_n^{*20}(H, \psi_0) T_n^h. \quad (3.38)$$

This is the formula employed to estimate the truncation error from a global geopotential model, e.g., GFZ93A, by taking $T_n^h \doteq T_n$.

In the process of downward continuation, the anomalies on the topography are known and anomalies on the co-geoid are to be determined. Thus, we are really interested in solving the inverse problem from what we have been discussing so far. This inverse problem implies that the system of equations (3.33) has to be solved. Denoting the mean anomalies on topography by vector \mathbf{b}^{20} and mean anomalies on the co-geoid by vector \mathbf{x}^{20} , the system of equations is abbreviated in a matrix notation as

$$\mathbf{b}^{20} = \mathbf{A}^{*20}(\psi_0) \mathbf{x}^{20} + \mathbf{t}^*(\psi_0), \quad (3.39)$$

where \mathbf{t}^* is the vector of the truncation errors, which is treated as a corrective quantity in the system.

The matrix \mathbf{A}^{*20} is non-symmetric, containing more zero elements than non-zero ones. It is regular and well conditioned when $5' \times 5'$ mean anomalies are considered. Its main diagonal elements are positive, smaller than 1 but larger than the off-diagonal elements. The off-diagonal elements grow even smaller in absolute value further away from the main diagonal.

For the downward continuation of $5' \times 5'$ mean Helmert's anomalies in an area of dimensions $17^\circ \times 22^\circ$ [Vaníček et al., 1996], the number of equations needed is large: $J=53856$. The direct solution of such a system of equations is not trivial and an iterative method has been employed by the authors. The iteration starts with the initial value

$$\mathbf{x}^{20(0)} = \mathbf{b}^{20} - \mathbf{t}^*. \quad (3.40)$$

To carry on with the iterations, the solution vector is corrected each time for the amount of the misclosure of the system. Iterations are continued until the convergence threshold of $10 \mu Gal$, in a Tchebyshev or a quadratic norm sense is met.

Downward continuation of $5' \times 5'$ mean Helmert anomalies in south-west Canada, [Vaníček et al., 1996] showed sizable values (hundreds of $mGal$) of a high-frequency character. The contribution of these values to the co-geoidal heights ranges between $0.10 m$ and $1.10 m$; interestingly it is positive everywhere, Fig. 3.6.

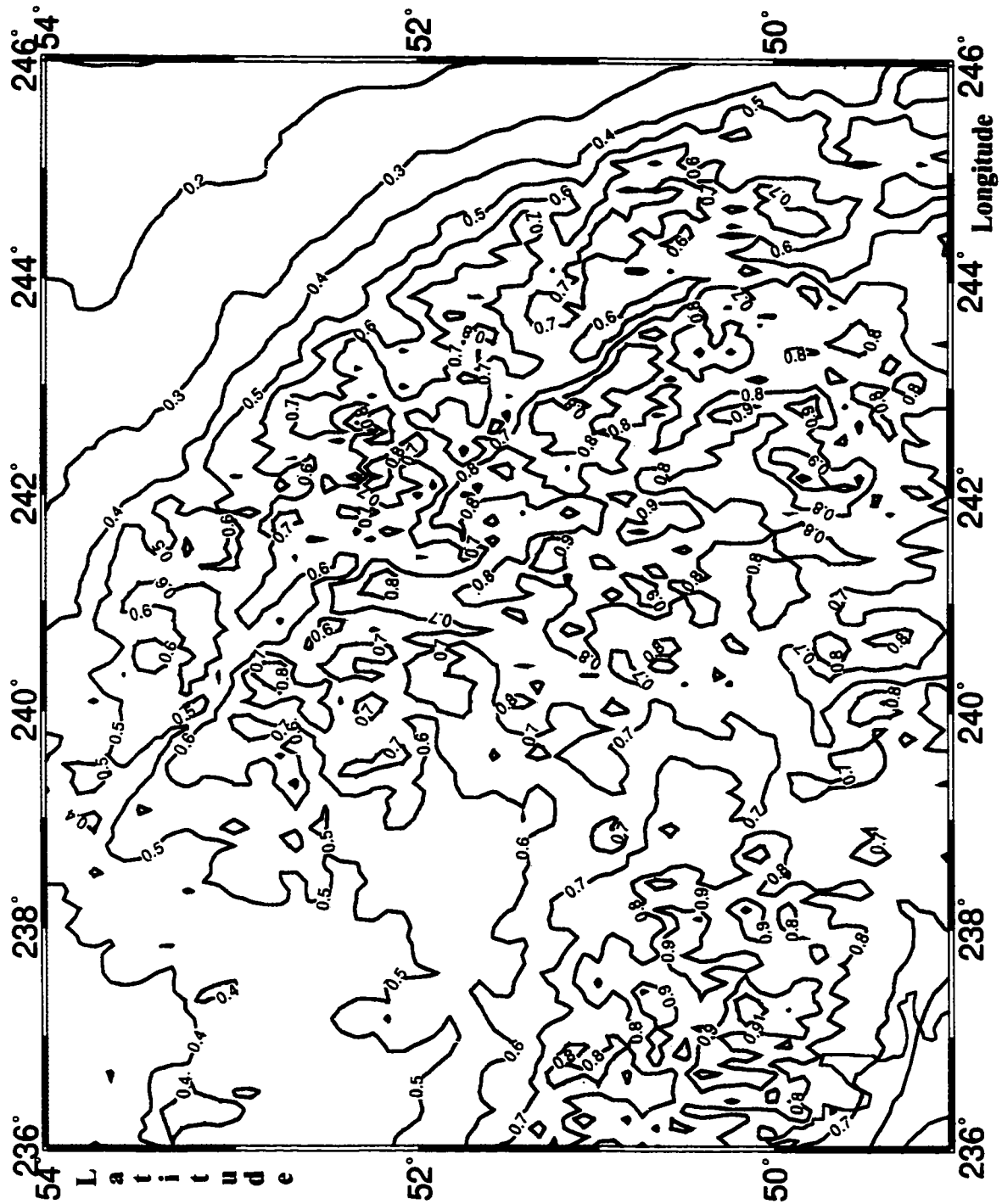


Figure 3.6: Contribution of downward continuation of Helmert's gravity anomaly to the Helmert co-geoid. Contour interval is 0.1 m.

Chapter 4

Numerical Results

4.1 Reference Quantities

4.1.1 Reference Spheroid of Degree 20 in Canada

Equation (2.101) describes the reference spheroid of degree L ($L=20$), using a satellite-derived disturbing potential. The equation as a harmonic series, could accommodate various geopotential models. In the least-squares adjustment of the GRIM4-S4 model [Schwintzer et al., 1995], an initial value of $GM^{\hat{}} = 0.398600440D + 15$ for the earth "geocentric constant" was selected. The 0-th degree coefficient was estimated as $\hat{W}_0 = 0.999999994D + 00$. This implies an a posteriori estimate of $GM^{\hat{}} = 0.3986004367D + 15$, which is different from the $GM^* = 0.3986005D + 15$ adopted for the GRS-80—the reference ellipsoid. This difference creates a 0-th degree term of

$$(N)_0 = -0.999 \text{ m}, \quad (4.1)$$

for the spheroid, referred to the ellipsoid. The estimation error is about $\pm 4 \text{ mm}$. The term is almost one metre and cannot be neglected. A different value of -1.025 m for $(N)_0$ was obtained for the GEM-T2 model [Marsh et al., 1990].

Figure 4.1 shows the spheroid of degree 20, denoted by N_{20} , referred to GRS-80, in Canada, using GRIM4-S4 geopotential model. The minimum and maximum values

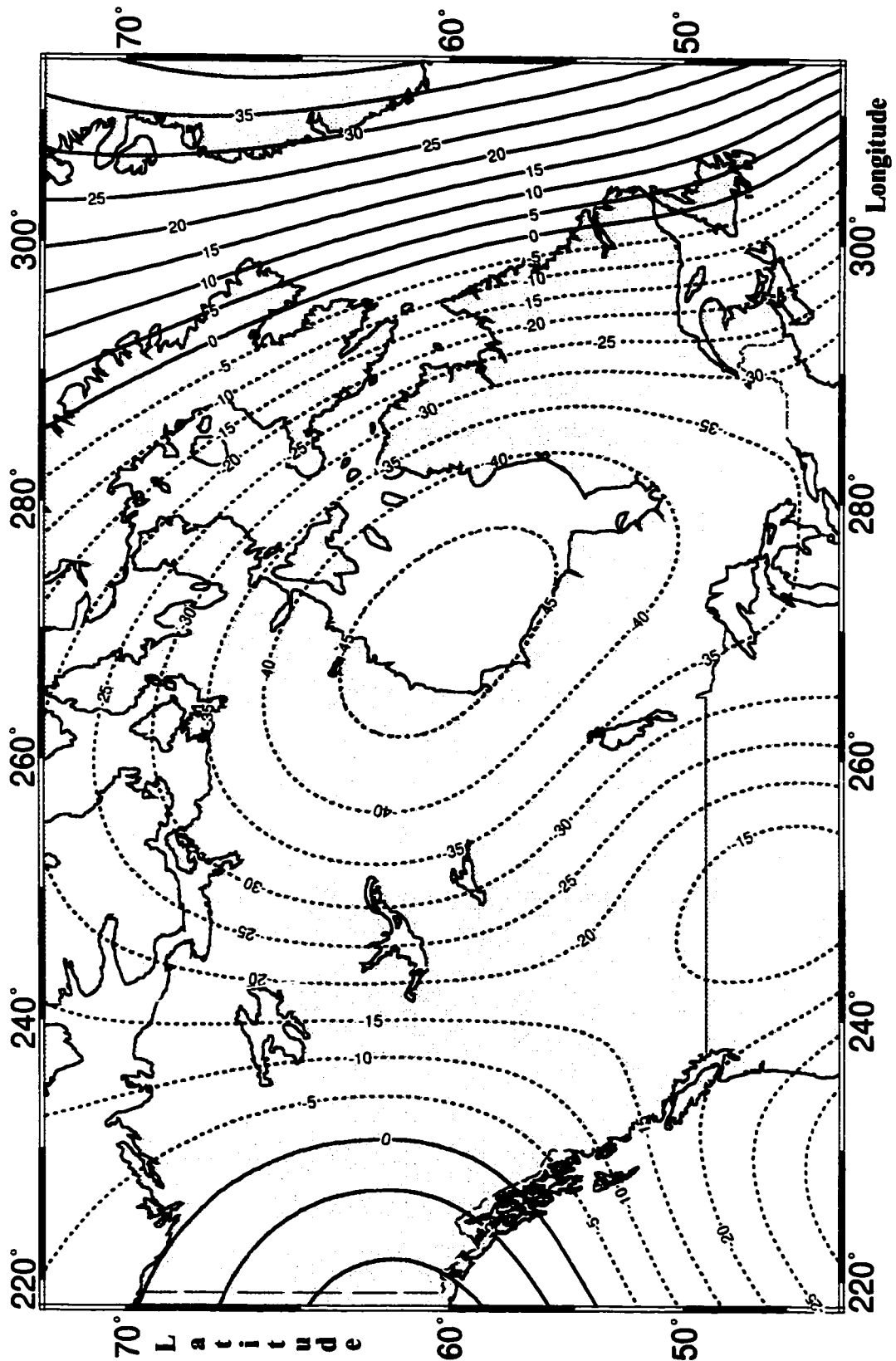


Figure 4.1: N_{20} derived from GRIM4-S4 model. Contour interval is 5 m.

of the spheroid, computed from different geopotential models are shown in Table 4.1.

Model Name	N_{20} [Min.(m), Max.(m)]	Mean Error(m)
GEM-T1 [Marsh et al., 1988]	-48.18, 42.89	1.06
GEM-T2 [Marsh et al., 1990]	-47.57, 43.68	0.90
GEM-T3S [Lerch et al., 1992]	-47.81, 43.02	0.28
GRIM4-S4	-47.38, 42.17	0.51

Table 4.1: Spheroid N_{20} in Canada and its mean "commission error"

The last column of the table shows the average "commission error" of the spheroids, an error due to the uncertainties associated with the satellite potential coefficients. This error is computed using eqn. (5.10).

The ellipsoidal correction to the spheroid, computed from the ellipsoidal correction on the potential (eqn. (2.99)), estimated from GRIM4-S4, ranges between $-0.88 m$ and $0.65 m$ in Canada, see Fig. 4.2. A higher-degree (higher than 2; the ellipsoid) approximation was obtained by evaluating the disturbing potential on the geoid, where we wrote

$$r_g(\Omega) = r_E(\Omega) + N_{20}(\Omega). \quad (4.2)$$

Then, the radial term in eqn. (2.97), attains a value

$$\left(\frac{\hat{a}}{r_E + N_{20}}\right)^{n+1} \doteq \left(\frac{\hat{a}}{r_E}\right)^{n+1} \left[1 - (n+1) \left(\frac{N_{20}}{r_E}\right) + \dots\right]. \quad (4.3)$$

This results in a maximum (absolute value) correction of $3 mm$, in addition to the ellipsoidal correction (approximation), to the spheroid in Canada, as shown in Fig. 4.3, and a maximum correction of $1 cm$ across the world not shown here). This "geoidal correction" can thus be safely neglected under present circumstances.

4.1.2 Reference Gravity Anomaly of Degree 20 in Canada

Reference gravity anomaly of degree 20 is computed using eqn. (2.38), evaluated on the geoid using the ellipsoidal approximation for r_g , i.e., putting $r_g \doteq r_E$.

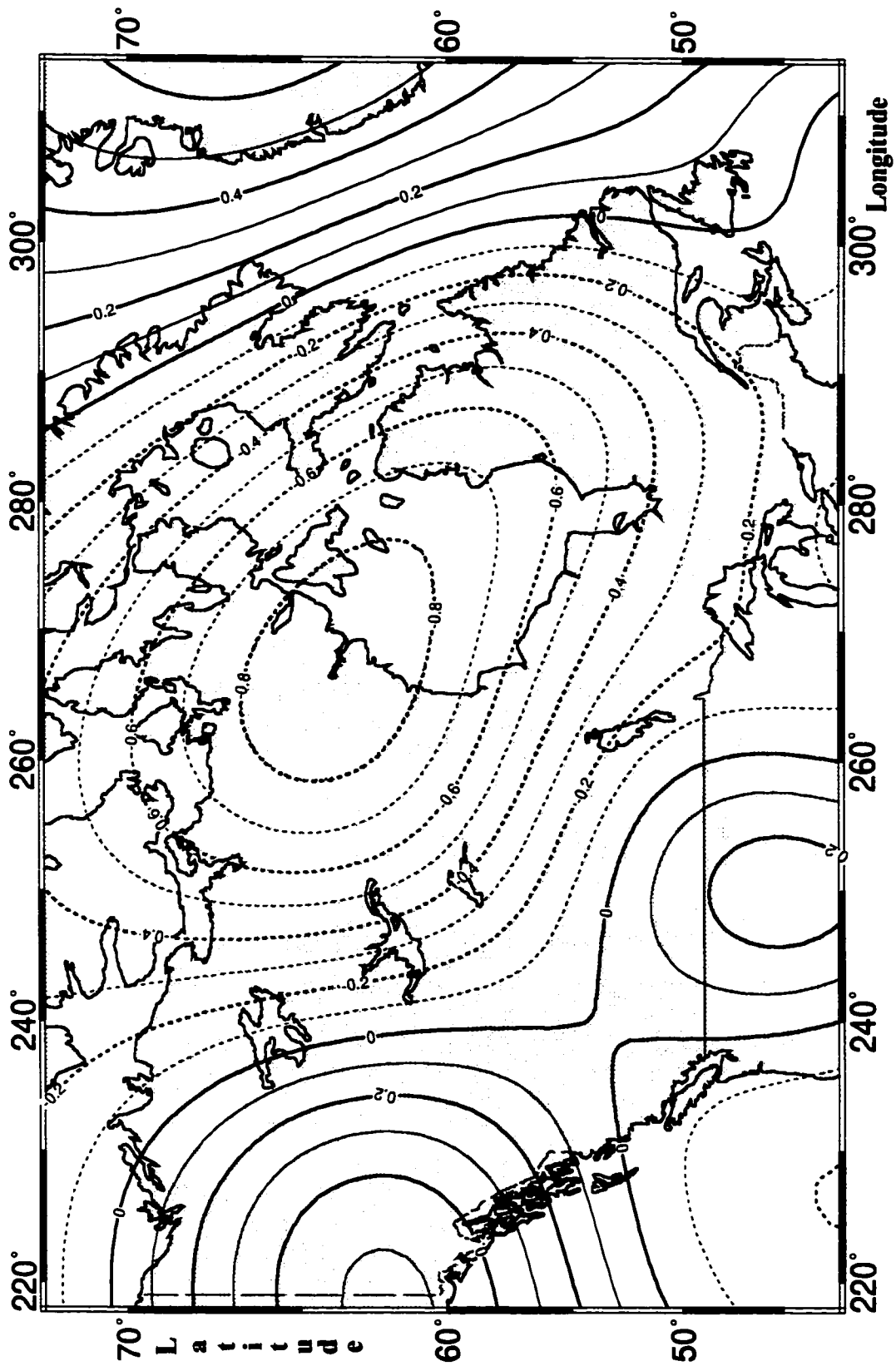


Figure 4.2: Ellipsoidal correction to N_{20} . Contour interval is 0.1 m .

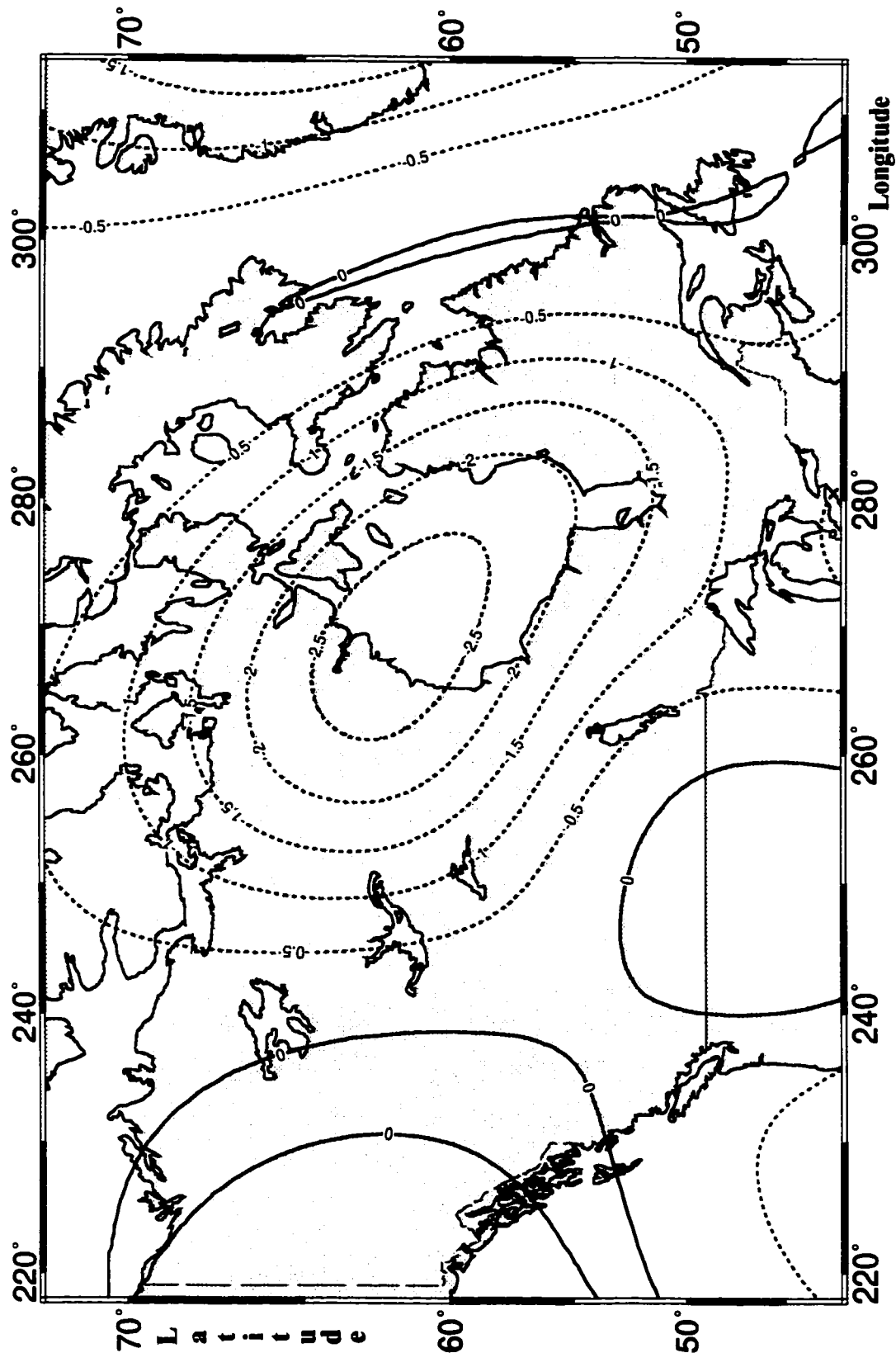


Figure 4.3: Higher-degree approximation of N_{20} , compared to the ellipsoidal approximation. Contour interval is 0.5 mm.

Figure 4.4 shows the reference gravity anomaly (Δg_{20}) in Canada, derived from the GRIM4-S4 model. Table 4.2 shows the minimum and maximum values and the mean "commission error" of the gravity anomaly, computed from different geopotential models.

Model Name	Min.(<i>mGal</i>),	Max.(<i>mGal</i>)	Mean Error (<i>mGal</i>)
GEM-T1	-43.484,	31.707	2.486
GEM-T2	-43.068,	33.654	2.134
GEM-T3	-43.740,	31.580	0.639
GRIM4-S4	-44.267,	29.745	1.223

Table 4.2: Δg_{20} in Canada and their mean "commission error"

The ellipsoidal correction, eqn. (2.100), to the reference gravity anomaly is shown in Fig. 4.5. The minimum and maximum values are -1.396 mGal and 1.093 mGal respectively.

4.2 Helmert's Reference Quantities in Canada

The residual topographical potential coefficients V_0 and V_{nm} , eqn. (2.71), were evaluated using squared topography, given by the TUG87 model. The direct topographical effect on spheroid, eqn. (2.93), was evaluated using ellipsoidal approximation. Figure 4.6 illustrates this effect, based on the conservation of the centre of mass of the earth. In Canada, the minimum and maximum values are -0.13 m and 0.18 m respectively. When condensation based on the conservation of mass of the earth is used, the extreme values in Canada change to -0.09 m and 0.25 m ; this result is not shown here.

The direct topographical effect on reference gravity (DTE_L), eqn. (2.86), evaluated on the geoid, using the ellipsoidal approximation is shown in Fig. 4.7, based on the conservation that conserves the centre of mass.

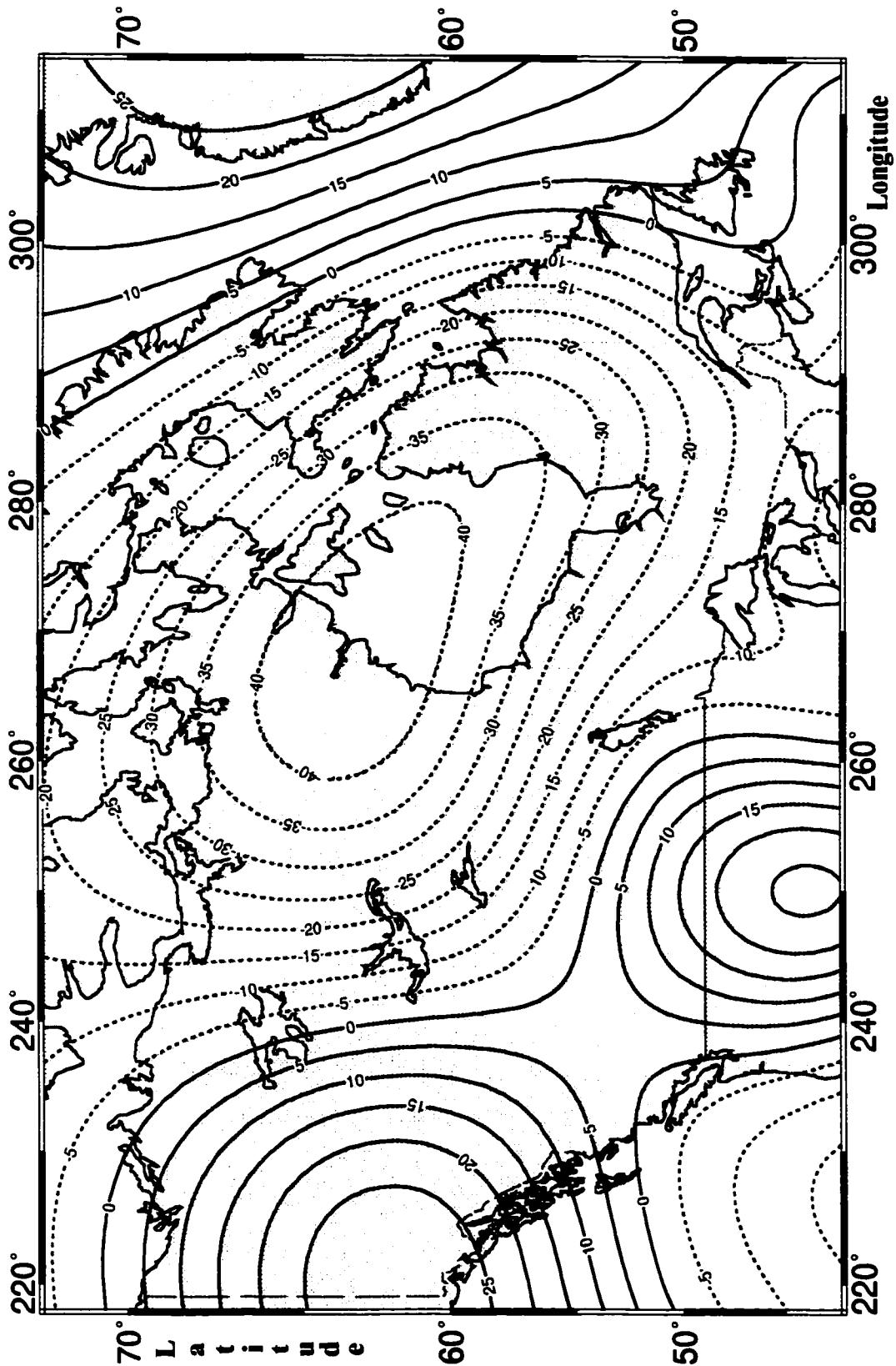


Figure 4.4: Δg_{20} derived from GRIM4-S4 model. Contour interval is 5 mGal.

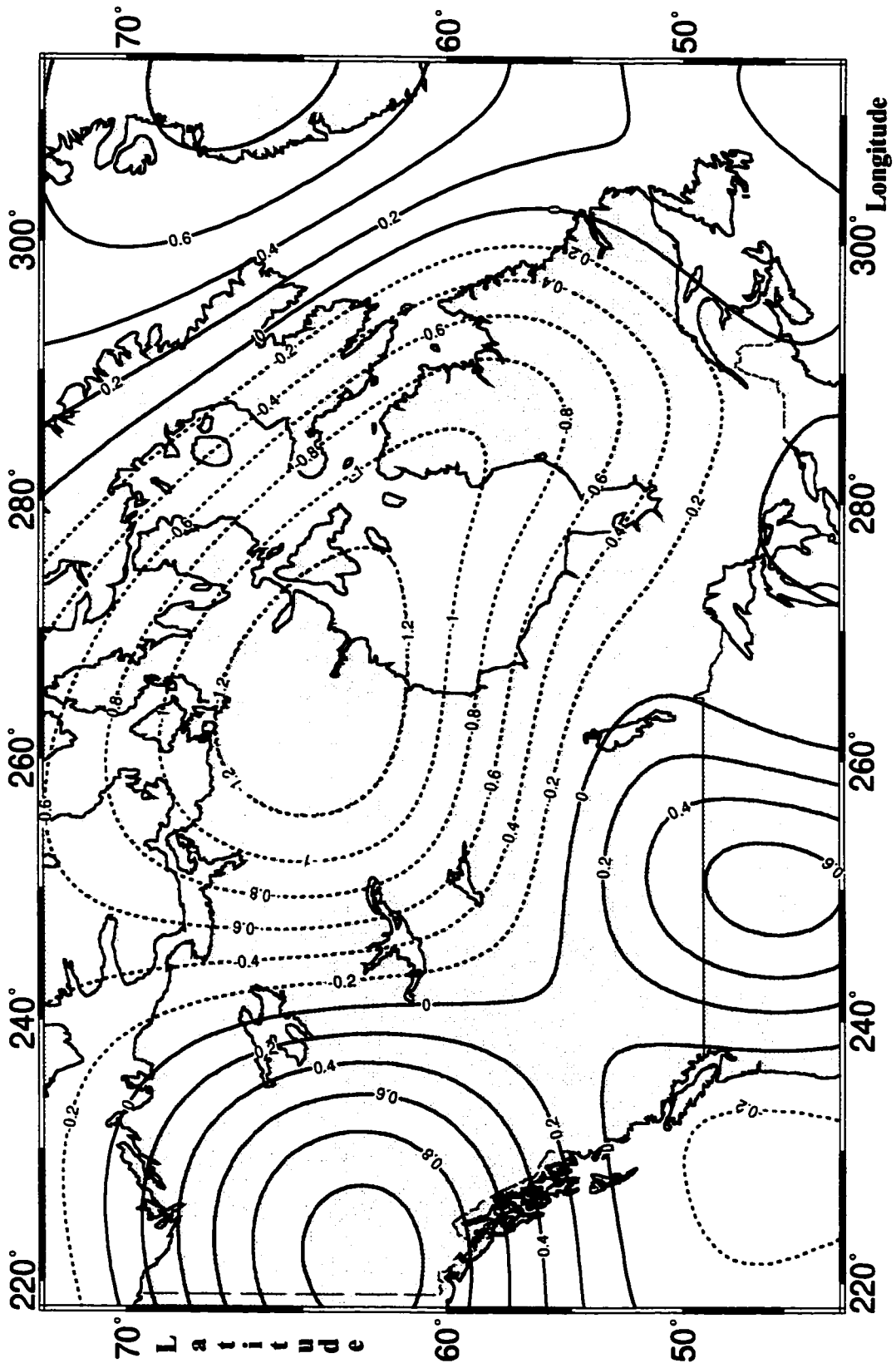


Figure 4.5: Ellipsoidal correction to Δg_{20} . Contour interval is 0.2 *mGal*.

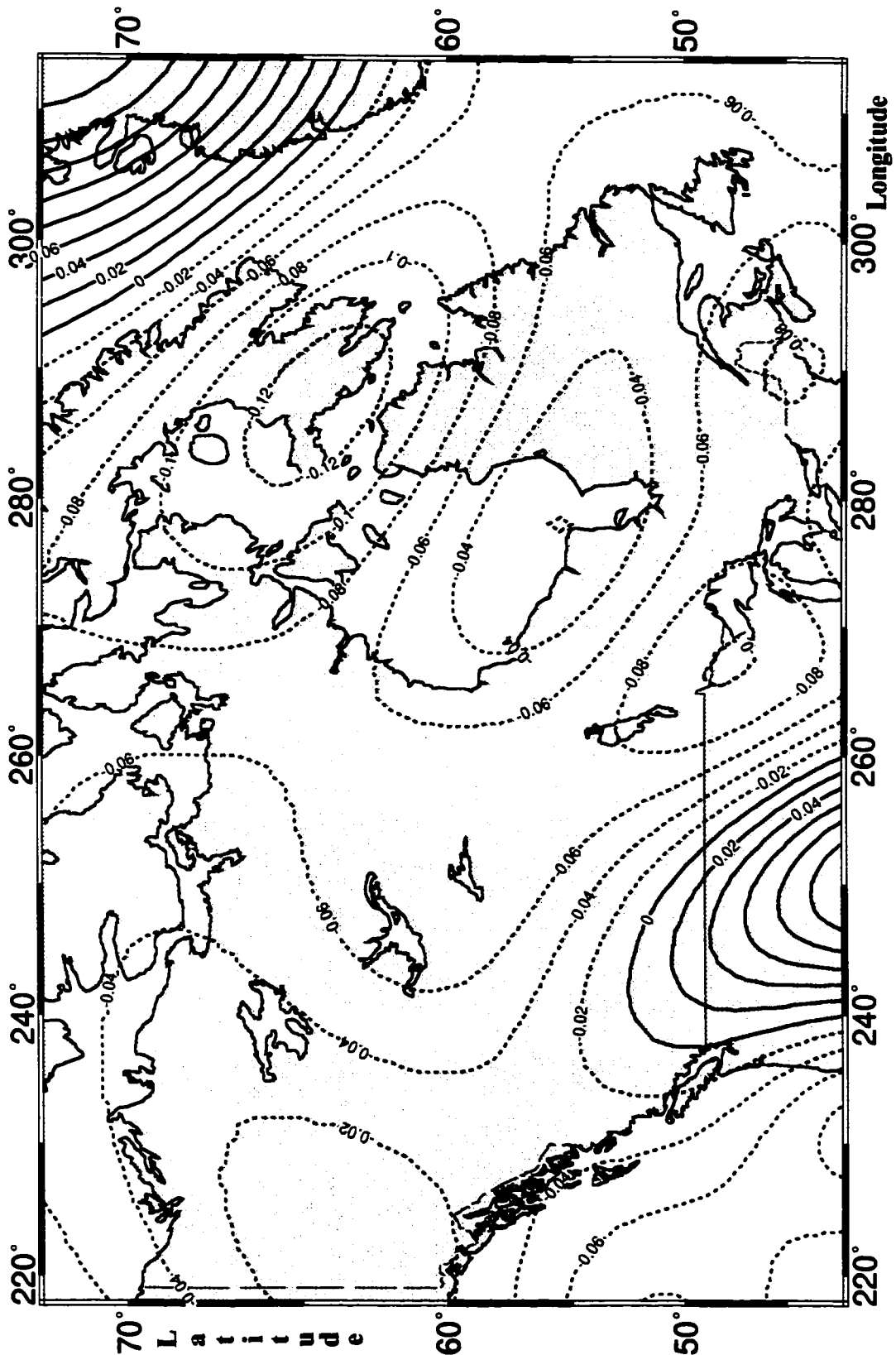


Figure 4.6: Direct topographical effect on spheroid, based on the centre of mass conservation model. Contour interval is 0.02 m.

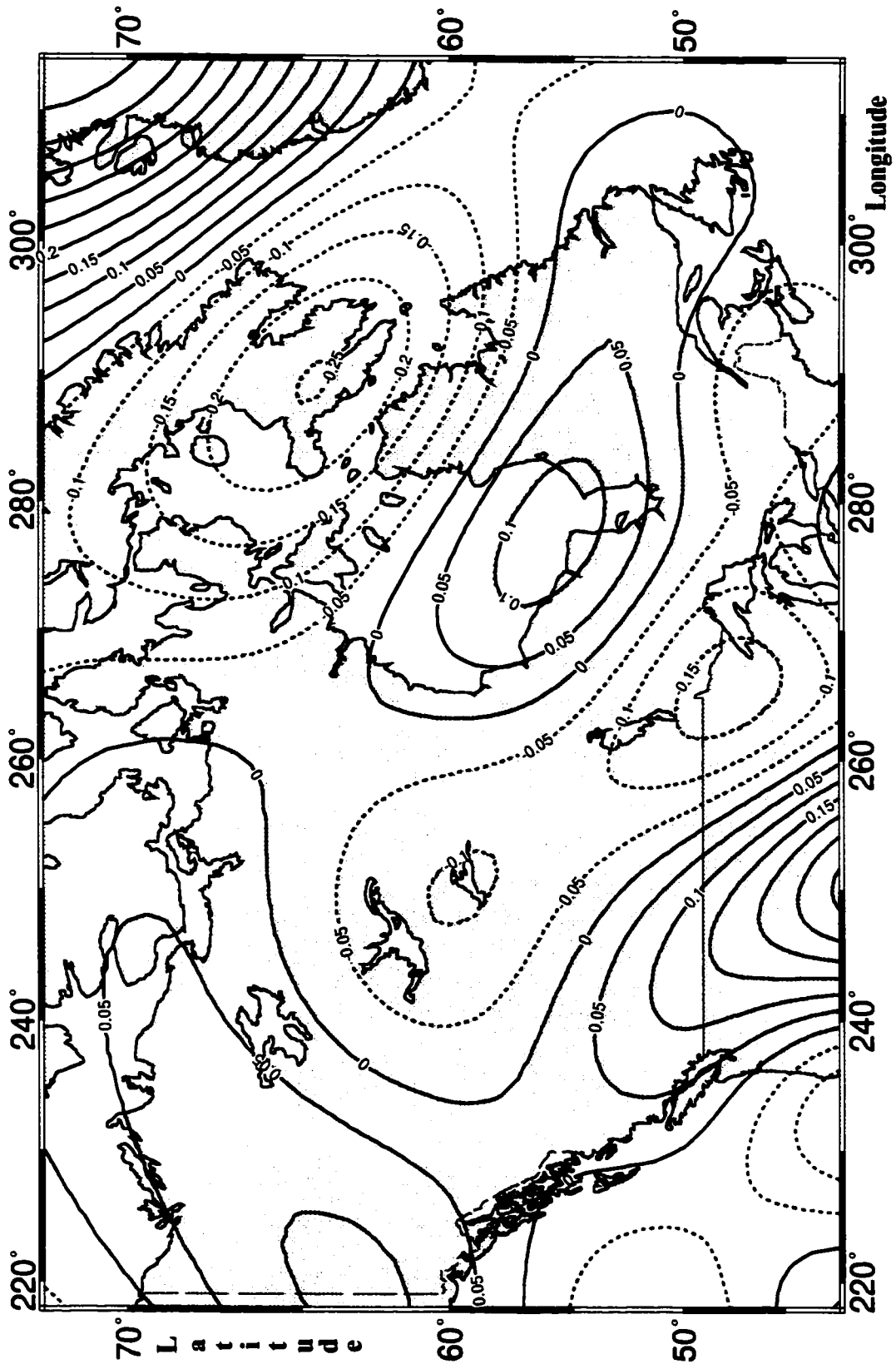


Figure 4.7: DTE_{20} , based on the centre of mass conservation model. Contour interval is 0.05 mGal .

The minimum and maximum values are -0.252 mGal and 0.500 mGal . These extreme values change to -0.258 mGal and 0.549 mGal when the other condensation model is applied.

The reference $SITE_L$ is the correction, before D_L^S , to be applied on the gravity anomaly. It was evaluated from eqn. (2.90). For the first condensation formula, it varies between -0.040 mGal , and 0.055 mGal in Canada, see Fig. 4.8. The last correction to the gravity anomaly is D_L^S , eqn. (2.103), with the extreme values -0.029 and 0.016 mGal in Canada, see Fig. 4.9.

Adding the direct topographical effect on spheroid (Fig. 4.6) to the N_{20} yields the Helmert reference spheroid, denoted by N_{20}^h , which can be also directly computed from eqn. (2.102). Applying the effect DTE_{20} (Fig. 4.7) to the Δg_{20} gives the Helmert reference gravity anomaly Δg_{20}^h , which could be also directly obtained from eqn. (2.87). The following Tables 4.3 and 4.4 show the range of variations of these Helmert reference quantities using different geopotential models.

Model Name	Min.(m),	Max.(m)
GEM-T1	-48.19,	42.75
GEM-T2	-47.57,	43.53
GEM-T3S	-47.81,	42.87
GRIM4-S4	-47.34,	42.09

Table 4.3: N_{20}^h in Canada

Model Name	Min.($mGal$),	Max.($mGal$)
GEM-T1	-43.486,	31.430
GEM-T2	-43.062,	33.346
GEM-T3	-43.729,	31.298
GRIM4-S4	-44.255,	29.639

Table 4.4: Δg_{20}^h in Canada

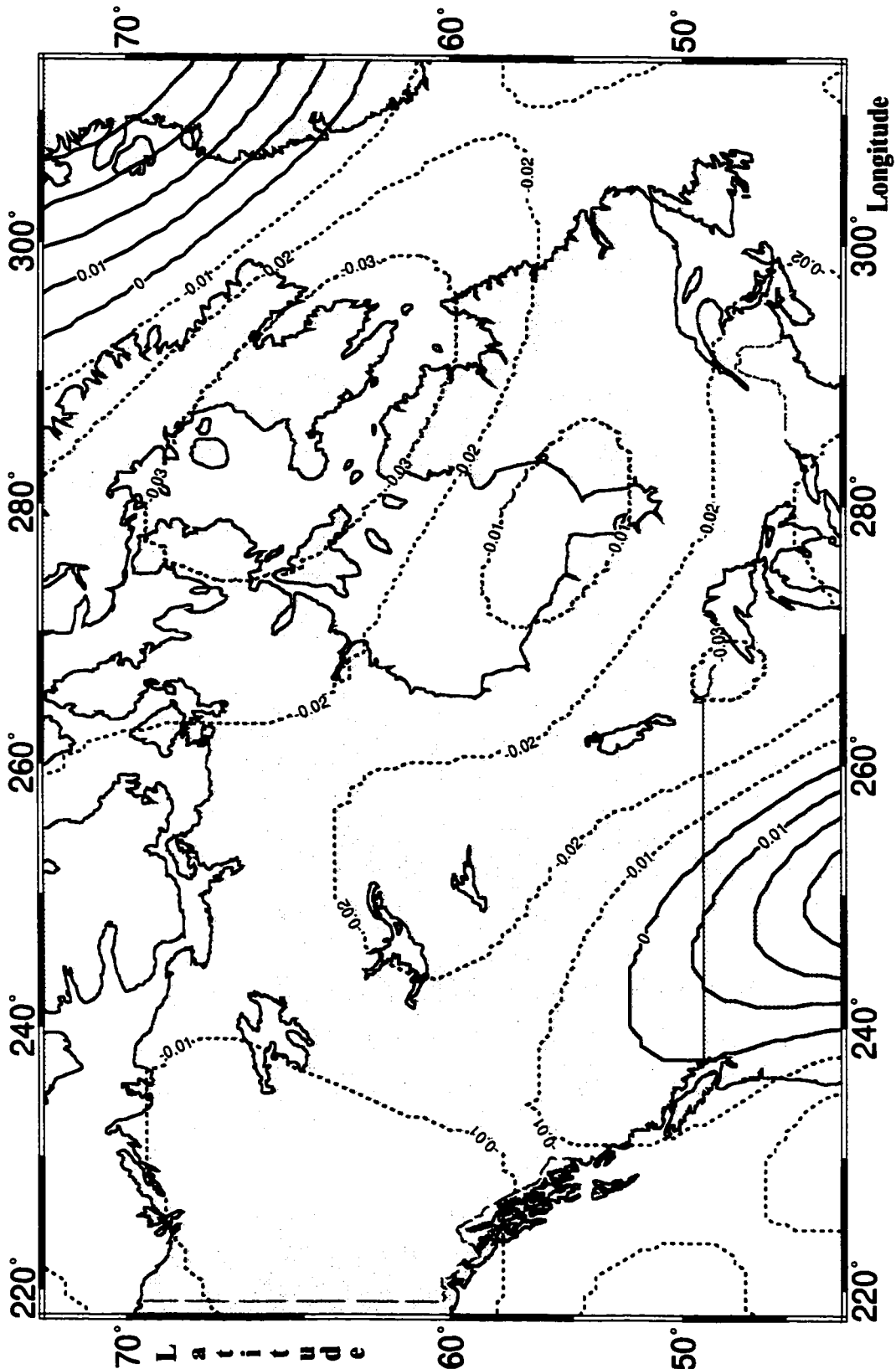


Figure 4.8: $SITE_{20}$, based on the centre of mass conservation model. Contour interval is 0.01 $mGal$.

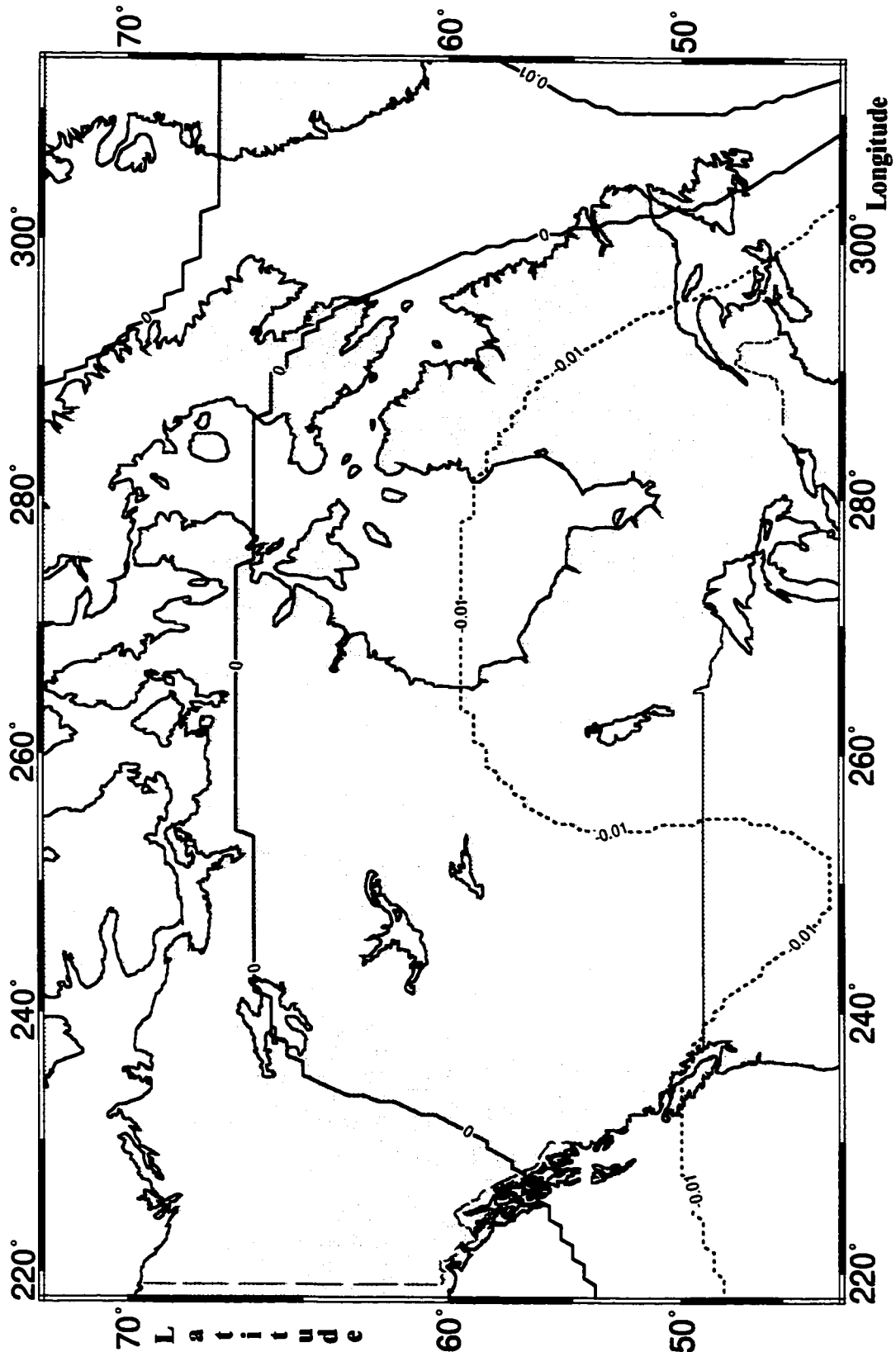


Figure 4.9: D_{20}^S (spherical correction to the Δg_{20}) in Canada. Contour interval is 0.01 mGal.

The Helmert spheroid, based on the conservation of the centre of mass condensation model, is geocentric by definition. It is, however, distorted in scale which shows as a constant depression of the geoid by 0.05 m along the vertical and can be described through the 0-th degree of the direct topographical effect on spheroid. The distortion is corrected when the *PITE*, based on the same conservation model, is applied to the Helmert co-geoid to obtain the final geoid.

Chapter 5

Accuracy of the Helmert Co-geoid

5.1 Introduction

In the Stokes-Helmert scheme, as it was shown, the geoid at each point is determined as the sum of the spheroid N_L^h (cf. eqn. (2.102)) and the residual geoid N^L (eqn. (3.1)). In this chapter, we will be talking about the accuracy of the geoid, rather than the Helmert co-geoid, i.e., ignoring the accuracy assessment of the transformations between real field and the Helmert space. By omitting the superscript "h" from the notations, and denoting N^L by δN^L we write

$$N = N_L + \delta N^L. \quad (5.1)$$

This new notation is used here to avoid confusion. For the error estimation, it is good enough to work with the spherical approximation of the spheroid:

$$N_L(\Omega) = R \sum_{n=0}^L T_n(\Omega), \quad (5.2)$$

[Vaníček and Krakiwsky, 1986], where R is the mean radius of the earth, $T_n(\Omega)$ are the surface harmonics of the disturbing potential, given by eqn. (2.13):

$$T_n(\Omega) = \sum_{m=0}^n [\bar{T}_{nm}^C \bar{Y}_{nm}^C(\Omega) + \bar{T}_{nm}^S \bar{Y}_{nm}^S(\Omega)], \quad (5.3)$$

and

$$\begin{pmatrix} \bar{Y}_{nm}^C(\Omega) \\ \bar{Y}_{nm}^S(\Omega) \end{pmatrix} = \begin{pmatrix} \cos m\lambda \\ \sin m\lambda \end{pmatrix} \bar{P}_{nm}(\sin \varphi) \quad (5.4)$$

are the fully normalized spherical harmonics, see eqns. (2.4). \bar{T}_{nm}^C and \bar{T}_{nm}^S are fully normalized satellite-derived disturbing potential coefficients.

The residual geoid is determined from the generalized Stokes integral, eqn. (3.1):

$$\delta N^L(\Omega) \doteq K \int \int_{C_0} \delta \Delta g^L(\Omega') S^{*L}(\psi(\Omega, \Omega')) d\Omega', \quad (5.5)$$

where

$$K = \frac{R}{4\pi\gamma_0}, \quad (5.6)$$

Ω' is the integration variable, ψ is a spherical distance, γ_0 is the normal gravity on the reference ellipsoid, and C_0 denotes the integration domain: a spherical cap of radius $\psi_0 = 6^\circ$ in our applications, and $\delta \Delta g^L$ is the residual Helmert gravity anomaly,

$$\delta \Delta g^L = \Delta g - \Delta g_L, \quad (5.7)$$

where Δg is the "observed" Helmert gravity anomaly and Δg_L is the (low-frequency) reference gravity anomaly.

5.2 Variance of the spheroid of degree L

For simplicity, let us omit the subscript L from the relevant symbols in this section, bearing in mind that all the discussion here is related to the spheroid of degree L . Uncertainties in the disturbing potential coefficients, are due to errors in the satellite potential coefficients estimated from satellite tracking. To estimate σ_N^2 , the variance of the spheroid, let us denote by σ_{nm}^2 the error variance of either cosine (\bar{T}_{nm}^C) or sine (\bar{T}_{nm}^S) satellite potential coefficients in eqn. (5.3). By applying covariance law to the equation, we get

$$\sigma_n^2(\varphi) = \sum_{m=0}^n \left[(\bar{Y}_{nm}^C(\Omega))^2 + (\bar{Y}_{nm}^S(\Omega))^2 \right] \sigma_{nm}^2, \quad (5.8)$$

where the sum in the square brackets (amplitude of the spherical harmonics) is derived from eqn. (5.4), resulting in

$$\sigma_n^2(\varphi) = \sum_{m=0}^n \overline{P}_{nm}^2(\sin \varphi) \sigma_{nm}^2, \quad (5.9)$$

where $\sigma_n^2(\varphi)$ is the error variance of the surface harmonic T_n and σ_{nm}^2 are the estimated variances from the satellite observations. The error variances $\sigma_n^2(\varphi)$ with respect to degree n , in different latitudes for the GRIM4-S4 "satellite only" model are shown in Fig. 5.1.

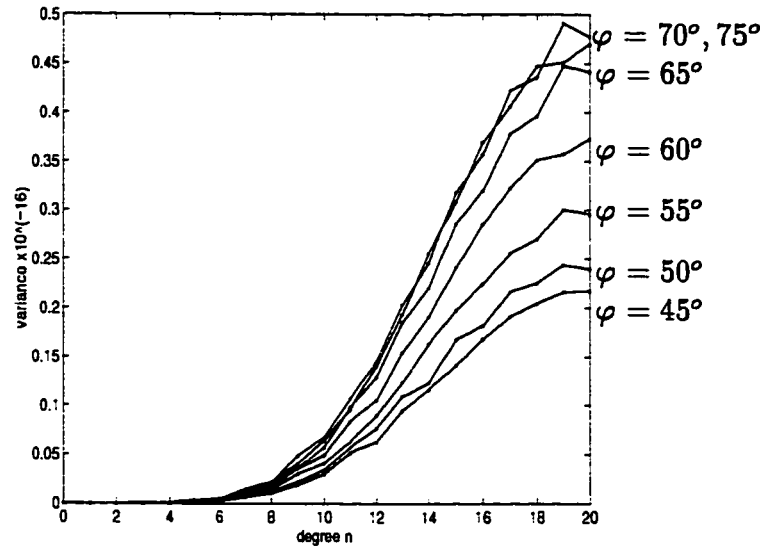


Figure 5.1: Accuracy (error variance) performance of GRIM4-S4 model in different latitudes

Applying now the covariance law to eqn. (5.2) yields

$$\sigma_N^2(\varphi) = R^2 \sum_{n=0}^L \sigma_n^2(\varphi), \quad (5.10)$$

where $\sigma_N^2(\varphi)$ is the variance of the spheroid, a function of the latitude of the computation point.

Let us look now at ΔN , the spheroidal height difference between points P_i and P_j ,

$$\Delta N = N_j - N_i. \quad (5.11)$$

The spheroidal heights N_i and N_j , determined from satellite potential coefficients at two points are statistically correlated. The correlation comes from the fact that the same potential coefficients are used in both computations. Applying the covariance law to eqn. (5.11), the variance of ΔN is obtained as

$$\sigma_{\Delta N}^2 = \sigma_N^2(P_i) + \sigma_N^2(P_j) - 2C_N(P_i, P_j), \quad (5.12)$$

where σ_N^2 is given by eqn. (5.10) and C_N is the error covariance function. It is expressed in terms of the error correlation function ρ_N as

$$C_N(P_i, P_j) = \rho_N(P_i, P_j) \sigma_N(P_i) \sigma_N(P_j). \quad (5.13)$$

To estimate $\sigma_{\Delta N}^2$, one has to estimate the two variances $\sigma_N^2(P_i)$, $\sigma_N^2(P_j)$, and the value of $C_N(P_i, P_j)$.

To derive the error covariance $C_N(P_i, P_j)$, let us assume a vector of spheroidal heights N computed at a mesh of m points, using satellite coefficients (see eqns. (5.2) and (5.3)). Let Φ be the Vandermonde matrix comprised of the spherical harmonic functions and t the vector of satellite-derived coefficients for the disturbing potential T (eqn. (5.3)). The following matrix equation is then valid,

$$N = \Phi^T t. \quad (5.14)$$

There is an estimated error covariance matrix (fully populated) associated with the vector t , derived from the adjustment of the satellite observations. Let us denote it by \hat{C}_t . Applying covariance law to the equation (above) yields the covariance matrix of N ;

$$C_N = \Phi^T \hat{C}_t \Phi. \quad (5.15)$$

The error covariance $C_N(P_i, P_j)$, the element located at i -th row and j -th column of the matrix C_N , is a quadratic form obtained as

$$C_N(P_i, P_j) = \Phi_i^T \hat{C}_t \Phi_j. \quad (5.16)$$

where Φ_i and Φ_j are the i -th and j -th columns of the Vandermonde matrix. Assuming a diagonal matrix \hat{C}_t , and considering eqns. (5.2) and (5.3) we obtain,

$$C_N(P_i, P_j) = R^2 \sum_{n=0}^L \sum_{m=0}^n \sigma_{nm}^2 \left[\bar{Y}_{nm}^C(\Omega_i) \bar{Y}_{nm}^C(\Omega_j) + \bar{Y}_{nm}^S(\Omega_i) \bar{Y}_{nm}^S(\Omega_j) \right], \quad (5.17)$$

where σ_{nm}^2 is the error variance of the satellite coefficients, Ω_i and Ω_j are the locations of points P_i and P_j .

The covariance function can now be computed, given the accuracy of the satellite coefficients. Fig. 5.2 illustrates the error variance as a function of degree n ($\sigma_n^2 = \sum_{m=0}^n 2\sigma_{nm}^2$), the error power spectrum of the gravity field determination by GRIM4-S4 global geopotential model [Schwintzer et al., 1995]. Fig. 5.3 shows the covariance function (eqn. (5.17)), along a meridian of the spheroid of degree 20, determined by the same model.

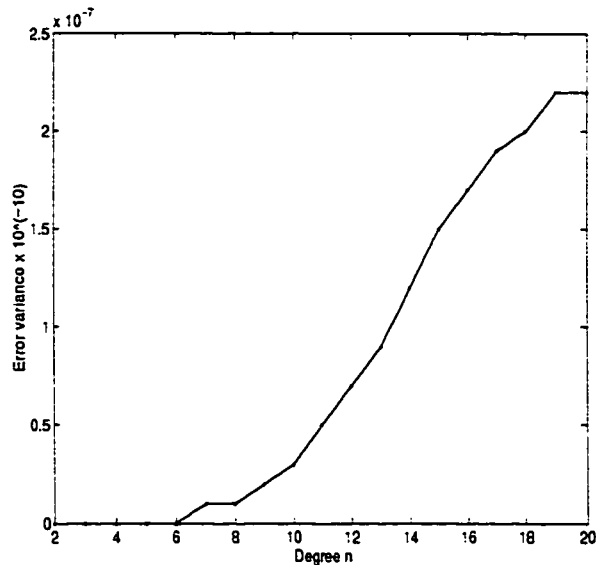


Figure 5.2: Error power spectrum of the GRIM4-S4 model

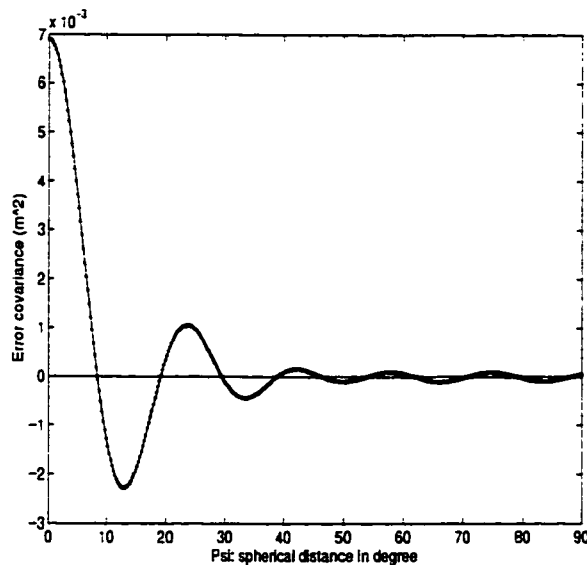


Figure 5.3: Error covariance function of the spheroid of degree 20 along a meridian

5.3 Variance of δN and $\Delta(\delta N)$

In this section, we also omit L , simplifying δN^L to δN . The residual geoid δN obtained from the Stokes integral (eqn. (5.5)) is subject to errors in the gravity anomalies $\delta \Delta g^L$ in the integration domain. The error variance of the geoid is derived by the covariance law applied to the Stokes integral. Let us call this variance by $\sigma_{\delta N}^2$. It will be derived in the next section.

The difference between residual geoidal heights at points P_i and P_j is given as

$$\Delta(\delta N) = \delta N_j - \delta N_i, \quad (5.18)$$

where δN_j or δN_i are both determined from eqn. (5.5). By applying the covariance law to eqn. (5.18), the variance of $\Delta(\delta N)$ is obtained as

$$\sigma_{\Delta(\delta N)}^2 = \sigma_{\delta N}^2(P_i) + \sigma_{\delta N}^2(P_j) - 2C_{\delta N}(P_i, P_j), \quad (5.19)$$

where $C_{\delta N}$ is the error covariance function of the residual geoid. It is related to the correlation function $\rho_{\delta N}$ by

$$C_{\delta N}(P_i, P_j) = \rho_{\delta N}(P_i, P_j) \sigma_{\delta N}(P_i) \sigma_{\delta N}(P_j). \quad (5.20)$$

5.3.1 Covariance of δN

Let us consider the errors in residual gravity anomalies $\delta\Delta g$ used in the Stokes integration to be statistically independent. The gravity anomalies are really not independent; they are at least correlated through errors in the reference gravity anomalies, see eqn. (5.7). Dealing with this problem is out of the scope of this paper. Assuming independent anomalies, the errors of geoidal heights δN_i and δN_j , computed at two points farther than $\psi = 12^\circ$ apart, would be statistically independent; the distance of 12° equals to twice the radius of the integration domain and for $\psi \geq 12^\circ$, there is no overlap of the two integration domains. The statistical correlation will arise though if some data are shared by the two integrals. This will be the case for points closer than 12° , i.e., when the integration domains intersect, see Fig. 5.4.

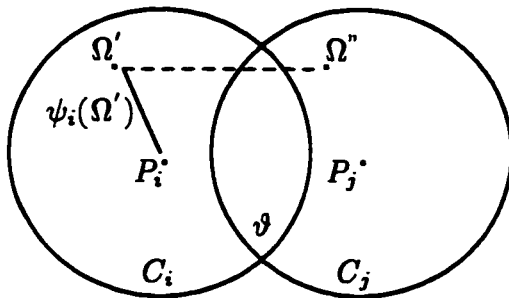


Figure 5.4: Intersection of the integration domains

The area $\vartheta = C_i \cap C_j$ contains the gravity data shared by the integrations over C_i and C_j .

To formulate the covariance function $C_{\delta N}$ (eqn. (5.20)), we again employ an algebraic approach. Denoting by δN the vector of the geoidal heights computed at a mesh of m points, and $\delta\Delta g$ the vector of gravity data required by the Stokes integral to compute δN , we can write the following system of linear equations

$$\delta N = S \delta\Delta g, \quad (5.21)$$

where S is the Stokes matrix operator, with its elements

$$s_{ik} = K_i S^{*L}(\psi_{ik}) \Delta a_{ik}, \quad (5.22)$$

being the values of the Stokes kernel ($S^{*L}(\psi_{ik})$) multiplied by the area of the surface integration element (Δa_{ik}) at the gravity point P_k and by K_i (see eqn. (5.5)). The kernel S^{*L} runs through the spherical cap C_i of radius $\psi = 6^\circ$, centred at point P_i . In other words, the i -th row vector of the matrix S multiplied by the vector $\delta \Delta g$ equals to the numerical integration (summation) of the Stokes's integral (over the cap C_i), resulting in the numerical value of residual geoidal height δN_i (element of vector δN).

Applying the covariance law to eqn. (5.21) yields

$$C_{\delta N} = S C_{\delta \Delta g} S^T, \quad (5.23)$$

where $C_{\delta \Delta g}$ is the covariance matrix of the gravity anomalies. The element c_{ij} of the matrix $C_{\delta N}$, is the covariance between δN_i and δN_j . This element can be obtained from the matrix equation (above) as the quadratic form

$$c_{ij} = S_i C_{\delta \Delta g} S_j^T, \quad (5.24)$$

where S_i and S_j are the i -th and j -th row vectors of the matrix S . The operator S_i , in the spherical coordinates system, has the form

$$S_i = [\dots, K_i S_i^{*L}(\Omega') \sin \psi_i(\Omega'), \dots], \quad (5.25)$$

where $\sin \psi_i(\Omega')$ is the Jacobian of the transformation to the spherical coordinates system and $\psi_i(\Omega')$ is the spherical distance of point " Ω' " (Fig. 5.4) from point P_i .

The compact form of c_{ij} , denoted by $C_{\delta N}(P_i, P_j)$ in eqn. (5.20) can be now written as

$$c_{ij} = C_{\delta N}(P_i, P_j) = K_i K_j \times \int \int_{C_i} S_i^{*L}(\Omega') \sin \psi_i(\Omega') \left(\int \int_{C_j} S_j^{*L}(\Omega'') \sin \psi_j(\Omega'') C_{\delta \Delta g}(\Omega', \Omega'') d\Omega'' \right) d\Omega', \quad (5.26)$$

where Ω' and Ω'' are two points in the domain $\mathfrak{R} = C_i \cup C_j$ (Fig. 5.4), $S_i^{*L}(\Omega')$ is the Stokes kernel defined in the cap C_i , $S_j^{*L}(\Omega'')$ is the kernel defined in the cap C_j , $\psi_j(\Omega'')$ is the spherical distance of point " Ω'' " from the centre P_j , K_i is the Stokes constant at P_i the centre of C_i , K_j is the constant at P_j ; the centre of C_j , and $C_{\delta\Delta g}(\Omega', \Omega'')$ is the covariance function (a kernel) defined for the pairs of points Ω' and Ω'' . The covariance function represents those "elements" of the covariance matrix $C_{\delta\Delta g}$ (eqn. (5.23)), in the compact space, that are contained in the domain \mathfrak{R} .

Assuming independent gravity anomalies ($\delta\Delta g$), the covariance function $C_{\delta\Delta g}(\Omega', \Omega'')$ reduces to a Dirac delta function [Korn and Korn, 1968], defined as

$$C_{\delta\Delta g}(\Omega' - \Omega'') = \begin{cases} 0 & \text{for } \Omega' \neq \Omega'' \\ \sigma_{\delta\Delta g}^2(\Omega') & \text{for } \Omega' = \Omega'' \end{cases}, \quad (5.27)$$

where $\sigma_{\delta\Delta g}^2(\Omega')$ is the variance of gravity anomaly at point Ω' . Taking the delta function into account, the eqn. (5.26) reduces to

$$C_{\delta N}(P_i, P_j) = K_i K_j \int \int_{C_i} S_i^{*L}(\Omega') S_j^{*L}(\Omega') \sin \psi_j(\Omega') \sin \psi_i(\Omega') \sigma_{\delta\Delta g}^2(\Omega') d\Omega'. \quad (5.28)$$

Further, the kernel $S_j^{*L}(\Omega')$ is different from 0 only in a portion of C_i , i.e., in the area ϑ . Hence, the integration domain (C_i) is reduced to ϑ ;

$$C_{\delta N}(P_i, P_j) = K_i K_j \int \int_{\vartheta} S_i^{*L}(\Omega') S_j^{*L}(\Omega') \sin \psi_j(\Omega') \sin \psi_i(\Omega') \sigma_{\delta\Delta g}^2(\Omega') d\Omega'. \quad (5.29)$$

This is the covariance function between residual geoidal heights (δN), at points P_i and P_j , see Fig. 5.4.

A special case of this function is the variance function $\sigma_{\delta N}^2(\Omega_i)$ at point P_i , when P_j moves towards the P_i , yielding

$$\sigma_{\delta N}^2(\Omega_i) \doteq K_i^2 \int \int_{C_i} [S_i^{*L}(\Omega') \sin \psi_i(\Omega')]^2 \sigma_{\delta\Delta g}^2(\Omega') d\Omega'. \quad (5.30)$$

As P_j moves to P_i , the integration domain ϑ increases to C_i . Writing variances at points P_i and P_j , and assuming uniform accuracy ($\sigma_{\delta N}^2(\Omega')$) for the gravity anomalies, and taking $K_i \doteq K_j$, the correlation function $\rho_{\delta N}$ is obtained from eqn. (5.20).

Substituting for the covariance and variances from eqns. (5.29) and eqn. (5.30) we get

$$\rho_{\delta N}(P_i, P_j) = \frac{\int \int_{\vartheta} S_i^{*L}(\Omega') S_j^{*L}(\Omega') \sin \psi_j(\Omega') \sin \psi_i(\Omega') d\Omega'}{\sqrt{\int \int_{C_i} [S_i^{*L}(\Omega') \sin \psi_i(\Omega')]^2 d\Omega'} \sqrt{\int \int_{C_j} [S_j^{*L}(\Omega') \sin \psi_j(\Omega')]^2 d\Omega'}}, \quad (5.31)$$

and realizing that $C_i = C_j = C_0$, we finally get

$$\rho_{\delta N}(P_i, P_j) = \frac{\int \int_{\vartheta} S_i^{*L}(\Omega') S_j^{*L}(\Omega') \sin \psi_j(\Omega') \sin \psi_i(\Omega') d\Omega'}{\int \int_{C_0} [S_0^{*L}(\Omega') \sin \psi_0(\Omega')]^2 d\Omega'}, \quad (5.32)$$

where $S_0^{*L}(\Omega')$ is the Stokes kernel, defined in the spherical cap C_0 . Clearly, as $P_j \rightarrow P_i$, $\rho_{\delta N}(P_i, P_j) \rightarrow 1$, as it should.

5.3.2 Numerical evaluation of the $\rho_{\delta N}$

The correlation function can now be numerically evaluated. The modified spheroidal Stokes kernel can be approximated within the 6° spherical cap by the function

$$S'(\psi) \doteq -32.43544 + \frac{1.99727}{\psi} - 3.44927 \ln\left(\frac{\psi}{2}\right) - 173.24417 \psi^2 \ln\left(\frac{\psi}{2}\right), \quad (5.33)$$

to the accuracy of better than 10^{-3} [Vaníček and Kleusberg, 1987]. The correlation function, eqn. (5.32), is the ratio of two surface integrals. In the denominator is the integral of the squared Stokes's kernel over the whole spherical cap of radius $\psi_0 = 6^\circ$. The integrand is singular at the centre of the cap, but the singularity is removed in the spherical coordinates system. The integral is finite and equals approximately to 0.9558. We note that this number seems to be acceptably close to 1.

The integral in the numerator is taken over the intersection area ϑ , and involves the product of two kernels, referred to points P_i and P_j , Fig. 5.5. The integral is written in a more explicit form as

$$\int \int_{\vartheta} S^{*L}(\psi_i(\Omega_i, \Omega')) S^{*L}(\psi_j(\Omega_j, \Omega')) \sin \psi_j(\Omega') \sin \psi_i(\Omega') d\Omega', \quad (5.34)$$

where Ω_i and Ω_j define the points P_i and P_j , ψ_i and ψ_j are the spherical distances, and Ω' defines the dummy point P' . At a first look, the integral seems to be a function of Ω_i and Ω_j , but writing the integral in the polar coordinate system at the pole P_i with polar coordinates of ψ_i and α (azimuth) as

$$I(\psi) = \int \int_{\vartheta} S^{*L}(\psi_i) S^{*L}(\psi_j(\psi, \psi_i, \alpha)) \sin \psi_j(\psi, \psi_i, \alpha) \sin \psi_i d\psi_i d\alpha, \quad (5.35)$$

where ψ_j (see the triangle $P_i P' P_j$) is a function of ψ_i , ψ , and the azimuth α , shows that the integral is really a function of ψ —the spherical distance between points P_i and P_j .

For the numerical evaluation of the correlation function, a planar approximation is employed: the spherical caps C_i and C_j are regarded as plane circles. Fig. 5.5 illustrates the case of $\psi < \psi_0$. In this case, the area of the integration is divided into four quadrants: OAD , OAB , OBC , and OCD . Because the Stokes kernel is homogeneous and isotropic, the integral over the area ϑ equals to four times the integral over, for instance, the area OAB ,

$$I(\psi) = 4 \int \int_{(OAB)} S^{*L}(\psi_i) S^{*L}(\psi_j) \sin \psi_j \sin \psi_i d\psi_i d\alpha. \quad (5.36)$$

In the area (OAB) , the kernel $S^{*L}(\psi_i)$ remains a regular function, while the kernel $S^{*L}(\psi_j)$ is singular at point P_j . The integration is carried out in the polar coordinate system with origin at P_i , and the singularity is treated separately. In the case $\psi > \psi_0$, see, i.e., Fig. 5.4, the integration can be again divided into 4 segments in the same coordinate system, provided that there would be no singularity of the Stokes kernels in this case. The correlation function obtained is shown in Fig. 5.6; it decreases monotonically, from unity at the 0° spherical distance to zero at a spherical distance of 12° . The integration was performed numerically for $\psi \in < 0, 12^\circ >$ at a step of 0.01 arc degree in both variables. For practical applications, the correlation function can be approximated by the following function

$$\rho_{\delta N}(\psi) = 1 + a \ln(1 + \psi) + b \psi^3, \quad (5.37)$$

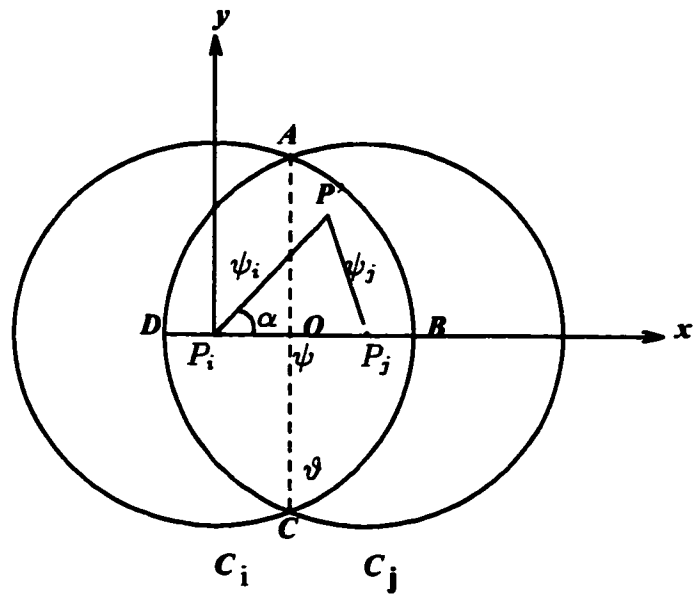


Figure 5.5: Integration over the area ϑ , for $\psi < \psi_0$

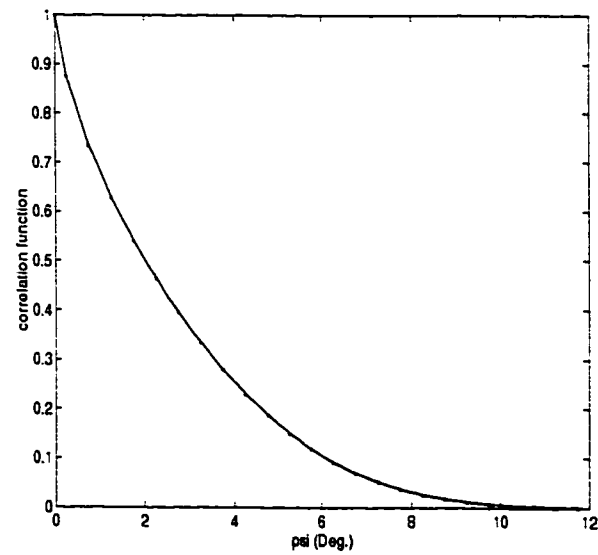


Figure 5.6: Correlation function of the residual geoid

to the accuracy of 0.01 (root mean squares error of fit), where

$$a = -0.46824364,$$

$$b = +0.00012060,$$

for ψ expressed in arc degrees.

5.3.3 Relative Accuracy of the Geoid

Accuracy of the geoid, σ_N^2 , is obtained from eqn. (5.1) by applying the covariance law;

$$\sigma_N^2 = \sigma_{N_L}^2 + \sigma_{\delta N^L}^2, \quad (5.38)$$

where on the right hand side are the variances of the spheroid and the residual geoid, considered here independent. In fact, these variances are statistically dependent (correlated), due to the use of Δg_L in derivation of $\delta \Delta g^L$ (see eqn. (5.7)). The correlations call for a separate investigation.

For the investigation of relative accuracy, eqn. (5.1) is re-written for the differences of quantities involved, as

$$\Delta N = \Delta N_L + \Delta(\delta N^L). \quad (5.39)$$

For the reason just discussed, the relative quantities (above) are also correlated. In the case of a higher degree spheroid (360×360) being used as a reference [She et al., 1993], there are even correlations between Δg_L and the "observed" Δg too. Assuming independency and applying the variance law to eqn. (5.39), we obtain the error variance of the geoid difference as the sum,

$$\sigma_{\Delta N}^2 = \sigma_{\Delta N_L}^2 + \sigma_{\Delta(\delta N^L)}^2, \quad (5.40)$$

of the variances of the two components.

After the correlation functions for the spheroid and the residual geoid are derived (eqns. (5.12) and (5.19)), they are added together to give the variance of the total

geoidal height differences. We obtain:

$$\begin{aligned} \sigma_{\Delta N}^2 &= \sigma_N^2(P_i) + \sigma_N^2(P_j) - 2\rho_N(P_i, P_j) \sigma_N(P_i) \sigma_N(P_j) + \\ &\quad \sigma_{\varepsilon N}^2(P_i) + \sigma_{\varepsilon N}^2(P_j) - 2\rho_{\varepsilon N}(P_i, P_j) \sigma_{\varepsilon N}(P_i) \sigma_{\varepsilon N}(P_j). \end{aligned} \quad (5.41)$$

Chapter 6

Conclusions and recommendations

6.1 The Stokes-Helmert Scheme

For the precise transformation of the "observed" gravity anomaly Δg_t on the topography to the Helmert gravity anomaly Δg_h^* on the geoid, eqn. (1.25), the series of corrections comprising *DTE* (eqn. (2.86)), *DAE*, *LE*, *AE* (eqns. (1.17)), $D\Delta g^h$ (Sec. (3.4)), *SITE* (eqn. (2.90)), and D^S (eqn. (2.103)) are required. The first two corrections provide the transformation from the real earth space to the Helmert space. The *DTE*—due to the difference between topographical masses and their condensation on the geoid, is weaker in the long wavelength part but more powerful in the short wavelength, i.e., its long wavelength contribution to the geoid is a few decimetres, Fig. 4.6, while its short wavelength contribution could reach up to a metre [Vaníček et al., 1995a]. For precise evaluation of the *DTE*, a more detailed topography (DTM) is required. The *DAE* hasn't been considered in the Stokes-Helmert scheme yet. This effect, even though smaller compared to *DTE*, has to be taken into account. This will complete the Helmertization (Sec. (2.4)).

It is worthwhile to mention here that the Helmert orthometric heights H using the Poincare-Pray gravity gradient ($0.0848 \text{ mGal}/m$), based on the simplified assumption of constant crustal density $\rho_0 = 2.67 \text{ g cm}^{-3}$, may be in error by a few decimetres due

to the actual density variations within the topography [Vaníček et al., 1995a]. This in turn can cause an error up to $100 \mu Gal$ in the upward continuation, eqn. (1.14), of the normal gravity, but has negligible impact on the LA and AE .

The $D\Delta g^h$ is determined through an iterative process. The number of iterations required, to meet the accuracy of $10 \mu Gal$ [Vaníček et al., 1996], increases with the height of the computation point. The downward continuation is a high-frequency phenomenon, it's contribution to geoidal height can reach up to a metre, Fig. 3.6. This cannot be ignored in the precise geoid determination.

The $SITE$ is a relatively small correction. It could reach up to a few μGal in the long wavelength part, but may attain larger values, e.g., $300 \mu Gal$ see Sec. (6.1), in the high-frequency part. The D^S is evaluated using a combined geopotential model, e.g., GFZ93A. The "commission error" due to the model is negligible.

6.2 The Helmert Reference Spheroid

The Helmert spheroid is obtained from the Helmert disturbing potential T_L^h . This potential is derived from the reference potential T_L , by subtracting from it the residual topographical potential V_L , eqn. (2.75). The potential V_L is two orders of magnitude smaller than T_L . This can be verified by the comparison of their extreme effects on equipotential surfaces, shown on Figs. (4.1) and (4.6). In the harmonic expansion, V_L is a function of mainly the squared-topography, eqns. (2.71). The "squared topography" model is derived from a global topographical model, e.g., TUG87. Any uncertainty of the model is propagated into the derived squared topographical model and finally to the potential V_L . Since the potential V_L is relatively small, the effect of the topographical error on the Helmert spheroid will be small too. Hence, the only error in the spheroid comes from satellite potential coefficients (commission error).

For the evaluation of the Helmert spheroid to a decimetre accuracy or better, the ellipsoidal approximation, Sec. (2.5), has to be implemented, since its impact on

the spheroid reaches up to a metre, Fig. 4.2. The same approximation must also be considered when evaluating the reference gravity Δg_L , see Fig. 4.5. Approximation to a degree higher than 2 (the ellipsoidal approximation) could improve the spheroid by a few millimetres, Fig. 4.3; this may be disregarded at the present time.

As seen in Sec. (4.1.1), different geopotential models estimate 0-th degree term differently. The differences imply error in the 0-th degree term of the spheroid, and it is translated as an error to the geoidal height. In relative accuracy assessment of the geoid, however, this error is immaterial.

6.3 Accuracy of the Geoid

The accuracy of the geoid was investigated in two parts: one reflecting the accuracy of the Helmert spheroid of degree 20; the other reflecting the accuracy of the residual geoid. Either one of the accuracies is a function of distance (isotropic) only.

Error in the spheroid is due to the "commission error" of the satellite potential coefficients. The derived spheroidal heights are highly positively correlated at neighbouring points, see Fig. 5.3. The correlations imply some statistical dependence of the spheroidal heights. The positive correlation, up to the distance of 900 *km*, indicates that the spheroidal height differences are determined to higher accuracy than the heights themselves, see eqns. (5.12). The correlation sign, however, starts alternating after 900 *km*.

The accuracy of the residual geoid was derived on the assumption of homogeneous and statistically independent residual gravity field. The positive correlation, Fig. 5.6, again indicates some functional relation among residual geoidal heights. Statistical independence of the gravity anomalies is a false assumption. They are certainly correlated through the methods of the prediction and densification used, as well as through the reference gravity. The correlation will have some effects on the correlation function, derived for the geoidal height.

6.4 Recommendations

During the computation of the precise geoid for Canada, we (the working group) discovered that the terrestrial data, i.e., the existing $5' \times 5'$ mean (Bouguer) gravity anomalies are not suitable (accurate) for a precise geoid. This has been verified by comparing some files of the mean anomalies with the satellite-derived anomalies of the same resolution. The discrepancies are far beyond the $10\mu Gal$, required for a centimetre geoid. The reason for this is that, the mean anomalies are based on sparse gravity (observed) network [Mainville and Veronneau, 1989], thus, mostly generated by prediction methods. The trace of systematic errors in the anomalies, as a result of these methods is evident [Vaníček et al., 1995a]. Another source, causing uncertainty is the height system to which the anomalies are referred. Hence, both a densified enough gravity network and a precise height network are fundamental for a precise determination of the geoid:

- A $5' \times 5'$ and higher resolution mean anomalies, required by a "centimetre geoid", demand much more gravity observations than exists today.
- A precise geoid could only stand on the bases of a reliable orthometric height network. This network is a base for both an unbiased gravity anomalies and a reliable topography model (DTM).

The atmospheric effects (*DAE* and *PIAE*) on the geoid are smaller, may be by one order of magnitude, than *DTE* (Fig. 4.6) and *PIE*. The effects are then still a few centimeters. For the precise geoid these effects have to be formulated and implemented in the Stokes-Helmert scheme.

The "GIN95.f" integrator is sensitive to low-frequency noise which may exist in the residual Helmert gravity anomaly. This is because the kernel used, contain low-frequency ($n \leq 20$) spectrum. This kernel translates any low-frequency noise (in the gravity data) to the noise in the geoidal height, i.e., correlating with the spheroid.

The noise could be developed either from the "observed" gravity anomalies or from the reference anomalies, see eqn. (5.7). To prevent the correlation with the spheroid, one has to make sure that the residual gravity anomalies are properly reduced to high-frequency component, or to account for the correlation by the propagation of the errors in the "observed" and reference gravity anomalies to the geoid.

It is seen from Fig. 3.5 that the geopotential models are not consistent in the estimation of the truncation error. This implies errors in a geopotential model which propagate, as an error, to the quantity (truncation error) estimated. The error will be evidently small on a small quantity. The minimum truncation error, then, will be estimated to a better accuracy by a geopotential model. This is why the generalized Stokes integral, using a modified kernel, is advantageous in the computation of a residual geoid.

Bibliography

Bomford, G. (1971). *Geodesy*. 3th ed., Oxford, at the Clarendon Press.

Forsberg, R. and M. G. Sideris (1993). Geoid Computation by the Multi-band Spherical FFT Approach. *Manuscripta Geodaetica*, 18, 82-90.

Gang Chang, R., N. Christou, and H. Fashir (1986). Software for Geoid Computations, Technical Memorandum (TM-10), Department of Surveying Engineering, University of New Brunswick, P.O.Box 4400, Fredericton, N.B., Canada

Gruber, T. and M. Anzenhofer (1993). The GFZ360 Gravity Field Model, the European geoid determination, Proceedings of session G3, European Geophysical Society XVIII General Assembly, Wiesbaden, May 3-7, 1993, published by the geodetic division of KMS, Kopenhagen.

Heck, B. (1992). A revision of Helmert's second method of condensation in geoid and quasigeoid determination. Paper presented at 7th Int. Symposium Geodesy and Physics of the Earth, IAG-Symposium, No. 112, Potsdam, October 1992.

Heiskanen, W. A. and H. Moritz (1981). *Physical Geodesy*. Reprinted in the Institute of Physical Geodesy, Technical University Graz, Austria, 1981.

Korn, G. A. and T. M. Korn (1968). *Mathematical Handbook for Scientists and Engineers*. McGraw-Hill book company, New York.

- Lerch, F. J., R. S. Nerem, B. H. Putney, T. L. Felsentreger, B. V. Sanches, S. M. Klosko, G. B. Patel, R. G. Williamson, D. S. Chinn, J. C. Chan, K. E. Rachlin, N. L. Chandler, J. J. McCatrthy, J. A. Marshall, S. B. Luthcke, D. W. Pavlis, J. W. Robbins, S. Kapoor, and E. C. Pavlis (1992). Geopotential Models of the Earth From Satellite Tracking, Altimeter and Surface Gravity Observations: GEM-T3 and GEM-T3S. NASA Technical Memorandum 104555, Goddard Space Flight Center, Greenbelt, MD.
- Mainville, A. and M. Veronneau (1989). Creating a Gravity Grid Over Canada Using Bouguer Anomalies and Digital Elevation Model. CGU Annual Meeting, Montreal, May, 1989.
- Martinec, Z. (1993). Effect of Lateral Density variations of Topographical Masses in View of Improving Geoid Model Accuracy Over Canada. Contract report for Geodetic Survey of Canada, Ottawa, June 1993.
- Martinec, Z. (1996). Stokes's two-boundary value problem. Department of geophysics, faculty of mathematics and physics, Charles University, Prague, Czech Republic.
- Martinec, Z. and P. Vaníček (1994a). The Indirect Effect of Topography in the Stokes-Helmert's Technique for a Spherical Approximation of the Geoid. *Manuscripta Geodaetica*, 19, 213-219.
- Martinec, Z. and P. Vaníček (1994b). Direct topographical effect of Helmert's condensation for a spherical approximation of the geoid. *Manuscripta Geodaetica*, 19, 257-268.
- Marsh, J. G., F. J. Lerch, B. H. Putney, D. C. Christodoulidis, D. E. Smith, T. L. Felsentreger, B. V. Sanchez, S. M. Klosko, E. C. Pavlis, T. V. Martin, J. W. Robbins, R. G. Williamson, O. L. Colombo, D. D. Rowlands, W. F. Eddy,

- N. L. Chandler, K. E. Rachlin, G. B. Patel, S. Ehati, and D. S. Chinn (1988). A New Gravitational Model for the Earth from Satellite Tracking Data: GEM-T1. *JGR*, Vol. 93, No. B6, p. 6169-6215, June 10, 1988.
- Marsh, J. G., F. J. Lerch, B. H. Putney, T. L. Felsentreger, B. V. Sanchez, S. M. Klosko, G. B. Patel, J. W. Robbins, R. G. Williamson, T. L. Engelis, W. F. Eddy, N. L. Chandler, D. S. Chinn, S. Kappoor, K. E. Rachlin, L. E. Braatz, and E. C. Pavlis (1990). The GEM-T2 Gravitational Model. *JGR*, Vol. 95, No. B13, p. 22043-22071, December 10, 1990.
- Molodenskij, M.S., V.F. Eremeev, and M.I. Yurkins, *Methods for Study of the External Gravitational Field and Figure of the Earth* (1960). (Translated from Russian by the Israel Program for Scientific Translation, Office of Technical Services, Department of Commerce, Washington, D.C., 1962.)
- Moritz, H. (1980). Geodetic Reference System 1980. *Bull. Géod.*, Vol. 66, NO. 2, p. 187, 1992.
- Schwarz, K. P., M. G. Sideris, R. Forsberg (1990). The Use of FFT techniques in Physical Geodesy. *Geophys. J. Int.* Vol. 100, pp. 485-514.
- Sjöberg, L. E. (1983). Land Uplift and its Implications on the Geoid in Fennoscandia, *Tectonophysics*, 97 (1983) 97-101.
- She, B. B., M. G. Sideris, and K. P. Schwarz (1993). A PC-based Unified Geoid for Canada. Final report for DSS contract No. 23244-0-4451/01-ET. The University of Calgary, department of Geomatics Engineering.
- Sideris, M. G. and Bin Bin She (1995). A new, high-resolution geoid for Canada and part of the U. S. by the 1D-FFT method. *Bull. Géod.*, Vol. 69, pp. 92-108.
- Sideris, M. G. and Ye Cai Li (1993). Gravity field convolution without windowing and edge effects. *Bull. Géod.*, Vol. 60, pp. 51-63.

- Schwintzer, P., Ch. Reigber, F. H. Massmann, W. Barth, J. C. Raimondo, M. Gerstl, H. Li, R. Biancale, G. Balmino, B. Moynot, J. M. Lemoine, J. C. Marty, Y. Boudon, and F. Barlier (1991). A New earth Gravity Field Model in Support of ERS-1 and SPOT-2: GRIM4-S1/C1. Final Report to the German Space Agency (DARA) and the French Space Agency (CNES). München/Toulouse 1991.
- Schwintzer, P., Ch. Reigber, A. Bode, Z. Kange, S. Y. Zhu, F. H. Massmann, J. C. Raimondo, R. Biancale, G. Balmino, J. M. Lemoine, B. Moynot, J. C. Marty, F. Barlier, and Y. Boudon (1995). Long-Wavelength Global Gravity Field Models: GRIM4-S4, GRIM4-C4. GeoForschungsZentrum (GFZ, Div. I), Potsdam, Germany and Groupe de Recherche de Géodésie Spatiale (GRGS), Toulouse, Grasse.
- Rapp, R. H., Y. M. Wang, and K. N. Pavlis (1991). The Ohio State 1991 geopotential and sea surface topography harmonic coefficient models. OSU report No. 410, Department of Geodetic Science and Surveying, The Ohio State University, Columbus, Ohio.
- Vaníček, P. and E. J. Krakiwsky (1986). *Geodesy: The Concepts*, 2nd corrected ed., North Holland, Amsterdam.
- Vaníček, P. and A. Kleusberg (1987). The Canadian Geoid- Stokesian Approach *Manuscripta Geodaetica* 12, 86-98.
- Vaníček, P. and L. E. Sjöberg (1991). Reformulation of Stokes's Theory for Higher than Second-Degree Reference Field and a Modification of Integration Kernels, *JGR* 96(B4), 6529-6539.
- Vaníček, P. and Z. Martinec (1994). The Stokes-Helmert Scheme for the Evaluation of a Precise Geoid. *Manuscripta Geodaetica*, 19, 119-128.

- Vaníček, P., A. Kleusberg, R. G. Chang, H. Fashir, N. Christou, M. Hofman, T. Kling, and T. Arsenault (1987). The Canadian Geoid. Department of Surveying Engineering, University of New Brunswick, P.O. Box 4400, Fredericton, N. B., Canada, E3B 5A3.
- Vaníček, P., A. Kleusberg, Z. Martinec, W. Sun, P. Ong, M. Najafi, P. Vajda, L. Harrie, P. Tomášek, and B. Ter Horst (1995a). Compilation of a Precise Regional Geoid. Final report on research done for the Geodetic Survey Division, Geomatics Sector, Natural Resources Canada, Ottawa, under a DSS contract No. 23244-1-4405/01-SS.
- Vaníček, P., M. Najafi, Z. Martinec, L. Harrie, and L. E. Sjöberg (1995b). Higher-Degree Reference Field in the Generalized Stokes-Helmert Scheme for Geoid Computation. *Journal of Geodesy* (1995) 70:176-182.
- Vaníček, P., W. Sun, P. Ong, Z. Martinec, M. Najafi, P. Vajda, and B. Ter Horst (1996). Downward Continuation of Helmert's Gravity Anomaly. *Journal of Geodesy* (accepted) for publication in *Journal of Geodesy* in July 1996.
- Wang, Y. M. and R. H. Rapp (1990). Terrain effects on geoid undulation computations. *Manuscripta Geodaetica*, 15, 23-29.
- Wichiencharoen, C. (1982). The indirect effects on the computation of geoid undulations. OSU Report No. 336, Department of Geodetic Science and Surveying, The Ohio State University, Columbus, Ohio.
- Wieser, M. (1987). The global digital terrain model TUG87. Internal report on set-up, origin and characteristics. Inst. of Mathematical Geodesy, University of Graz, Austria.

Vita

Candidate's full name: Mehdi Najafi-Alamdari

Place and date of birth: Iran (Alamdari), 22 April, 1947.

Permanent Address: No. 6 Bahar-e-azadi Ave., Peyambar crossing, Ashrafi-esfahani HWY., Tehran, Iran.

Schools attended: Nezami Junior high school, Alamdar (1959-1962), Iran. Ferdosi high school, Tabriz (1962-1965), Iran.

Universities attended: University of Tehran, BSc. in physics, Tehran (1966-1970), Iran. University of New Brunswick, MSc. in Surveying Engineering, Fredericton (1978-1981), Canada.

Publications:

Najafi, M. (1981). *Local Evaluation of the Geoid From Gravity Data*. M. Sc. thesis, Department of Surveying Engineering, University of New Brunswick, Fredericton, N. B., Canada.

- Vaníček, P., W. Sun, P. Ong, Z. Martinec, M. Najafi, P. Vajda, and B. Ter Horst (1994). Downward Continuation of Helmert's Gravity Anomaly. *Journal of Geodesy* (accepted for publication in July 1996).
- Vaníček, P., A. Kleusberg, Z. Martinec, W. Sun, P. Ong, M. Najafi, P. Vajda, L. Harrie, P. Tomášek, and B. Ter Horst (1995). Compilation of a Precise Regional Geoid. Final report on research done for the Geodetic Survey Division, Geomatics Sector, Natural Resources Canada, Ottawa, under a DSS contract No. 23244-1-4405/01-SS.
- Vaníček, P., M. Najafi, Z. Martinec, L. Harrie, and L. E. Sjöberg (1995). Higher-degree Reference Field in the Generalized Stokes-Helmert Scheme for Geoid Computation. *Journal of Geodesy* 70:176-182.
- Vaníček, P., M. Najafi, and A. M. Abolghasem (1995). The Need for a Precise Geoid and How to Get It. In Farsi, Journal of NCC, Iran.
- Vaníček, P. and M. Najafi (1996). Proposed New Cartographic Mapping For Iran. Contract Report for NCC, Iran. Department of Geodesy and Geomatics Engineering, University of New Brunswick, Fredericton, N.B., Canada, E3B 5A3.
- Najafi, M., P. Vaníček, P. Ong, and M. Craymer (1996). Accuracy of a Regional Geoid. *Journal of Geodesy* (in preparation).
- Featherstone, W. E., M. W. Schouten, M. Najafi, P. Vaníček, A. Kleusberg, and P. Novak (1996). Numerical Validation of the GIN95.f Geoid Computation Software at UNB. *Geomatica* (in preparation).